TECHNISCHE UNIVERSITÄT DARMSTADT

Antibody-mediated inhibition of MHC class I chain-related protein A shedding for tumor therapy

vom Fachbereich Chemie

der Technischen Universität Darmstadt

zur Erlangung des Grades

Doctor rerum naturalium

(Dr. rer. nat.)

Dissertation von

Veronika Liptáková

Erstgutachter: Prof. Dr. Harald Kolmar

Zweitgutachter: Prof. Dr. Alexander Steinle

Darmstadt 2023

Tag der Einreichung: 17.05.2023

Tag der mündlichen Prüfung: 10.07.2023

Liptakova, Veronika: Antibody-mediated inhibition of MHC class I chain-related protein A shedding for tumor therapy

Darmstadt, Technische Universität Darmstadt

Year thesis published in Tuprints 2023

Contents

Summary

The NKG2D/NKG2D ligand pathway mediates cancer immunosurveillance by cytotoxic lymphocytes. Natural killer group 2 member D (NKG2D) is a homodimeric C-type lectin like receptor expressed on almost all human cytotoxic lymphocytes (NK, $CD8^+$ and γδ T cells) and serves as a primary activating receptor on NK cells. In humans, there are eight NKG2D ligands (MICA/MICB and ULBP1-6), among which MICA/B (MHC class I chain-related sequence A/B) have been best characterized. MICA and MICB are ´sister´ molecules that share around 91 % identity in their coding sequences. The domain structure of MICA/B consists of three extracellular domains, the α1α2 MHC class I-like superdomain and the Ig-like α3 domain. Under normal physiological conditions, MICA/B glycoproteins usually are not expressed in healthy tissues, but MICA/B cell surface expression can be induced by various stress conditions (e.g., virus infection, malignant transformation). MICA/B-NKG2D interaction promotes immune recognition and cytolysis of MICA/B-expressing stressed cells. However, tumor cells often escape from NKG2D-mediated recognition, apparently also by shedding of MICA molecules from the cell surface by various metalloproteases (e.g., ADAM10 and ADAM17). There is a negative correlation of elevated soluble MICA/B (sMICA/B) levels in serum of cancer patients (as a consequence of MICA/B shedding) with overall survival. Moreover, sMICA/B was suggested as a cancer marker. Hence, these properties mark the shedding of MICA/B as an attractive target for cancer studies. Numerous clinical studies attempted to target metalloproteases in order to block their action to treat malignant diseases in patients. Unfortunately, these attempts were unsuccessful due to important biological roles of these proteases in processes. As a result, there is an urgent need to develop other means of cancer treatment that lead to inhibition of MICA shedding from tumors.

The aim of this thesis was to characterize the MICA/B-monoclonal antibody (mAb) BAMO3, which inhibits MICA/B shedding, and test the therapeutic efficacy of BAMO3-mediated inhibition of MICA shedding in aggressive syngeneic mouse tumor models. In addition, particular amino acids in the transmembrane and α3 domain in the MICA molecule and their role in MICA shedding and eventually their role in affecting BAMO3-mediated MICA shedding inhibition were studied. Lastly, therapeutic efficacy of another MICA antibody conjugated to toxin was tested.

Previously, the Steinle laboratory generated the mAb BAMO3 specific for MICA and MICB. This thesis demonstrates BAMO3 proteolytic shedding inhibition of MICA/MICB from different tumor cells in a dose-dependent and cell-specific manner *in vitro*. The shedding inhibition was very efficient as BAMO3 was able to prevent MICA/B shedding at very low concentrations, as low as 0.1 µg/ml, and at 10 µg/ml the MICA/B shedding was almost completely blocked. BAMO3 is

widely applicable as it prevented shedding of different MICA and MICB allelic variants expressed by various cancer cell lines. To elucidate the molecular action of BAMO3, the epitope of BAMO3 was mapped to the membrane proximal site of the MICA α3 domain suggesting that BAMO3 acts by steric hindrance of metalloprotease cleavage.

MICA is highly polymorphic and there are over 100 different alleles recognized in the current literature. Several alleles possess two, four or even nine GCT repeats, in the transmembrane region of MICA, respectively. The results of this study suggest that the length of alanine repeats in the transmembrane domain of MICA does not affect MICA shedding inhibition by BAMO3.

Next, a cysteine in position 250 in MICA (positioned in the α3 domain), that does not seem to form an intramolecular disulfide bond with any cysteine partner, was studied. Mutation of this cysteine (Cys250Ala) led to mitigation of shedding intensity of Cys250Ala MICA from B16F10 cells. Moreover, the surface expression of Cys250Ala MICA was increased while ADAM10 metalloprotease surface expression was decreased. Further, co-immunoprecipitation experiments indicated a lower intensity interaction between Cys250Ala MICA and ADAM10.

Finally, anti-tumor effects of anti-MICA antibodies were studied *in vivo*. Administration of BAMO3 delayed growth of RMA-MICA lymphoma in a syngeneic mouse model in MICA transgenic (MICAgen) mice and thereby improved survival of tumor-bearing mice. Tumor-infiltrating NK cells expressed higher NKG2D levels upon BAMO3 treatment as compared to control-treated mice. Overall, these data demonstrated therapeutic efficacy of BAMO3 treatment in the mouse RMA lymphoma model, and, together with other data from our laboratory, endorse BAMO3 treatment as a potential novel immunotherapeutic approach for treatment of human malignant diseases.

In addition, therapeutic efficacy of a drug-conjugated antibody against MICA (19E9-PBD) was tested in MICAgen mice bearing various aggressive mouse tumors. 19E9-PBD demonstrated a tremendous efficiency in delaying the tumor growth and improving survival of MICAgen mice. A decreased MICA expression on immunosuppressive myeloid-derived suppressor cells (MDSCs) was detected in the tumors. Moreover, the combination therapy of 19E9-PBD together with an anti-PD-1 antibody showed therapeutic efficacy in delaying the growth of MICA-expressing tumors.

In conclusion, these results presented powerful antibody-based agents for tumor elimination of MICA-positive tumors. They may be used to complement and enhance the antineoplastic effects of other anti-cancer therapeutics or immune checkpoint inhibitors that are currently used for patients with various malignancies.

Zusammenfassung

Die NKG2D/NKG2D-Liganden Achse ermöglicht die immunologische Kontrolle von entarteten Zellen durch zytotoxische Lymphozyten. NKG2D gehört zur Familie der C-Typ ähnlichen Rezeptoren und wird als Homodimer auf zytotoxischen Lymphozyten (NK, $CD8^+$ und γδ T Zellen) exprimiert, wo es als aktivierender Rezeptor fungiert. Bislang sind acht NKG2D Liganden (NKG2DL) im Menschen beschrieben. Neben MICA und MICB Molekülen, welche eine zentrale Rolle in dieser Arbeit einnehmen, sind die NKG2DL ULBP1-6 zu erwähnen. MICA und MICB weisen drei extrazelluläre Domänen (α1-α3) auf und 91% Sequenzidentität. Unter normalen physiologischen Bedingungen ist keine Expression von MICA/B auf gesunden Zellen nachweisbar. Zahlreiche Stressoren wie z.B. eine Virusinfektion, oder eine maligne Transformation vermögen jedoch die Oberflächenexpression von MICA/B zu induzieren, sodass es zu einer Immunantwort (Zytolyse) durch $NKG2D^+$ Zellen kommen kann. Entartete Zellen können jedoch einer NKG2D-vermittelten Immunantwort entgehen, indem MICA/B Moleküle proteolytisch durch Metalloproteasen (ADAM10/17) von der Zelloberfläche abgetrennt werden („*shedding*“). Studien zufolge korreliert das Überleben von Krebspatienten negativ mit der Menge an löslichen MICA/B im Serum, weshalb MICA/B als Biomarker in Frage kommen. In zahlreichen klinischen Studien versuchte man Metalloproteasen zu blockieren. Bisher waren diese therapeutischen Ansätze jedoch aufgrund erheblicher Nebenwirkungen erfolglos, da Metalloproteasen auch in wichtige biologische Prozesse involviert sind. Es ist deshalb von großem Interesse eine Therapie zu entwickeln die MICA shedding auf anderem Wege gezielt inhibiert.

Ziel dieser Arbeit war die Charakterisierung des MICA/B-spezifischen monoklonalen Antikörpers BAMO3 hinsichtlich dessen Verwendung als Inhibitor von MICA shedding *in vitro* und *in vivo*.

Diese Doktorarbeit zeigt den inhibitorischen Einfluss von BAMO3 auf das proteolytische „*Shedding*“ von MICA/B in Tumorzellen *in vitro.* Bereits eine geringe Konzentration [0.1 µg/ml] an BAMO3 vermag das shedding verschiedener MICA/B Allele in unterschiedlichen Tumorzelllinien zu reduzieren. Mit Hilfe von Alaninmutagenese wurde das Epitop von BAMO3 an einer membranproximalen Stelle der MICA α3 Domäne kartiert. In unmittelbarer Nähe liegt die Schnittstelle der Metalloproteasen, weshalb der inhibitorische Effekt von BAMO3 wahrscheinlich auf eine sterische Blockade zurückzuführen ist.

MICA ist polymorph, wobei die Literatur bislang über hundert verschiedene Allele beschreibt. So finden sich auch repetitive GCT Sequenzmotive in der Transmembrandomäne von

MICA. Diese Arbeit zeigt, dass die Anzahl der GCT- Repetitionen keinen Einfluss auf die BAMO3 vermittelte Inhibierung des MICA- „Shedding“ hat.

Des weiteren zeigt diese Arbeit, dass die Substitution von Cystein an Position 250 durch Alanin im MICA Molekül (α3 Domäne) zur Verminderung des „Sheddings“ führt. Zugleich nimmt die Oberflächenexpression der Metalloprotease ADAM10 ab. In Folge dessen steigt die Dichte der MICA Moleküle auf der Zelloberfläche. Des Weiteren wurde auch eine verringerte Interaktion zwischen ADAM10 und MICA (C250A) beobachtet.

Abschließend widmet sich diese Arbeit der therapeutischen Verwendung von anti-MICA Antikörpern in Maustumormodellen. Die therapeutische Gabe von BAMO3 vermag nicht nur das Wachstum des $MICA^+$ Lymphoms RMA in einem syngenen MICA-transgenen Mausmodell zu verzögern, sodass das Überleben signifikant verlängert werden konnte. Daneben führte die BAMO3-Behandlung auch zu einer erhöhten NKG2D-Oberflächenexpression auf Tumor-infiltrierenden NK Zellen. Daneben wurde auch wird die Effizienz des Wirkstoff-konjugierten anti-MICA Antikörper 19E9-PBD sowohl in der Monotherapie, als auch in der Kombinationstherapie mit einem anti-PD-1 Antikörper beschrieben. Beide Ansätze zeigen - wie auch die BAMO3 Behandlung – ein verzögertes Tumorwachstum sowie einen positiven Effekt auf das Überleben. Darüber hinaus verringern sie die MICA Expression myeloider Suppressorzellen (MDSC), deren immunsuppressive Eigenschaften gegenüber T-Zellen maßgeblich an der Immunevasion maligner Tumore beteiligt sind.

Zusammenfassend demonstriert diese Arbeit die Wirkungsweise und das immunotherapeutische Potential von BAMO3 zur Elimination MICA-positiver Tumore. Eine Kombinationstherapie mit bereits zugelassenen antineoplastischen Krebsmedikamenten könnte synergistisch wirken und wird Bestandteil künftiger Studien sein.

Abbreviations

Abs	Absorbance
ADAM	A disintegrin and metalloproteinase
ADC	Antibody drug-conjugate
ADCC	Antibody-dependent cellular cytotoxicity
AICL	Activation-induced C-type lectin
Ala	Alanine
AML	Acute myeloid leukaemia
ANOVA	Analysis of Variance
APC	Antigen presenting cell
ATM	Ataxia telangiectasia mutated
ATR	Ataxia-telangiectasia mutated and Rad3-related
BB94	Batimastat
bp	Base pair
BTLA	B and T lymphocyte attenuator
CAR	Chimeric antigen receptor
CCL	Chemokine (C-C motif) ligand
CCR	Chemokine receptor
CD	Cluster of differentiation
CEACAM1	Carcinoembryonic antigen-related cell adhesion molecule 1
CLEC	C-type lectin-domain family member
CO-IP	Co-immunoprecipitation
CTLA-4	Cytotoxic T-lymphocyte-associated protein 4
Cys	Cysteine
Da	Dalton
DAP10	DNAX-activating protein of 10 kDa
DAP12	DNAX-activating protein of 12 kDa
DC	Dendritic cell
DMEM	Dulbecco's Modified Eagle's Medium
DMSO	Dimethyl sulfoxide
DNA	Deoxyribonucleic acid
DNAM-1	DNAX accessory molecule-1
dNTPs	Deoxyribonucleotide triphosphates
DOX	Doxorubicin
E.coli	Escherichia coli
E:T	Effector to target ratio
ecto-CRT	Ecto-calreticulin
EDTA	Ethylenediaminetetraacetic acid
EGF	Epidermal growth factor
ELISA	Enzyme-Linked Immunosorbent Assay
EndoH	Endoglycosidase H
ERp5	Endoplasmic reticulum protein 5
FACS	Fluorescence-activated cell sorter
Fc	Fragment crystalizable
FCS	Fetal calf serum
Fcγ	Fc gamma receptor
fw	Forward

GM-CSF	Granulocyte macrophage colony-stimulating factor
GPI	Glycosylphosphatidylinositol
Grb2	Growth Factor Receptor-bound protein 2
GRP78	Glucose-regulated protein 78 kDa
H60 family	The histocompatibility 60 family
HDACi	Histone deacetylase
HER2	Human epidermal growth factor receptor 2
HLA	Human leukocyte antigen
HMGB1	High mobility group box
HRP	Horseradish peroxidase
IFNβ1	Interferon beta 1
IFN-γ	Interferon gamma
Ig	Immunoglobulin
IL	Interleukin
IMDM	Iscove's Modified Dulbecco's Medium
iNKT	Invariant natural killer T
IP	Immunoprecipitation
ITAM	Immunoreceptor tyrosine-based activation motif
ITIM	Immunoreceptor tyrosine-based inhibitory motif
kDa	Kilodalton
KIR	Killer cell immunoglobulin-like receptors
KLRK1	Killer cell lectin-like receptor subfamily K, member 1
LAG3	Lymphocyte-activation gene 3
LAT	Linker for activation of T cells
LB	Luria-Bertani
LFA-1	Lymphocyte function-associated antigen 1
LILRB1	Leukocyte immunoglobulin-like receptor B1
LN	Lymph node
mAb	Monoclonal antibody
MDSC	Myeloid-derived suppressor cell
Met	Methionine
MFI	Median fluorescence intensity
MHC	Major histocompatibility complex/class
MICA	MHC class I chain-related protein A
MICAgen	MICA transgenic
MICB	MHC class I chain-related protein B
MIP-1b	Macrophage inflammatory protein *1α*
MM	Multiple myeloma
MMP	Matrix metalloproteinase
MULT-1	Murine UL16-binding protein-like transcript-1
Nck	Non-catalytic region of tyrosine kinase
NK cell	Natural killer cell
NKC	Natural killer gene complex
NKG2D	Natural killer group 2, member D
NKG2DL	NKG2D ligand
NP-40	Nonidet P-40
PAMP	Pathogen-associated molecular pattern
PAO	Phenylarsine oxide
PBD	Pyrrolobenzodiazepine
PBS	Phosphate-buffered saline

PCR	Polymerase chain reaction
PD-1	Programmed death-1
PDGF-DD	Platelet-derived growth factor D
PD-L1	Programmed death-ligand 1
PEI	Polyethylenimine
PI3K	Phosphatidylinositol-3 kinase
PLCγ	Phospholipase C-γ
PMA	Phorbol 12-myristate 13-acetate
PNGase F	Peptide -*N*-Glycosidase F
PRRs	Pattern recognition receptors
PVDF	Polyvinylidene difluoride
Rae-1	Retinoic acid early inducible-1
RPMI	Roswell Park Memorial Institute 1640 Medium
RT	Room temperature
rv	Reverse
SA	Streptavidin
scFv	Single chain variable fragment
SCID	Severe combined immunodeficiency
SDS PAGE	Sodium dodecyl-sulfate polyacrylamide gel electrophoresis
Ser	Serine
SFI	Specific fluorescence intensity
SH2 domain	Src homology domain 2
SHP-2, -3	SH2 Src-homology domain 2, -3
SLP-76	Lymphocyte cytosolic protein 2 (SH2 domain containing leukocyte protein of 76kDa)
sMICA	Soluble MICA
sMICB	Soluble MICB
SNP	Single nucleotide polymorphism
STR	Short tandem repeat
Syk	Spleen tyrosine kinase
TCR	T cell receptor
tdLN	Tumor-draining lymph node
TGF	Transforming growth factor
T_H1 cell	T helper type 1 cell
TIGIT	T cell immunoglobulin and ITIM domain
TIL	Tumor infiltrating lymphocyte
TIM3	T-cell immunoglobulin and mucin-domain containing-3
TIMP-1	Tissue inhibitor of metalloproteinases 1
TNF-α	Tumor necrosis factor α
TRAIL	TNF-related apoptosis-inducing ligand
TRAIL-R1/R-2	TNF-related apoptosis-inducing ligand receptor 1/-2
T_{regs}	Regulatory T cells
ULBP	UL 16-binding protein
Val	Valine
WB	Western blot
XCL-1	Chemokine (C motif) ligand
ZAP-70	Zeta-chain-associated protein kinase 70
Zn	Zinc

1 Immune system

The immune system is a complex network of cells, tissues, and organs that work together to defend the body against infection and disease. It is responsible for identifying and destroying pathogens, such as bacteria, viruses, fungi, and parasites, as well as abnormal or cancerous cells that arise within the body. The immune system is composed of two main parts: the innate immune system and the adaptive immune system. The innate immune system is the body's first line of defence and is responsible for providing immediate protection against a wide range of pathogens. It includes physical barriers, such as the skin and mucous membranes, as well as specialized cells and molecules, such as phagocytes, natural killer cells, and complement proteins. The adaptive immune system, on the other hand, is a more specialized component of the immune system that develops over time in response to exposure to specific pathogens. It is responsible for providing long-term, specific protection against pathogens that the body has previously encountered. The adaptive immune system includes B cells, T cells, and specialized molecules, such as antibodies. All immune cells arise from one progenitor cell called pluripotent hematopoietic stem cell in the bone marrow. These pluripotent cells divide and produce two types of stem cells – common lymphoid progenitors (giving rise to B, T and NK cells) and common myeloid progenitors which are precursors of dendritic cells, granulocytes (neutrophils, eosinophils, basophils), monocytes, macrophages and mast cells. They also give rise to erythrocytes and platelets (Murphy et al., 2017).

1.1 Principle of the innate immune system

Innate immunity is the first line of defence against invading pathogens that provides immediate protection to the body. One of the key components of the innate immune system are so called pattern recognition receptors (PRRs). PRRs are molecules expressed by cells of the immune system, such as macrophages and dendritic cells that can recognize conserved molecular patterns present on a wide range of pathogens. These conserved patterns are known as pathogen-associated molecular patterns (PAMPs). Once a PAMP is recognized, PRRs can activate a variety of downstream signalling pathways that lead to the production of different cytokines, chemokines, and antimicrobial peptides, as well as to the activation of other cells of the immune system. The recognition of PAMPs by PRRs is critical for the innate immune response, as it allows the immune system to quickly detect and respond to a wide range of pathogens (Mogensen., 2009; Li & Wu., 2021).

Some of the key cells of the innate immune system include neutrophils that are among the first cells to respond to an infection. Neutrophils can engulf and digest invading pathogens, as well as release antimicrobial molecules (Borregaard, 2010). Other phagocytic cells able to engulf and digest larger pathogens, such as bacteria and fungi are called macrophages. They play an important role in presenting antigens to the adaptive immune system (Murray & Wynn, 2011). Dendritic cells also belong to antigen presenting cells (APCs) that can engulf and present antigens to the adaptive immune system, helping to generate a more specific immune response (Banchereau & Steinman, 1998). Eosinophils, specialized granulocytes, are involved in the response to parasitic infections, as well as allergic and inflammatory responses (Rothenberg & Hogan, 2006). Basophils play an important role in allergic and inflammatory responses as well. These immune cells release histamine and other molecules such as leukotrienes, different chemokines or tumor necrosis factor α (TNF-α), that can cause inflammation and increase blood flow to affected tissues (Zhang et al., 2021). Mast cells are tissue-resident cells that are involved in allergic and inflammatory responses. Similar to basophils, mast cells also release histamine and other molecules in response to stimuli such as allergens or pathogens (Galli & Tsai, 2010). Natural killer (NK) cells are specialized lymphocytes that can recognize and kill infected or abnormal cells, such as those infected with a virus or that have become cancerous (Vivier et al., 2008).

2 Natural killer cells

Greenberg and colleagues first described natural killer (NK) cells in 1973 as ´null lymphoid cells´ (Greenberg et al., 1973). Two years later Kiessling and colleagues already called these cells natural killer cells in their publication (Kiessling et al., 1975). NK cells are usually described as cytotoxic lymphocytes, members of the innate lymphoid cell family (Diefenbach et al., 2014). They are large granular lymphocytes possessing the ability to recognize and eliminate infected and cancer cells as well as to fine-tune other aspects of the immune system responses via cytokine and chemokine production (Caligiuri, 2008; Orr & Lanier, 2010). They differ from T and B lymphocytes in several aspects. In particular, T cells develop in the thymus, and they become activated upon T cell receptors' (TCRs) encounter with peptidic antigen carried on major-histocompatibility complex (MHC) molecules, together with costimulatory ligands expressed on APCs. In contrast, NK cells develop and mature primarily outside of the thymus, including bone marrow, tonsils, spleen and lymph nodes (Scoville et al., 2017). Moreover, NK cells do not express a TCR and do not require foreign antigen presentation through MHC in order to elicit cytotoxic immunity. Rather, NK cells respond to germ-line encoded markers of transformation present on the surface of stressed cells (e.g., infected or cancer cells) (Raulet & Guerra, 2009; Lanier et al., 1986). NK cells can be found not only in blood but also in lymphoid and non-lymphoid tissues (Vivier et al., 2008).

In humans, based on the expression patterns of these markers, two major subsets of NK cells are defined into $CD56^{dim}CD16^{+}$ and $CD56^{bright}CD16^{-}$ cells. $CD56^{dim}CD16^{+}$ NK cells form around 90% of peripheral blood and spleen NK cells, express perforin and are known to be cytotoxic NK cells producing cytokines and chemokines upon activation (Anfossi et al., 2006; Fauriat et al., 2010). They express killer cell immunoglobulin-like receptors (Cooper et al., 2001). Additionally, the expression of an Fc receptor (CD16) enables NK cells to exert a process termed as antibody-dependent cell-mediated cytotoxicity (ADCC) (Lanier et al., 1986 b). On the other hand, the subset $CD56^{bright}CD16^{-}$ NK cells lack perforin, are tissue-resident and are able to produce large quantities of cytokines (Ferlazzo & Munz, 2004; Cooper et al., 2001). They produce cytokines in response to stimulation with interleukin (IL)-12, IL-15 and IL-18 (Cooper et al., 2001).

In mice, NK cells differ in their expression of CD11b and CD27 markers and are categorized as $CD11b^{dull}$ $CD27^{+}$, $CD11b^{+}CD27^{+}$ and $CD11b^{+}CD27^{dull}$ NK cells (Vivier et al., 2008). Some literature includes another subset as double negative $CD11b^{-}CD27^{-}$ (Chiossone et al., 2009). They differ in tissue distribution as well as in their functionality. $CD11b^{+}CD27^{+}$ and $CD11b^{+}CD27^{dull}$ NK cells have cytotoxic capacities and secrete IFN-γ upon stimulation, but $CD11b^{+}CD27^{dull}$ NK cells are in a state of so called replicative or cellular senescence (Hayakawa et al., 2006).

Of note, CD56 is not expressed on mouse NK cells. However, mouse and human NK cells share a common marker, NKp46 (CD335) (Walzer et al., 2007).

NK cells are principally regarded as cytotoxic lymphocytes and their cytotoxicity is mediated via two diverse and complex mechanisms. Upon activation, NK cells release lytic granules (large specialized secretory lysosomes) containing perforin and granzymes and granulysin in humans (Clément et al., 1990; Pena et al., 1997; Stenger et al., 1998). Perforin induces pore formation in the stressed target cell allowing granzymes to enter the cell and induce subsequent apoptosis (Lieberman, 2003; Voskoboinik et al., 2006; Mace et al., 2014). The second mechanism by which NK cells can induce cell death, involves activation of the death receptor pathway. Death-inducing ligands expressed by activated NK cells (FAS ligand, and/or TRAIL) bind to their respective receptors expressed on the target cells (Fas/95 and TRAIL-R1/R-2 receptors), triggering cell death (Zamai et al., 1998, 2007; Voskoboinik et al., 2006; Takeda et al., 2001; Prager & Watzl, 2019).

Besides the cytotoxic function of NK cells, they have abilities to modulate immune responses via secretion of different cytokines and chemokines, for example IFN-γ, GM-CSF, TNF-α, XCL-1, CCL3, CCL4 and CCL5 (Kiessling et al., 1975; Böttcher et al., 2018; Robertson, 2002; Pallmer & Oxenius., 2016). Therefore, they are considered as bridge between innate and adaptive immune responses as they are able to communicate with dendritic cells (DCs), macrophages, neutrophils and T cells directly via cell-cell interactions and soluble factors (Bottcher et al., 2018; Pallmer & Oxenius., 2016; Bernardini et al., 2012). For example, NK cells are able to recruit dendritic cells into solid tumors by the secretion of CCL5, XC-chemokine ligand 1 and 2 (XCL-1/-2) (Bottcher et al., 2018). NK cells can also influence T cell responses by releasing IFN-γ and therefore promote polarization of T_H1 cells (T helper type 1 cells) or even reducing the expansion of T cells (Morandi et al., 2006; Pallmer & Oxenius., 2016). IFN-γ production by NK cells further promotes DCs activation via an engagement of the activating receptor NKp30 (Ferlazzo et al., 2002; Ferlazzo & Moretta., 2014).

NK cells have been historically considered innate lymphocytes, a part of the rapid innate immunity. However, some studies described NK cell memory formation under certain instances. Memory NK cells are a unique subset of NK cells that exhibit long-term antigen-specific memory and enhanced effector functions upon re-exposure to a previously encountered pathogen or antigen. Antigen-specific memory of NK was first recognized in several studies in mice (O'Leary et al., 2006; Sun et al., 2009; Paust et al., 2010). These studies showed NK cell-mediated long-lived, antigen-specific adaptive recall responses independent of B cells and T cells.

A fundamental function of NK cells lies in the elimination of cells with absent or reduced expression of MHC class I molecules, a phenomenon known as ´missing self´ principle. Missing self was hypothesized by Klas Kärre and colleagues in 1986 based on the fact that tumor cells with defective or low MHC-I expression were unable to inhibit triggering of NK cell-mediated lysis (Kärre et al., 1986). These activated NK cells then produce cytokines and possess cytotoxic functions. On the other hand, NK cells possess mechanisms allowing them to distinguish unhealthy cells from healthy cells. NK cells recognize stress-induced molecules that are not expressed or are expressed at low levels on healthy cells, but which are upregulated due to the activation of pathways associated with stress. This process is often referred to as an `induced self` hypothesis (Bauer et al., 1999; Diefenbach and Raulet, 2001). NK cell function is regulated by a large number of germ-line encoded receptors (Lanier, 2005). These receptors can be defined as activating and inhibitory receptors and a complex balance between the activating and inhibitory signals triggers NK cell-mediated cytotoxicity (Lanier, 2005) (Figure 1).

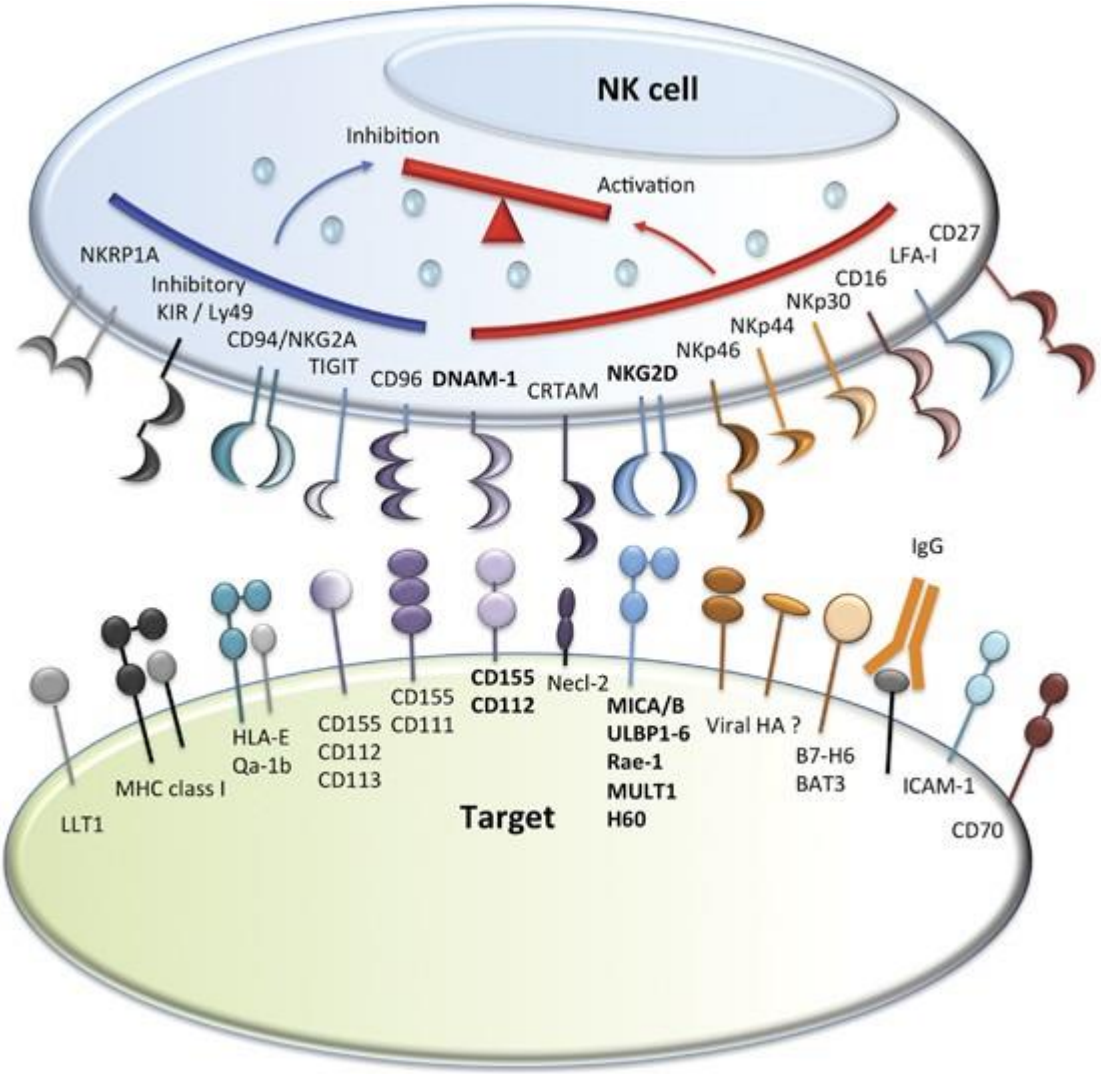

Figure 1. Major cell surface receptors expressed on murine and human NK cells and their ligands. Taken from Chan et al., 2014.

As mentioned earlier, NK cells express on their surface activating and inhibitory receptors and the balance in their signalling ensures their further activity via their activating ITAM and inhibitory ITIM, respectively (Long, 1999; Vivier et al., 2004; Lanier, 2008). When inhibitory receptor is triggered, the ITIM is tyrosine phosphorylated and SH2 domain (Src homology domain 2) – containing protein phosphatases SHP-1/2 or phosphatidylinositol phosphatase SHIP are recruited (Vivier et al., 2004). Dephosphorylation of the signalling molecules of the activation pathways by these phosphatases results in inhibition of cell activation. In principle, the inhibitory signal comes from the interaction of inhibitory receptors with normal physiological levels of MHC-I molecules. However, CD94/NKG2A heterodimer (also inhibitory receptor) is capable of recognizing non-classical MHC-I class (e.g., HLA-E in humans and Qa-1^b in mice) (Ravetch & Lanier., 2000). When an ITAM is triggered, Src protein tyrosine kinases are recruited as a result.

This leads to phosphorylation of the ITAM that causes recruitment and activation of the SH2 domain-containing tyrosine kinases Syk and ZAP-70. This signalling cascade then results in a recruitment and phosphorylation of number of signalling molecules (e.g., LAT, SLP-76, PI3K, PLCγ, Grb2, Vav, Cbl and Nck). This is followed by effector function of the triggered NK cell (Tomasello et al., 2000).

2.1 Inhibitory receptors and their ligands

The following chapters describe the most relevant inhibitory and activating receptors together with their ligands, according to the current literature.

Members of the KIR (killer cell Ig-like receptor) family in humans and of the C-type lectin-like Ly49 receptors in mice are important inhibitory receptors expressed on NK cells. They recognize the expression of different allelic variants of MHC-I molecules (Lanier, 2005; Yokohama, 1993; Moretta et al., 1996; Long et al., 1997). The first identified MHC-I specific inhibitory receptors were the Ly49 receptors (Karlhofer et al., 1992; Yokohama and Seaman, 1993). Both Ly49 and KIR genes are highly polymorphic and are expressed not only on NK cells but also on memory T cells (Karlhofer et al., 1992; Moretta et al., 1996; McMahon & Raulet., 2001; VIvier & Anfossi, 2004). KIR encode for both activating and inhibitory receptors, and they engage different HLA molecules (i.e., HLA-A, -B, -C). In humans, KIR2D family recognizes polymorphic HLA-C ligands, while other KIR3D family of receptors engages with HLA-A and HLA-B ligands (Parham, 2005).

A heterodimer CD94/NKG2A is shared by human and mice and is classified as an inhibitory receptor recognizing changes in MHC-I molecules. The CD94/NKG2A receptor recognizes as its ligand human HLA-E and murine Qa-1^b (Ravetch & Lanier., 2000). Around 50% of NK cells and some CD8 T cells express CD94/NKG2A inhibitory receptors on their surface. The NKG2A subunit contains an ITIM, responsible for the inhibitory properties (Raulet & Vance, 2006).

Other inhibitory receptors expressed by human and murine NK cells include the NKC-encoded KLRG1 (Corral et al., 2000; Voehringer et al., 2000) and it was shown that KLRG1 binds to cadherins (Grundemann et al., 2006; Ito et al., 2006; Tessmer et al., 2007). There are other receptors that bind so called non-MHC-encoded self-surface molecules. Except KLRG1, there is a human receptor NKR-P1A engaging LLT1 cadherin and murine Nkrp1d receptor engaging Clr-b (Iizuka et al., 2003; Aldemir et al., 2005; Rosen et al., 2005; Grundemann et al., 2006; Ito et al., 2006).

LILRB1 (also referred to as LIR1 or ILT2) is another ITIM-bearing inhibitory receptor present on NK cells as well as on T cells, B cells and myeloid cells (Colonna et al., 1997; Cosman et al., 1997). LILRB1 receptor can sense all human HLA-I molecules and has highest affinity to HLA-G (Shiroshi et al., 2006).

TIGIT inhibiting receptor (of the Ig superfamily) is found on both mouse and human NK cells, while approximately 50% of human peripheral blood NK cells express on their surface this receptor (higher on $CD56^{dim}$ cells compared to $CD56^{bright}$ cells) (Wang et al., 2015; Yin et al., 2018). TIGIT is expressed on human NK cells under both physiological and pathological conditions. The literature suggests that TIGIT inhibits function of NK cells not only with help of an ITIM motif but also via other mechanisms. For example, TIGIT was shown to compete for its ligand with the activating receptor DNAM-1 (Yu et al., 2009). TIGIT has two known ligands – CD155 (poliovirus receptor) and CD112 (nectin adhesion molecule) expressed mostly on APCs, T cells as well as on tumor cells and virus-infected cells (Casado et al., 2009; Stanietsky et al., 2009).

NK cells express several other inhibitory receptors on their surface. TIM3 is another inhibitory NK cell receptor expressed by both murine and human NK cells. Mature human NK cells express TIM3 constitutively on their surface while their expression can be upregulated by different cytokines (Ndhlovu et al., 2012). While TIM3 does not possess the characteristic inhibitory ITIM motif, it forms homodimers with CEACAM1, which appears to contain such inhibitory motif in its structure (Huang et al., 2015). Numerous ligands have been described for TIM3 – for example galectin-9, phosphatidylserine, HMGB1 (Das et al., 2017).

There are other receptors expressed on the surface of either human or murine NK cells, that serve inhibitory functions. To name a few, CD96 binding CD155, CD112R binding CD112, but as well as other T-cell associated immune checkpoints, such as PD-1, CTLA-4, BTLA or LAG-3 (reviewed in Buckle & Guillerey, 2021).

2.2 Activating receptors and their ligands

NK cells express a wide range of activating receptors (Figure). Among earliest identified receptors were the natural cytotoxicity receptors (NCRs) NKp30, NKp44 and NKp46 that are responsible for recognizing tumor cells and inducing cytotoxic functions (Koch et al., 2013). These NCRs are categorized as type I transmembrane receptors belonging to the immunoglobulin superfamily. NKp30 and NKp46 are largely expressed on activated and resting NK cells, while NKp44 expression is induced upon NK cell activation, for example by IL-2 (Cantoni

et al., 1999; Vitale et al., 1998; Pende et al., 1999; Sivori et al., 1997). Tumor-expressed B7-H6 was identified as a cellular ligand for NKp30 (Brandt et al., 2009; Kaifu et al., 2011).

NKp44 is an activating receptor that is expressed on activated NK cells, but also on a subgroup of ILC3. It is not expressed in mice. NKp44 associates with the adaptor protein DAP12, and it recognizes ligands, such as platelet-derived growth factor D (PDGF-DD) or nidogen 1 (Barrow et al., 2018; Gaggero et al., 2018).

NKp46 is the only NCR conserved among all mammalian species and is expressed by all mature NK cells. NKp46 is also expressed by other cells belonging to innate lymphoid cells ILC1 and ILC3 (Simoni & Newell, 2017). NKp46 recognizes several ligands, such as complement factor p (properdin), viral hemaglutinins or ecto-calreticulin (ecto-CRT) (Narni-Mancinelli et al., 2017; Mandelboim et al., 2001; Sen Santara et al., 2023).

CD16 receptor is expressed on both murine and human NK cells, and it associates with FcRγ homodimers (murine) and FcRγ and CD3ζ homodimers or heterodimers (human) (Lanier et al., 1989; Lanier et al., 1991). There are two isoforms of CD16 receptor – CD16 A and CD16 B. CD16A binds Fc domains of IgG1 and IgG3 expressed by NK cells and CD16B is mainly expressed on neutrophils (Medjouel Khlifi et al., 2022). Triggering of the CD16 receptor initiates ADCC (Hatjiharissi et al., 2007). Upon this engagement, target cells are killed by release of cytotoxic granules. Moreover, triggering of CD16 can affect NK cell survival (Waren & Kinnear., 1999).

Activating KIRs (killer cell immunoglobulin-like receptors) are located on human chromosome 19 in the leukocyte receptor complex. KIR gene family includes 15 genes and 2 pseudogenes. Their nomenclature is indicating their structure and also function, such as numbers of extracellular domains (2D and 3D), length of cytoplasmic tail (short S, long L) (Vivier et al., 2011). Upon engagement with their respective ligands (HLA-A/B/C), NK cells promote their cytotoxic functions via DAP12 adaptor protein bearing the ITAM motif (Lanier et al., 1998).

DNAM-1 (DNAX accessory molecule-1) is an activating receptor containing an Ig-like domain in its structure (Shibuya at al., 1995; Zhang et al., 2015; Long et al., 2013) and is expressed by both human and murine NK cells. Other immune cells were described to express DNAM-1 receptor as well ($CD8^+$ T cells or myeloid cells) (Bottino et al., 2003). Two ligands are recognized by DNAM-1 activating receptor, namely CD155 and CD112 that are upregulated on stressed cells but can be also expressed on healthy cells (Bottino et al., 2003; Pende et al., 2005). Engagement of DNAM-1 with its ligands significantly strengthens anti-tumor NK cell cytotoxicity (Pende et al., 2005; Carlsten et al., 2007). Human DNAM-1 also engages LFA-1 (β2-integrin) (Shibuya et al., 1999).

Human NK cells express a receptor NKp80**,** which belongs to a family of C-type lectin-like receptors. It is a homodimeric type II transmembrane protein that is expressed on all NK cells in the peripheral blood. NKp80 interacts with its ligand called AICL (activation-induced C-type lectin), expressed on activated NK cells, monocytes, macrophages and granulocytes (Welte et al., 2006; Klimosch et al., 2013).

2B4 (CD244**)**, another activating NK cell receptor belongs to the SLAM (signalling lymphocytic activation molecule) family of receptors. Interestingly, 2B4 receptor has appeared to be activating in humans (Chuang et al., 2000; Mathew et al., 2005) but inhibitory in mice (Lee et al., 2004; Vaidya et al., 2006). 2B4 receptor interacts with CD48 that is expressed on all hematopoietic cells (Mathew et al., 2009). 2B4 has two functional isoforms: h2B4-A and h2B4-B, where the A form elicits a stronger cytotoxic function of NK cells compared to the B form (Mathew et al., 2009).

Except of the already above-mentioned receptors, activating murine receptors include Ly49 family – Ly49D and Ly49H that associate with ITAM-bearing adaptor DAP12 (Moretta et al., 2001; Lanier, 2005).

The NKG2 family is formed in total by seven different receptors (NKG2A, B, C, D, E, F, H). They are type II transmembrane proteins, contain a C-type lectin-like extracellular domain, a transmembrane domain and a cytoplasmic tail. As already mentioned, some members of this family belong to inhibitory receptors due to the ITIM motif in their cytoplasmic region (i.e., NKG2A/B). Except NKG2D and NKG2F, all other NKG2 members associate with CD94 by disulfide bonds (Borrego et al., 2006). The activating NKG2C receptor is found to be expressed on adaptive NK cells, and similarly to the inhibitory receptor NKG2A, recognizes HLA-E molecules (Vales-Gomez et al., 1998). In humans, NKG2C has been reported as human cytomegalovirus (HCMV) specific (Guma et al., 2004). NKG2C receptor is an equivalent to the murine receptor Ly49H that can also directly recognize the mouse cytomegalovirus antigen (Brown et al., 2001; Arase et al., 2002). One of the most significant members of this family is the NKG2D activating receptor.

3 The Natural Killer Group 2 Member D – NKG2D and NKG2D ligands

NKG2D is encoded by the *KLRK1* gene (killer cell lectin-like receptor subfamily K, member 1) on mouse chromosome 6 or human chromosome 12 (Houchins et al., 1991; Ho et al., 1998). NKG2D is characterized as a homodimeric type II membrane glycoprotein receptor constitutively expressed by most cytotoxic lymphocytes in humans, on virtually all human NK cells, all peripheral blood $CD8^+$ T, γδ T cells and some subsets of $CD4^+$ T cells (Bauer et al., 1999). NKG2D was found to be expressed by human iNKT cells (Gumperz et al., 2002) as well as by some $CD4^+CD28^-$ T cells in patients with various autoimmune diseases (Groh et al., 2003; Dai et al., 2009). NKG2D expression differs in mice and humans in some respects. In particular, naïve murine $CD8^+$T cells do not express NKG2D receptor on their surface, while upon activation, murine $CD8^+$ T cells express high levels of NKG2D (Bauer et al., 1999; Diefenbach et al., 2000). NKG2D structure consists of two β-sheets, two α-helices and four disulfide bonds (Wolan et al., 2001; Li et al., 2001).

In mice, there are two isoforms of the NKG2D receptor (NKG2D-L (long) and NKG2D-S (short)) that differ by length in 13 amino acids (Diefenbach et al., 2002; Gilfillan et al., 2002). The NKG2D-L isoform is constitutively expressed on NK cells, while resting mouse NK cells express less NKG2D-S and its expression is induced when NK cells are activated (Diefenbach et al., 2002; Rabinovich et al., 2006). Mouse $CD8^+$ T cells do not express neither of the isoforms in resting state, only after TCR stimulation and activation. NKG2D does not have a signalling motif within its intracellular domain, however, it associates with adaptor protein DAP10 and DAP12 (Gilfillan et al., 2002). NKG2D receptor requires the association with its adaptor proteins for surface expression and signal transduction. The NKG2D-L binds DAP10 and NKG2D-S is able to pair with both DAP10 and DAP12. The only isoform that is expressed by humans corresponds to NKG2D-L and is associated only with DAP10 (Bauer et al., 1999; Wu et al., 1999; Rosen et al., 2004). DAP12 possesses the ITAM motif within its structure that recruits Syk and ZAP70 tyrosine kinases (Lanier et al., 1998). In contrast, DAP10 has a YINM motif, that in turn recruits the p85 subunit of the PI3 kinase and the Vav-1 signalling complex (Wu et al., 1999; Upshaw et al., 2006).

There is a 55-60 % sequence identity between human and mouse NKG2D receptors. Interestingly, it was shown that the mouse NKG2D receptor is able to engage also human NKG2D ligands MICA and MICB (Wolan et al., 2001; Diefenbach et al., 2000). A positive signal from NKG2D can override signals delivered by inhibitory receptors to NK cells, thus resulting in the destruction of cells with normal expression of MHC class I (Bauer et al., 1999; Wu et al., 1999).

NKG2D is a primary NK cell activating receptor and acts as a co-activating or co-stimulatory receptor for T cells (Groh et al., 2001; Maasho et al., 2005) because apparently in the case of T cells, NKG2D activation is insufficient to trigger their cytotoxicity (Bauer et al., 1999; Ehrlich et al., 2005). However, in the presence of high levels of IL-15, $CD8^+$T cells can be activated via NKG2D in a TCR-independent manner (Meresse et al., 2004). NKG2D-DAP10/12 complex activates NK cell-mediated cytotoxicity upon engagement of NKG2D ligands (NKG2DL) (Diefenbach et al., 2002). Activation of NK cells by engagement of NKG2D with its ligands, triggers cytotoxicity and leads to production of cytokines (IFN-γ, TNF-α and MIP-1β (Slavuljica et al., 2011). On the other site, some cytokines modulate expression of NKG2D receptor on NK cells and $CD8^+$T cells. For example, IL-2, IL-7, IL-12 or IL-15 upregulate the NKG2D receptor (Roberts et al., 2001; Maasho et al., 2005; Park et al., 2011; Zhang et al., 2008). Others, such as TGF-β, IFNβ1 or IL-21 downregulate NKG2D (Castriconi et al., 2003; Crane et al., 2010; Muntasell et al., 2010; Burgess et al., 2006). NKG2D is a potent activating immunoreceptor that enables cytotoxic lymphocytes to recognize and destroy tumor cells. Studies on NKG2D-deficient mice showed a clear NKG2D-dependent immunoediting of tumors (Guerra et al., 2008). NKG2D deficiency resulted in a higher occurrence in malignant prostate adenocarcinomas and this deficiency accelerated a progression of Eμ-myc-induced lymphomas. Interestingly, NKG2D deficiency did not lead to a global impairment of NK cell functions *in vivo* and did not alter functional recognition by other NK receptors.

The NKG2D receptor binds to inducible ligands expressed on the surface of stressed or transformed cells. These ligands are distantly related to MHC class I proteins. Human NKG2D ligands (NKG2DL) are represented by two families, the MIC family and ULBP family (Steinle et al., 2001; Ullrich et al., 2013; Lanier, 2015). The MIC family consists of two members, the sister molecules MICA and MICB. The ULPB family comprises six proteins ULBP 1-6. MICA, MICB, ULBP4 and ULBP5 contain transmembrane domains while other human NKG2DL are GPI-anchored in the membrane. In mice, there are other NKG2DL, namely MULT-1, members of the retinoic acid early inducible 1 (Rae 1) (Rae-1 α-ε) and H60 family of glycoproteins (H60a-c) (Raulet et al., 2013) (Figure 2). MULT-1, H60a and -b are transmembrane anchored and other mouse NKG2DL are GPI-anchored (Cerwenka et al., 2000; Diefenbach et al., 2001; Carayannopoulos et al., 2002; Takada et al., 2008). All NKG2DL have α1 and α2 extracellular domains (with MICA and MICB having an additional α3 domain) with homology to MHC class I proteins, but they do not bind peptides, nor they engage with β2-microglobulin (Cosman et al., 2001; Ullrich et al., 2013; Li & Mariuzza, 2014). The NKG2DL expression is regulated by different mechanisms on transcriptional, translational and posttranslational levels (Raulet et al., 2013) and is usually attributed to cellular

stress. In the context of tumorigenesis, upregulation of NKG2DL can be mediated via DNA damage sensors and serine/threonine protein kinases (ATM (ataxia telangiectasia mutated), ATR (ATM and RAD-3 related)) that are constitutively active in cancer. DNA damage activates ATM and ATR that mediate DNA repair and cell cycle arrest (Cerboni et al., 2014; Bartkova et al., 2005). NKG2DL can be also upregulated as a result of oxidative stress and endoplasmic reticulum stress (Borchers et al., 2006; Venkataraman et al., 2007; Hosomi et al., 2018). Moreover, aberrant expression of NKG2DL was reported in inflamed tissues as well as in connection with different autoimmune disorders, such as celiac disease, diabetes, atherosclerosis or even Crohn´s disease (Guerra et al., 2013).

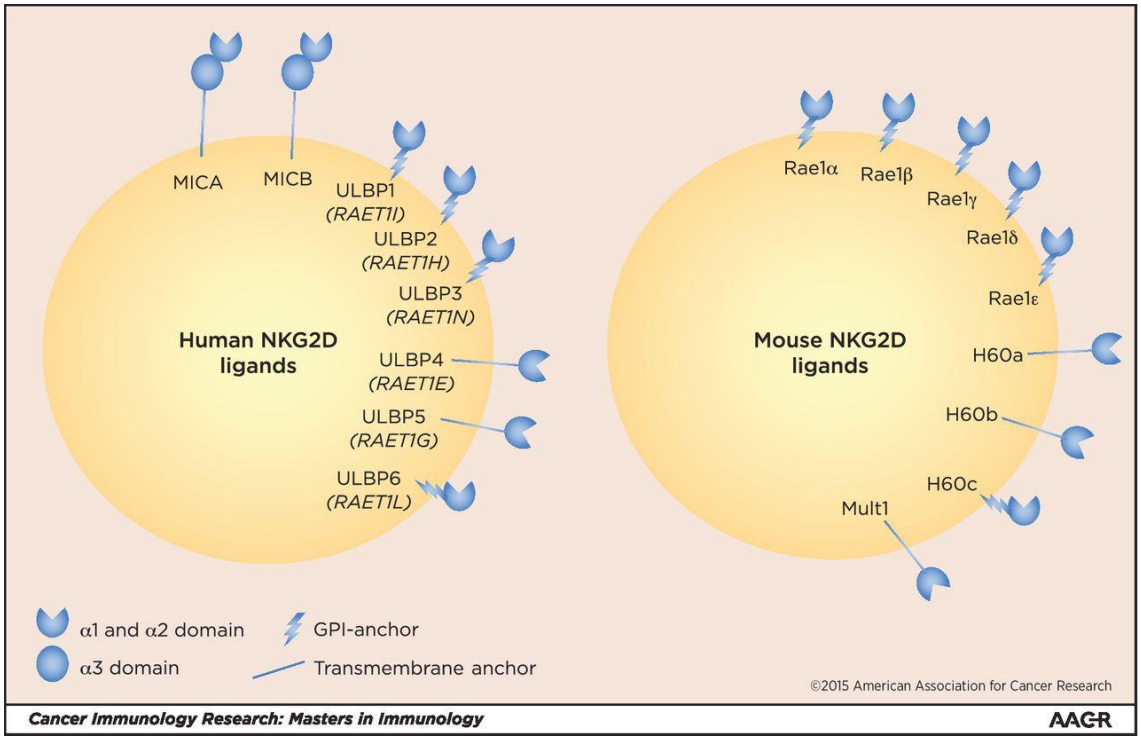

Figure 2. Human and mouse NKG2D ligands. Taken from Lanier, 2015.

4 MHC class I polypeptide–related chain A/B (MICA/B)

MICA is one of the eight human ligands for the activating NKG2D receptor which is expressed on the surface of essentially all cytotoxic lymphocytes (Li et al., 1999; Bauer et al., 1999; Groh et al., 2001).

The domain structure of MICA/B, similar to MHC class I molecules (Bahram et al., 1996), consists of α1, α2 and α3 extracellular domains, a hydrophobic transmembrane domain and a cytoplasmic tail. α1 and α2 domains of the molecule directly bind to NKG2D (Li et al., 1999; Li et al., 2001; Steinle et al., 2001). MICA/B are known to be highly polymorphic (http://hla.alleles.org/alleles/classo.html) (Li et al., 1999; Stephens, 2001). Currently, approximately 108 alleles of MICA encoding for 87 protein variants and 43 alleles of MICB encoding for 31 protein variants have been identified in humans so far (Yang et al., 2018). MICB and MICA have a sequence identity of 86% (Bahram et al., 1996). Furthermore, different MICA alleles are characteristic for triplet repeat microsatellite polymorphism (GCT) or so called short tandem repeats (STR) in their transmembrane region, encoded by exon 5. This polymorphism consists of 4-10 repetitions of GCT encoding alanine (A4,5,6,7,8,9, and 10 respectively) (Fodil et al., 1996; Mizuki et al., 1997; Ota et al., 1997; https://www.uniprot.org/uniprot/Q29983) (or 5 GCT repetitions with an additional G nucleotide insertion: A5.1) (Choy and Philips 2010). The latter polymorphism GGCT/AGCC is causing a frame shift resulting in a premature stop codon at the end of the transmembrane region. An example of such a MICA allele is MICA*008. MICA*008 is characterized by a GPI (glycosylphosphatidylinositol) anchor replacing the transmembrane domain, which is found in other MICA alleles (Ashiru et al., 2013).

Polymorphism of MICA was massively studied for its importance in cancer, e.g., cervical cancer was among the first cancer studied in association with MICA polymorphism (Chen & Gyllesten, 2014). The report of Onyeghala and colleagues associated the presence of at least one copy of the allele of MICA A5.1 with an increased risk of pancreatic cancer in patients. Additionally, these patients had elevated levels of sMICA in their serum. Several other studies reported on similar findings in cervical carcinoma (Chen et al., 2013) or hepatocellular carcinoma in the Chinese population (Jiang et al., 2012) and oral squamous cell carcinoma in a Japanese case-control study (Tamaki et al., 2008). Another study reported on overexpression of the MICA-A4 allele found in Spanish patients with hepatocellular carcinoma (HCC) and end-stage liver disease (Lopez-Vazquez et al., 2004). A great number of studies investigated the MICA polymorphism and its therapeutic potential application. Among all, MICA-129Met/Val dimorphism in the alpha2 domain (encoded by exon 2) has gained most interest. Isernhagen and colleagues studied the MICA-129Met and MICA-129Val variants for their impact on MICA

shedding and surface expression. They observed that the MICA-129Met/Val dimorphism influenced shedding of MICA. Further, their results revealed the fact that MICA-129Met was more susceptible to shedding than the MICA-129Val isoform. They speculated that the polymorphism could directly correlate with MICA surface expression intensity and thereby control the shedding of MICA (Isernhagen et al., 2016). Tong and colleagues studied MICA polymorphism in correlation with soluble MICA (sMICA) serum levels in patients with hepatitis B virus-induced HCC. Notably, this study associated significantly higher sMICA levels in serum of these patients with the MICA175Ser and MICA251Arg and microsatellite variants A4 and A9 (Tong et al., 2013). Another SNP (single nucleotide polymorphism) of MICA (rs2596542) was reported to be expressed at low levels on the surface of HCC cells in response to HCV infection which led to the progression of the disease and development towards HCC (Goto & Kato; 2014).

4.1 MICA shedding

Although MICA and MICB genes are transcribed in all cells (Venkataraman et al., 2007), expression of MICA/B proteins is highly restricted to a few tissues (mainly gastrointestinal epithelium) in healthy tissues, whereas many human tumors upregulate MICA/B expression on their cell surface (Groh et al., 1996; Groh et al., 1998; Raulet at al., 2013). Interaction of NKG2D and MICA triggers cytotoxicity toward a target cell and cytokine release of NK cells. Moreover, this interaction provides co-stimulatory function for $CD8^+$ T cells (Groh et al., 2001).

Nevertheless, tumor cells have evolved many immune escape mechanisms. One of them represents a release of soluble forms of MICA/B from the cell surface to the periphery. Consequently, these tumor cells are less well recognized by cytotoxic lymphocytes and can further proliferate.

There have been studies proposing that MICA shedding operates as a mechanism of tumor escape of NKG2D-mediated immune surveillance (Salih et al., 2002; Groh et al., 2002; Waldhauer et al., 2008; Wiemann et al., 2005). Elevated levels of sMICA/B correlated with cancer stage, metastasis and poor prognosis of patients. Soluble MICA was also proposed as an independent prognostic factor in multiple myeloma patients (Rebmann et al., 2007). Soluble MICA may impair the NKG2D/NKG2DL axis by downregulating NKG2D receptor (by endocytosis and internalization) and thereby preventing immune recognition (Groh et al., 2002). However, there is a report challenging this opinion as it was observed that mouse soluble NKG2DL MULT-1 demonstrated a protective role in tumorigenesis and promoted NK cell activity. As a result, they observed tumor rejection *in vivo*. The mechanism lies in the high affinity of sMULT-1 to NKG2D that in turn was

preventing the engagement of NKG2D with NKG2DL expressed by tumor-associated cells, such as myeloid-derived suppressor cells (MDSCs) (Deng et al., 2015).

Sheddases are membrane-bound enzymes able to induce cleavage of extracellular domains of different transmembrane proteins, producing soluble forms of these proteins. There are two families of sheddases belonging to the family of matrix metalloproteinase (MMP) or to the aspartic protease family (Lichtenthaler at al., 2018). Sheddases of MICA and MICB have been very well studied and investigated, in particular MMPs and A Disintegrin and Metalloproteinases (ADAMs).

The ADAMs are multifunctional proteins that are found among mammals and are members of zinc protease superfamily. Members of ADAM family exert important roles in many physiological processes in a cell, such as proteolytic cleavage of different receptor ectodomains and protein processing or cell signaling (Nyren-Erickson et al., 2013; Giebeler & Zigrino., 2016; Mittal et al., 2016). There are 21 members of ADAM family in humans but only 13 of them are functionally active due to a Zn-binding motif in the catalytic site. In general, the structure of ADAMs consists of the following structural elements: A signal peptide (marking the protein for its secretory pathway), a pro-domain (responsible for folding of the protein), a metalloproteinase domain (with potential proteolytic activity), a disintegrin domain (highly conserved, important for cell adhesion and binding to integrins), a cysteine-rich domain (necessary for substrate recognition and adhesion), an EGF-like domain (function unknown, not present in ADAM10 and ADAM17), a transmembrane region and a cytoplasmic tail (Murphy, 2008).

Cleavage of tumor-associated MICA from the surface of cancer cells is thought to be an important factor for tumor immune escape (Waldhauer et al., 2008). Shedding of MICA primarily depends on a proteolytic cleavage involving different enzymes. ADAMs are often upregulated by many tumor cell lines (Zocchi et al., 2012) and are known to be involved in the process of promotion of tumor growth and metastasis (reviewed in Nyren-Erickson et al., 2013). Many studies showed an involvement of different ADAMs in cancer in terms of their overexpressed levels in cancer patients (reviewed in Walkiewicz et al., 2018). Experiments with ADAM12 knockout mice showed that these mice with missing ADAM12 developed tumors at much slower rate. Their tumors had reduced growth capacity and had less lung metastases in comparison to the control mice with ADAM12 (Frohlich et al., 2011).

In 2002, Salih and colleagues described a spontaneous release of sMICA from MICA transfected cell lines which was subsequently blocked by metalloproteinases inhibitors together with a substantial increased MICA on the cell surface. This study also analyzed sMICA levels in

the patient sera with gastrointestinal carcinomas. The sera of cancer patients contained significantly higher levels of sMICA than sera of healthy donors. Correlation between elevated serum levels of sMICA and malignancy incidence led to the conclusion that MICA is released from tumor cells *in vivo*. Similar observations were observed for MICB and published later by the same group in 2006 (Salih et al., 2006). Later in 2008, Waldhauer and colleagues described metalloproteinases ADAM10 and ADAM17 as critical molecules involved in the tumor-associated proteolytic release of sMICA. By silencing RNA of ADAM10/17, they reduced sMICA levels by 50% while levels of MICA transcripts or surface expression was unaffected. This paper provided substantial evidence that sMICA comprises the entire ectodomain (α1, α2 and α3) and therefore this observation led to the conclusion of MICA proteolytic cleavage atop of the plasma membrane. Deletions in the stalk region of MICA molecule caused reduced release of sMICA but also an impairment in MICA surface expression when compared to wild type MICA. This report showed that the ADAM proteases involved in proteolytic shedding of MICA likely do not recognize a specific sequence in MICA molecule but rather seem to be susceptible to the shortening of the stalk region between alpha3 domain and the plasma membrane (Waldhauer et al., 2008). Furthermore, this paper reported on MICA cleavage occurring at the surface on tumor cells and further cleaved in the stalk region proximal to the membrane. Later, in 2009 the metalloproteinase ADAM17 was reported to be involved in the shedding of another NKG2D ligand – MICB (Boutet et al., 2009) where inhibition and knockdown of this metalloproteinase resulted in inhibition of MICB shedding. Moreover, detergent-resistant membrane microdomains (DRMs) were important sites for proteolysis of MICB. Inhibition of ADAM10 with TIMP-1 did not reduce shedding of MICB in the presence of PMA (Boutet et al., 2009). Chitadze and colleagues also studied ADAM10 and ADAM17 involvement in proteolytic cleavage of tumor-associated MICA (Chitadze et al., 2013). In this paper, the authors analyzed several human tumor cell lines including mammary, pancreatic and prostate carcinomas. Using small molecule inhibitors or siRNA treatments, they demonstrated that ADAM10 and 17 are responsible for the generation of sMICA/B. Pharmacological inhibition of these metalloproteases led to reduced levels of sMICA/B and increased expression levels of MICA on the surface of the cells. Studies using siRNA confirmed an important role of ADAM10/17 in NKG2D ligand shedding and furthermore a tumor cell-specific role of ADAM10/17 in shedding of MICA and MICB was reported. Moreover, this study showed differential roles of ADAM10 and ADAM17 where the single knockdown of these metalloproteases did not result in significant decrease of MICA shedding, however, a double knockdown led to reduced levels of sMICA in the Pand89 cell supernatant. Authors of this study suggested that both proteases are important for MICA shedding, and they can replace each other. Interestingly, downregulation of ADAM17 almost completely blocked MICB shedding

where downregulation of ADAM10 had a minor effect. In another cell line (PancTu-I) MICA shedding was mainly mediated by ADAM17, and MICB appeared to require both ADAM10 and ADAM17. The breast cancer cell line (MDA-MB-231) showed dependency on ADAM17. Altogether, it seems that shedding of MICA and MICB can be differently regulated in a given tumor cell. A report from 2009 by Kohga and colleagues revealed that ADAM10 but not ADAM17 is required for MICA shedding in human HCC cells. Upon downregulation of ADAM10, they observed increase of surface MICA on HepG2 and PLC/PRF/5 cells simultaneously with decrease of sMICA in the culture supernatants. In contrast, same experiment with knockdown of ADAM17 showed no effect on MICA surface expression or the production of sMICA (Kohga et al., 2009). Furthermore, the authors postulated that a treatment of HCC cells with commercially available chemotherapeutic drugs led to downregulation of ADAM10 expression and activity together with inhibition of MICA ectodomain shedding. On the contrary, another report showed an opposite effect of chemotherapeutic drugs with similar mechanism of action (i.e., Doxorubicin (DOX) and Melphalan) on ADAM10 expression and activation (Zingoni et al., 2015). DOX treatment of SKO-007 (J3) and U266 cell lines led to an induced release of sMICA and sMICB, while no change in ADAM17 and Erp5 was observed. The authors tested several multiple myeloma (MM) cell lines and observed similar effects. Combination therapy of chemotherapeutic drugs together with metalloproteinase inhibitors preserved MIC molecules on the cell surface. When assessing the question whether the effect of this chemotherapeutic drug was MICA allele dependent, several MICA alleles were tested including MICA*019 (representing a long form of MICA alleles) and MICA*008 which is known to be released independent from metalloproteases (Ashiru et al., 2013). In 2010, another sheddase, ADAM9, was studied in HCC cells and appeared to be involved in MICA ectodomain shedding (Kohga et al., 2010). Knockdown of ADAM9 in HepG2 and PLC/PRF/5 cells resulted in increased membrane bound MICA and decreased levels of sMICA released in their culture supernatants. They identified a potential cleavage site of ADAM9 (*in vitro*) located in the intracellular domain of MICA, more precisely at a site between Gln347 and Val348 of MICA. There were two options considered in regard to the mode of action of ADAM9 proteolytic shedding of MICA. For one, ADAM9 is able to activate other proteases to enable intracellular cleavage, or direct cleavage of MICA by ADAM9 during the process of shifting of the intracellular domain to the extracellular site via flip-flop mechanism described in other lipids (Devaux et al., 2008).

It is proposed that MICA forms a complex with a disulphide isomerase called ERp5 (endoplasmic reticulum protein 5**,** also known as protein disulfide isomerase family A, member 6, (PDIA6) a thiol isomerase)) which leads to a conformational change of the MICA molecule that

is enabling proteolytic cleavage by ADAM proteases (Kaiser et al., 2007; Waldhauer et al., 2008). MIC proteins are highly glycosylated and therefore, this can affect the overall structure of the molecule and alter the accessibility of the cleavage site. Kaiser and colleagues showen that on the surface of several tumor cell lines (A375, HeLa, U266) MICA molecule is associated with ERp5. When treating these cell lines with PAO (phenylarsine oxide), which inhibits protein disulphide isomerase function, sMICA release in the culture supernatant was reduced. This report showed that an ERp5 target site exists in the α3 domain of the MICA molecule. Knockdown of ERp5 mRNA decreased MICA tetramer binding and ERp5 surface expression, when MICA expression was not altered. Thus, this provided evidence that Erp5 function is indeed critical for MICA shedding (Kaiser et al., 2007). Wang and colleagues identified a six-amino acid motif (i.e., NGTYQT) in the α3 domain of MICA critical for the physical MICA/B – ERp5 interaction. The authors claimed that mutation of this motif prevented MICA shedding, but not MICA surface expression and did not interfere with NKG2D mediated recognition of the MICA molecule. Importantly, this motif is highly conserved among all recognized MICA and MICB alleles and therefore it was postulated that this motif was evolutionarily selected to be conserved for a specific function (Wang et al., 2009). Huergo-Zapico and colleagues reported on ERp5 and GRP78 (Glucose-regulated protein 78 kDa) expression on the surface of B cells in CLL patients and healthy donors suggesting that ERp5 and GRP78 are expressed on the surface of cells of B cell origin (Huergo-Zapico et al., 2012). ERp5 and GRP78 expression levels were significantly elevated in progressed malignomas. They also showed that inhibition of ERp5 activity in some B-cell lines or in stimulated primary leukemia cells considerably caused a decrease in sMICA shedding (Huergo-Zapico et al., 2012). ERp5 was shown to be expressed on the surface of several cancer cells which has been associated with MICA shedding (Jinushi et al., 2008). Another report suggested a metastasis-promoting activity of ERp5 (Gumireddy et al., 2007). Gumireddy and colleagues observed a link between expression of ERp5 and tumor development showing that overexpression of ERp5 promoted migration and invasion (*in vitro*) and metastasis (*in vivo*) of breast cancer cells. When BALB/cJ mice were transplanted with ERp5 overexpressing 168FARN breast cancer cells into the mammary fad pad, they developed lung metastasis after 6-8 weeks while the mice transplanted with control cells did not (Gumireddy et al., 2007).

5 Targeting NKG2D/NKG2DL for cancer immunotherapy

As outlined above, the expression of NKG2DL is strictly regulated in healthy tissues, and upon e.g., cellular stress, their expression is induced. Moreover, the NKG2D receptor substantially contributes to tumor surveillance. Hence, the NKG2D/NKG2DL axis represents an ideal candidate for development of therapeutic agents targeting either NKG2DL ligands, as they help to distinguish healthy and diseased cells, and also targeting NKG2D receptor to exploit cytotoxic potency of NKG2D and strengthen tumor surveillance. There are several approaches that are exploited to target this important axis:

1. Targeting NKG2DL on tumor cells or NKG2D receptor on cytotoxic lymphocytes to recruit them into tumors, by bispecific antibodies.

   Bispecific antibodies are usually designed with two binding sites for two different antigens. A study from 2006 developed an NKG2D ligand-antibody fusion construct (ULBP2-BB4) with the aim to recruit NKG2D expressing NK cells to human multiple myeloma (MM) cells that overexpress a tumor antigen CD138 (targeted by the BB4 antibody fragment) and is absent on other hematopoetic cells (von Strandmann et al., 2006). ULBP2-BB4 protein enhanced the NK-mediated lysis of two $CD138^+$ human MM cell lines *in vitro*. Additionally, *in vivo* combination therapy with human peripheral blood lymphocytes abrogated tumor growth of MM tumors in mice.

   Another group generated two different bispecific fusion proteins that targeted NKG2DL. They consist of the extracellular domain of NKG2D as targeting moiety fused to Fab-fragments of CD3 (NKG2D-CD3) or CD16 (NKG2D-CD16) antibodies. NKG2D-CD16 successfully activated NK cells (shown by CD69 and CD25 upregulation), resulted in degranulation (shown by CD107a expression) and IFN-γ production and subsequent lysis of acute myeloid leukaemia (AML) cell lines and patient AML cells. Both NKG2D-CD16 and NKG2D-CD3 induced granzyme B and perforin secretion of peripheral blood mononuclear cells (PBMCs) from healthy patients. Both of the fusion proteins NKG2D-CD16 and NKG2D-CD3 showed a profound capacity to stimulate NK cells and T cells, respectively (Märklin et al., 2019). Raynaud and colleagues developed a bispecific anti-NKG2DxHER2 antibody that engage HER2 on tumor cells and NKG2D on NK cells. This antibody elicited cytotoxicity of unstimulated NK in a tumor-specific manner (Raynaud et al., 2020).

2. Administration of various cytokines to enhance NKG2D expression by NK cells.

   Various cytokines can positively modulate the expression of NKG2D on the surface and this was proposed as another strategy in antitumor therapy (Ghasemi et al., 2016;

Banerjee et al., 2021; Easom et al., 2018; Konjević et al., 2010). One of the examples is the cytokine IL-2. IL-2 is known as a crucial cytokine used in cancer therapy because it has the ability to enhance the NKG2D expression on NK cells and thereby enhances NK cell-mediated cytotoxicity in patients with different malignant diseases (Rosenberg, 2014). Administration of cytokines IL-2 and TNF-α is able to significantly induce upregulation of NKG2D expression on NK cells, especially on the cytotoxic $CD16^{bright}$ NK cell subset (Konjević et al., 2010). However, administration of IL-2 can lead to severe systemic side effects in patients, that include vascular leak syndrome, hypotension, fever or organ necrosis due to activation of the vascular endothelium (Rosenberg., 2014; Cotran et al., 1988; Lotze et al., 1985). Moreover, IL-2 causes an expansion of immunosuppressive regulatory T cells (T_{regs}) that have a negative impact on anti-tumor immune response (Cesana et al., 2006). To prevent all of these negative side effects of IL-2 treatment, another group generated and tested a recombinant fusion protein comprising of a cowpox virus encoding NKG2D binding protein (OMCP) and a mutated form of IL-2 with poor affinity for IL-2Rα. IL-2Rα expression on T_{regs} and on vascular endothelium is responsible for the above-mentioned life-threatening complications in patients. OCMP did not cause IL-2 associated toxicity and showed high efficacy in mouse tumor models (Ghasemi et al., 2016). In 2021, the same group showed that their NKG2D-retargeted IL-2 (called OMCPmutIL-2) expanded tumor-infiltrating lymphocytes and provided tumor control (Banerjee et al., 2021).

3. <u>Targeting tumor associated NKG2DL to enhance their expression.</u>

   Enhanced NKG2DL expression on cancer cells has been shown to promote tumor susceptibility to NK cell-mediated immunosurveillance in clinical practice (Krieg et al., 2012; Zingoni et al., 2017). There are numerous chemotherapeutic drugs currently used for cancer treatment that show the ability to increase MICA on the surface of various cancer cells. For example, cisplatin that is used to treat patients with ovarian, testicular cancer or head and neck cancer (Brown et al., 2019) upregulated expression of MICA on tumor cells (Okita et al., 2016; Okita et al., 2019). As a result, NKG2D-mediated cytotoxicity of NK cells is enhanced (Okita et al., 2016). Histone deacetylase inhibitors (HDACi) displayed their potential to increase MICA expression on the surface of tumor cells (Yamanegi et al., 2010; Goto et al., 2016), even to increase NKG2D expression by NK cells *in vitro* (Zhu et al., 2015). There are other agents that were able to enhance cytotoxicity mediated by NKG2D on NK cells by upregulation of MICA and MICB ligands on cancer cells. Romidepsin significantly induced NK cell-mediated cytotoxicity against acute lymphoblastic leukemia and non-Hodgkin lymphoma *in vivo* and *in vitro* (Satwani

et al., 2014). Bortezomib (proteasome inhibitor) and ionizing radiation increased expression of MICB and ULBP1 on MM cells (Lee et al., 2018).

4. Targeting tumor associated NKG2DL to inhibit their shedding.

   Since the release of soluble NKG2DL (sNKG2DL) appears to be a major mechanism of tumors to escape immune recognition by cytotoxic lymphocytes (Waldhauer & Steinle, 2008; Ullrich et al., 2013), targeting shedding of tumor ligands MICA and MICB by monoclonal antibodies appears to be a very promising strategy for tumor therapy. Sera of cancer patients contain elevated levels of sNKG2DL MICA/B compared to healthy patients´ sera and it is associated with disease progression and shorter overall survival (Salih et al., 2002; Holdenrieder et al., 2006 a; Holdenrieder et al., 2006 b). Therefore, strategy to block sNKG2DL shedding and thereby strengthening NKG2D/NKG2DL axis seems to be an attractive immunotherapy approach. Recently, Wucherpfennig and colleagues established the antibody 7C6 which inhibits MICA/B cleavage from tumor cells. This monoclonal antibody was able to preserve the expression of MICA/B on tumor cells and thereby boost NKG2D-dependent activation of NK cell cells. Later, the same group showed that antibody-mediated MICA shedding inhibition promoted macrophage-driven immunity against acute myeloid leukemia (Ferrari de Andrade et al., 2018; Ferrari de Andrade et al. 2020; Alves da Silva et al., 2022). Another antibody preventing MICA/B shedding, CLN-619, entered a clinical trial phase I for the therapy in patients with advanced solid tumors. CLN-619 is administered either as a monotherapy or in combination with PD-1 inhibitor pembrolizumab (ClinicalTrials.gov, Identifier: NCT05117476). Preclinical studies in BALB/c SCID mice bearing human lung cancer xenograft cells demonstrated a potent anti-tumor activity of CLN-619 antibody as a result of an enhanced interaction of MICA with NKG2D (Whalen et al., 2022). Our group also generated a monoclonal antibody, BAMO3, that inhibits MICA/B shedding from tumor cells and it differs from 7C6 with regard to some details that are discussed in this thesis in later chapters. Therapeutic administration of BAMO3 leads to tumor control and improves survival of tumor-bearing immunocompetent MICAgen mice. Overall, these data provide evidence in support of antibody-mediated MICA/B shedding inhibition as a potential immunotherapy tool for malignant diseases.

5. Targeting tumor-associated NKG2DL MICA with toxin-conjugated antibodies to inhibit tumor growth.

   The increasing global incidence of cancer each year represents a major challenge to scientists and clinicians. Global cancer statistics have shown that in 2020 there were about 18.1 million cancer cases in the world. Despite a tremendous success of many

treatments to cure various type of cancer in patients, there are still patients who do not respond to them. Therefore, it is necessary to develop new therapeutics to help treating patients who failed to respond to other treatments. One of the treatment options are antibody drug conjugates (ADCs), which have gained more and more attention as a therapy option in recent years and are currently tested in many clinical trials (Tolcher et al., 2020). ADCs combine the specificity of a monoclonal antibody with the toxicity of a conjugated drug. One of the advantages that ADCs offer is the specific targeting of the cytotoxic agent to tumor cells while minimizing toxicity against healthy tissues and thereby allowing a maximal anti-cancer potency. Bléry and colleagues reported on a novel MICA antibody conjugated to a toxin payload PBD (pyrrolobenzodiazepine). This antibody conjugate MICAB1-ADC demonstrated an optimal tumor control in several solid tumor models *in vivo*, including patient-derived xenografts and carcinogen-induced tumors in MICAgen transgenic mice (Bléry et al., 2021). This thesis also shows the therapeutical efficacy of the MICA-ADC in MICAgen mice against various aggressive MICA-expressing murine tumor models and further details are elaborated in the results chapter.

6. NKG2D-CAR cells.

CAR or chimeric antigen receptor is defined as a recombinant synthetic receptor for antigens with potency to alter the specificity of cytotoxic cells, most commonly T cells but also NK cells, to recognize and eliminate target cancer cells. NK cells and T cells recombinantly expressing CAR are then targeted and triggered by cells expressing a specific tumor antigen that is recognized by the portion of CAR (usually a single chain variable fragment of a murine or human antibody (scFv)) (Sterner & Sterner, 2021). CARs consist of four main components: an extracellular antigen-binding domain, a hinge region, a transmembrane domain and intracellular signalling domain(s) (Zhang et al., 2017). NKG2D-based CARs usually contain the NKG2D ectodomain and the intracellular signalling domain almost always consists of the CD3ζ signalling moiety that is fused to one or more co-stimulatory domains (Weinkove et al., 2019; Lazarova et al., 2020).

Hence, such NKG2D-CAR T/NK cells are directed towards NKG2DL expressing tumor cells and this interaction leads to a signalling cascade to finally eliminate the target cells. Safety of NKG2D-based CAR T cells in patients with acute myeloid leukemia/myelodysplastic syndrome or relapsed/refractory multiple myeloma was also shown previously in a clinical trial phase I (Baumeister et al., 2019). Currently, a number of clinical trials harnessing NKG2D as a CAR are ongoing (*clinicaltrials.gov*). As of May 2023, there are 11 trials using NKG2D-CAR T cells, one trial investigates NKG2D-CAR γδ

T cells, and 7 trials are using NKG2D-CAR NK cells (one of them for COVID-19 patients). It is therefore clear that NKG2D CARs have gained an increased attention for utilization in clinical practice. Several groups reported on NKG2D CAR-T cells and showed their ability to recognize NKG2DL on tumor cells and increase production of proinflammatory cytokines (Sentman & Meehan, 2014). A combination therapy of bispecific antibody against NKG2D and tumor-associated antigen HER2, and NKG2D-based CAR T and NK cells showed their synergistic effect and successfully enhanced NKG2D-mediated cytotoxicity *in vivo* in a murine glioblastoma model (Zhang et al., 2021). Autologous NKG2D-CAR NK cells reportedly displayed safety and potent anti-myeloma activity *in vitro* and *in vivo* (Leivas et al., 2021).

Considerable efforts are being made to develop and clinically test NKG2D-based CARs to improve outcome of malignant diseases in patients as employing the NKG2D axis for therapeutic benefit is an exciting immunotherapy strategy (Curio et al., 2021).

6 Material and methods

6.1 Materials

6.1.1 Devices

Name	Company
BD FACS Canto II	BD Biosciences
CASY TT Cellcounter	OLS OMNI Life Sciences
Fusion SL image acquisition system	Vilber Lourmat
Gene Pulser Xcell electroporation system	Bio-Rad
Multiskan™ FC Microplate Photometer	Thermo Scientific

6.1.2 Primary antibodies

FACS: Flow cytometry, WB: Western Blot, IP: Immunoprecipitation. All listed laboratory-made antibodies were generated in the laboratory of Prof. Alexander Steinle.

Specificity	Clone	Conjugate	Isotype (species)	Method	Origin
α-MICA	AMO1	-	IgG1 (mouse)	FACS: 10 µg/ml ELISA: 5 µg/ml (coating Ab)	Laboratory-made
	AMO1	Biotin	IgG1 (mouse)	FACS: 10 µg/ml	Laboratory-made
	AMO1	AlexaFluor647	IgG1 (mouse)	FACS: 1:150	Laboratory-made
α-MICB	BMO2	-	IgG1 (mouse)	FACS: 10 µg/ml ELISA: 5 µg/ml (coating Ab)	Laboratory-made
	BMO2	Biotin	IgG1 (mouse)	ELISA: 1 µg/ml (capture Ab)	Laboratory-made
α-MICA/B	BAMO1	-	IgG1 (mouse)	FACS: 10 µg/ml ELISA: 5 µg/ml (capture Ab) WB: 2.5 µg/ml	Laboratory-made
	BAMO1	Biotin	IgG1 (mouse)	FACS: 10 µg/ml ELISA: 1 µg/ml	Laboratory-made

	BAMO3	-	IgG2a (mouse)	FACS: 10 µg/ml ELISA: 1 µg/ml *In vivo*: 10 µg/ml *In vitro*: 0.1 – 30 µg/ml	Laboratory-made
	BAMO3	Biotin	IgG2a (mouse)	FACS: 10 µg/ml ELISA: 1 µg/ml	Laboratory-made
	6D4	-	IgG2a, kappa, (mouse)	IP: 2 µg/ml	Invitrogen, 14-5788-82
α β-Actin	AC-15	HRP	IgG1 (mouse)	WB: 1:10000	Sigma-Aldrich A5441
α -ADAM10	139712	-	IgG2a (rat)	WB: 1:400	R & D, MAB946
α -ADAM10	139712	PE	IgG (rat)	FACS: 1:25	R & D, FAB946P
α – human ERp5/PDIA6	polyclonal	-	Rabbit	WB: 1:1000	LS Bio, LS-C97795
CD3e	145-2C11	PE/Cy7	Armenian Hamster IgG	FACS: 1:100	BioLegend, 100320
CD3e	145-2C11	AlexaFluor647	Armenian Hamster IgG	FACS: 1:100	BioLegend, 100322
CD4	GK1.5	AlexaFluor647	Rat IgG2b	FACS: 1:100	BioLegend, 100424
CD8	53-6.7	APC/Cy7	Rat IgG2a	FACS: 1:100	BioLegend, 100714
CD11b	M1/70	Pe/Cy7	Rat / IgG2b	FACS: 1:800	Invitrogen, 25-0112-82
CD19	6D5	APC/Cy7	Rat IgG2a	FACS: 1:200	BioLegend, 115530
CD31	MEC13.3	APC	Rat IgG2a	FACS: 1:100	Biolegend, 102510
CD39	Duha59	APC	Rat IgG2a k	FACS: 1:100	BioLegend, 143810
CD45	104	PerCP	IgG2a	FACS: 1:100	BioLegend, 109826
CD103	2E7	PE	Armenian Hamster IgG	FACS: 1:100	BioLegend, 121406
CD274 (PD-L1)	10F.9G2	PE	Rat IgG2b k	FACS 1:100	BioLegend, 124308
CD279 (PD-1)	29F.1A12	BrilliantViolet421	Rat IgG2a	FACS: 1:800	BioLegend, 135218
CD314 (NKG2D)	CX5	BrilliantViolet421	Rat IgG1	FACS: 1:100	BD Biosciences, 562800

CD335 (NKp46)	29A1.4	FITC	Rat IgG2a	FACS: 1:100	BioLegend, 137606
Gr1	RB6-8C5	PE	Rat IgG2b	FACS: 1:100	BioLegend, 108408
TCRγδ	GL3	PE	Armenian Hamster IgG	FACS: 1:100	BioLegend 118108

6.1.3 Fluorescent stains

FACS: flow cytometry.

Specificity	Method	Origin
DAPI (4',6-diamidino-2-phenylindole)	FACS: 1:300	AppliChem (Darmstadt, DE), A1001,0010
eBioscience™ Fixable Viability Dye eFluor™ 506	FACS: 1:1000	Thermo Fisher Scientific, 65-0866-14

6.1.4 Isotype control antibodies

Specificity	Clone	Conjugate	Method	Origin
Rat IgG1, k	R3-34	BrilliantViolet421	FACS: 1:100	BD Biosciences , 562868
Mouse IgG1	-	Biotin	FACS: 10 µg/ml	Laboratory-made
Mouse IgG2a	-	-	FACS: 10 µg/ml *In vitro*: 0.1 – 30 µg/ml *In vivo*: 10 µg/ml	Laboratory-made

6.1.5 Secondary antibodies

Specificity	Species	Conjugate	Method	Origin
Streptavidin	-	BrilliantViolet421	FACS: 1:200	Biolegend, 405225
	-	PE	FACS: 1:200	Jackson Immunoresearch, 016-110-084
	-	HRP	WB: 1: 10000	Jackson Immunoresearch, 016-030-084
Mouse IgG	Goat	PE	FACS: 1:200	Jackson Immunoresearch, 115-115-164
	Goat	HRP	WB: 1:10000	Jackson Immunoresearch, 115-035-003
Rabbit IgG	Goat	HRP	WB: 1:10000	Scientific Research Antibody, AS014
Rat IgG	Goat	HRP	WB: 1:10000	Jackson Immunoresearch, 112-035-003

6.1.6 Buffers, media and SDS-gel

Name	**Composition**
2X YT medium	Trypton 16 g/L Yeast Extraxt 10 g/L NaCl 5 g/L in millipore H_2O
50 x TAE buffer	Tris-Base 2 M EDTA 0,05 M Acetic acid 5,7 % v/v in millipore H_2O
Blocking solution for Western blot	Non-fat dry milk 5 % w/v in TBS-T buffer
ELISA washing buffer	1 x PBS Tween-20 0,05 v/v
FACS Buffer	FCS 2 % v/v EDTA 2 mM NaN3 0,01 % v/v 1 x PBS
IP buffer (7.2 pH at RT)	Tris 25 mM NaCl 150 mM in millipore H_2O
LB agar	LB medium 25 g/L Agar for bacteriology 15 g/L in millipore H_2O
LB medium	25 g/L in millipore H_2O If needed, these antibiotics were added 100 µg/ml Ampicillin 50 µg/ml Kanamycin 100 µg/ml Zeocin
Loading buffer for Western blot (Laemmli)	Tris (pH 6,8) 62,5 mM Glycerol-solution 5 % v/v SDS 1 % w/v Bromophenol blue 0,0025% w/v in millipore H_2O
Loading buffer Orange G	Glycerol 30 % v/v Orange G 0,25 w/v in 1 x TAE buffer
Non-reducing loading buffer for Western blot (Laemmli)	100 µl Millipore H_2O 400 µl Loading buffer
NP-40 Protein lysis buffer (pH 8 at RT)	Tris-HCl 50 mM NaCl 150 mM NP-40 1 % v/v in millipore H_2O
10 X PBS	95,5 g/L in millipore H_2O
Polyacrylamide separation gel	1.5 M Tris pH 8.6 (HCL)

	SDS 10% v/v Acrylamid 40% v/v APS 10% v/v TEMED 0,05 % v/v in millipore H_2O
Polyacrylamide stacking gel 4.5%	1 M Tris pH 6.8 (HCL) SDS 10% v/v Acrylamid 40% v/v APS 10% v/v TEMED 0,05 % v/v in millipore H_2O
Reducing loading buffer for Western blot (Laemmli)	100 µl β-Mercaptoethanol 400 µl Loading buffer
SDS running buffer	Tris-base 25 mM Glycin 192 mM SDS 0,1 % v/v in millipore H_2O
SOB medium	26,64 g/L in millipore H_2O
TBS-T buffer	NaCl 150 mM Tris-Base 10 mM Tween-20 0,05% v/v in millipore H_2O
Western blot transfer buffer	Tris-base 25 mM Glycin 192 mM Methanol 20 % v/v in millipore H_2O

6.1.7 Cell culture media composition

Cells	**Name**	**Supplements**
293 F	FreeStyle™ F17 Expression Medium	L-Glutamine 1%
293 T (HEK) **B16F10** **B16F10 transfected** **A375**	DMEM (Dulbecco's Modified Eagle's Medium)	FBS 10% Penicillin/Streptomycin 1% L-Glutamine 1% Sodium pyruvate 1% For transfected cells added 1 mg/ml G418
B16F10 MICA*001 transduced **MC38-MICA*004**	DMEM (Dulbecco's Modified Eagle's Medium)	FBS 10% Penicillin/Streptomycin 1% L-Glutamine 1% Sodium pyruvate 1% Non-essential amino acid solution (100x) 1%
C1R **C1R transfected**	RPMI (Roswell Park Memorial Institute 1640 Medium)	FBS 10% Penicillin/Streptomycin 1% L-Glutamine 1%

RMA **RMA transfected**		Sodium pyruvate 1% For transfected cells added 1 mg/ml G418
COS7	IMDM (Iscove's Modified Dulbecco's Medium)	FBS 10% Penicillin/Streptomycin 1% L-Glutamine 1% Sodium pyruvate 1%
NKL	RPMI (Roswell Park Memorial Institute 1640 Medium)	FBS 10% Penicillin/Streptomycin 1% L-Glutamine 1% Sodium pyruvate 1% 10 % Horse serum and IL-2 (200 U/ml)

B16F10 MICA*001 and MC38-MICA*004 transductants were kindly provided by Innate Pharma, France.

6.1.8 Supplements for cell culture media

Name	**Origin**
Fetal Bovine Serum	Sigma-Aldrich, 7524
G418	NeoFroxx, 1150GR010
Horse serum	Sigma-Aldrich, H1138
IL-2 (Proleukin S)	Miltenyi Biotec, 130-097-743
L-glutamine solution (200 mM)	Sigma-Aldrich, G7513
MEM Non-Essential Amino Acids (100x)	Sigma-Aldrich, M7145
Penicillin/Streptomycin (100X)	Sigma-Aldrich, P0781
Sodium Pyruvate (100 mM)	Sigma-Aldrich, S8636

6.1.9 Reagents

Name	**Origin**
1 kb Plus DNA marker	New England Biolabs, N0469S
10x DNase Buffer	Promega, M198A
50 bp DNA marker	Fermentas, SM0373
Albumin Fraktion V min. 98%, protease free (BSA)	Carl Roth, T844.3
Applifect	Applichem, A8886,0001,
Batimastat (BB94)	Sigma-Aldrich, SML-0041-5MG
BD Pharm Lyse Lysisg buffer	BD Biosciences, 555899
Cell Dissociation Buffer, enzyme-free, PBS	Life Technologies, 13151014
Complete Protease Inhibitor	Roche, 4693116
Corning® Matrigel® Basement Membrane Matrix, 5ml vial	Corning, 356234
DNase	Promega, M610A
DNase stop solution	Promega, M199A
dNTPs (10 mM)	Thermo Fisher Scientific, R0181
Endoglycosidase H	New England BioLabs, P0702S
EZ-Link® Sulfo - NHS-LC-LC-Biotin	Thermo Fisher Scientific, 21338

Ficoll Paque Plus	GE Healthcare, 17-1440-02
HRP-juice PLUS	PJK, 103 15
Ionomycin	LC Laboratories, I-6800
Lipofectamine® LTX Reagent	Invitrogen, P/N 94754
M-MLV 5X Reaction Buffer	Promega, M1705
M-MLV Reverse Transcriptase	Promega, M1705
PageRulerTM Prestained Protein Ladder	Thermo Fisher Scientific, 26616
peqGOLD TriFast ™	Peqlab, 30-2010
Phorbol 12-myristate 13-acetate (PMA),	Sigma-Aldrich, P8139
Phusion-Polymerase	New England BioLabs, F630L
Pierce™ Protein A/G UltraLink™ Resin	Thermo Fisher Scientific, 53132
Plus ™ Reagent	Invitrogen, P/N 10964-040
PNGaseF	New England BioLabs, P0704S
Polyethylenimine, Linear, MW 25000, Transfection Grade (PEI 25K™)	Polysciences, 23966-1
Protease Inhibitor Cocktail (cOmpleteTM)	Roche, 4693116001
Quickload 2-log marker	New England Biolabs, N3200S
Quickload 50 bp marker	New England Biolabs, N0473S
Random Primer (500 ng/µl)	Promega, C1181
ReBlot Plus Mild Solution	Merck Millipore, 2502
Recombinant RNasin ® Ribonuclease Inhibitor	Promega, N2511
Roti-Nanoquant 5x	Carl Roth, K880.1
Shrimp Alkaline Phosphatase (rSAP)	Biolabs, MO371S
SOB medium powder	Carl Roth, AE27.1
Taq-Polymerase	New England Biolabs, M0267L
TEMED (100 ml),	Carl Roth, 2367.1
TMB Microwell Peroxidase Substrate System	KPL (SeraCare), 5120-0047 (50-76-00)
Triton X-114	AppliChem, A3848,0500
Trypsin-EDTA solution	Sigma-Aldrich, T3924
Ultra Comp eBeads	Invitrogen, 01-2222-42
UltraPure ™ Distilled Water DNase/RNase-free	Invitrogen, 10977-035

6.1.10 Kits

Name	**Origin**
CytoTox 96 ® Non-Radioactive Cytotoxicity Assay	Promega, G1780
EZ-PCR-Mycoplasma Test Kit	BioFroxx, 20-700-20
Mouse IgG Library set	ProGen, F-2010
NucleoSpin Plasmid Easy Pure kit	Macherey Nagel, 740727.250
Plasmid Maxi Kit	Qiagen, 12163
QIAquick Gel Extraction Kit	Qiagen, 28706
ToxinSensor™ Chromogenic LAL Endotoxin Assay Kit	GenScript, L00350

6.1.11 Restriction endonucleases and buffers

For all restriction endonucleases CutSmart buffer was used (New England Biolabs, B7204).

Name	**Origin**
AdhI	New England Biolabs, R0584S
BamHI-HF	New England Biolabs, R3136S
EcoRV-HF	New England Biolabs, R3195S
NheI-HF	New England Biolabs, R3131S
ScaI-HF	New England Biolabs, R3122 S

6.1.12 Bacteria used for transformation

Name	**Origin**
Escherichia Coli Top10	Thermo Fisher Scientific, C404003
Escherichia Coli XL1-Blue	Agilent Technologies, 200236

6.1.13 Oligonucleotides

All oligonucleotides used in this thesis were purchased from Sigma-Aldrich. fw=forward, rv=reverse

Primer name	**Sequence**
1. MICA frag1 fw	GCATGCAGACTGCCTGCAGGAACTACGGCGATATCTAAAATC CGGCGTAGTCCTG
2. MICA frag1 M1 rv	GGCGCCCGCTGCGGCCGCACTGCGGGCGACAGCCACCGCG GGGGGCACTGTTCTCCTCAGGACTACGCCGGATTTTAG
3. MICA frag2 M1 fw	CAGTGCGGCCGCAGCGGGCGCCATTACCGTGACATGCAGGG CTTC
4. MICA frag2 rv	CTCATCAATGTATCTTATCATGTCTGGCCAGCTAGCACCTAATG GTGGTGATGATGGTGTTC
5. MICA frag1 M2 rv	GCCCAGGGATAGAAGCCAGCAGCCGCGCATGCCACGGTAAT GTTGCCCTCTGAG
6. MICA frag2 M2 fw	GCTGGCTTCTATCCCTGGGCTATCGCACTGAGCTGGCGTCAG GATGGGG
7. MICA frag1 M3 rv	GGCGGCGGCCAAAGCTACCCCAGCCGCAGCCCAGCTCAGTG TGATATTCCA
8. MICA frag2 M3 fw	GGGGTAGCTTTGGCCGCCGCCACCCAGCAGTGGGGGGATGT CCTGCCT
9. MICA frag1 M4 rv	AGCCCCAGCAGGCAGGACAGCCCCCCACTGCGCGGTGTCGT GGCTCAAAGATAC
10. MICA frag2 M4 fw	CTGTCCTGCCTGCTGGGGCTGGAACCTACCAGACCTGGGTG GCCACC
11. MICA frag1 M5 rv	GGCAATCGCGGTGGCCACCCAGGTCTGGT
12. MICA frag2 M5 fw	CCTGGGTGGCCACCGCGATTGCCCAAGGAGAGGAGCAGAG GTTC

13. MICA frag1 M6 rv	AGCGCTGGCAGCCCCGCTGTGTGCCATGTAGCAGGTGAACG CCGCCTCCGCTCCTGCGCAAATCCTGGTGGCCACCCA
14. MICA frag2 M6 fw	ACAGCGGGGCTGCCAGCGCTCACCCTGTGCCCTCTGGGAAA GTGCTG
15. MICA frag1 M3-1 rv	CCCAGCCGCAGCCCAGCTCAGTGTGATATTCCAGGGATAGAA GCCAGA
16. MICA frag2 M3-1 fw	CTGAGCTGGGCTGCGGCTGGGGTATCTTTGAGCCACGACAC CCAGCAG
17. MICA frag1 M3-2 rv	GGCGGCGGCCAAAGCTACCCCATCCTGACGCCAGCTCAGTG TGATATTCCA
18. MICA frag2 M3-2 fw	GGGGTAGCTTTGGCCGCCGCCACCCAGCAGTGGGGGGATGT CCTG
19. MICA frag1 M6-1 rv	CGCCGCCTCCGCTCCTGCGCAAATCCTGGTGGCCACCCAGGT CTG
20. MICA frag2 M6-1 fw	TGCGCAGGAGCGGAGGCGGCGTTCACCTGCTACATGGAACA CAGC
21. MICA frag1 M6-2 rv	AGCGCTGGCAGCCCCGCTGTGTGCCATGTAGCAGGTGAACC TCTGCTCCTC
22. MICA frag2 M6-2 fw	GCACACAGCGGGGCTGCCAGCGCTCACCCTGTGCCCTCTGG GAAAGTGCTG
23. MICA frag1 M7 rv	CGCGGTGGCCACCCAGGTCTGGTAGGTTCCAGCCCCATCAG GCAGGACATCCCCCCA
24. MICA frag2 M7 fw	CAGACCTGGGTGGCCACCGCGATTTGCCAAGGAGAGGAGC AG
25. MICA frag2 M3-2 fw	GTAGCTTTGGCCGCCGCCACCCAGCAGTGGGGGGATGTCCT G
26. MICA frag2 M3-2 fw	ACCCAGCAGTGGGGGGATGTCCTG
27. MICA frag1 M3-1.1 rv	CCCATCCTGAGCCCAGCTCAGTGTGATATTCCAGGGATA
28. MICA frag2 M3-1.1 fw	CTGAGCTGGGCTCAGGATGGGGTATCTTTGAGCCACGACAC C
29. MICA frag1 M3-1.2 rv	CCCATCCGCACGCCAGCTCAGTGTGATATTCCAGGGATA
30. MICA frag2 M3-1.2 fw	CTGAGCTGGCGTGCGGATGGGGTATCTTTGAGCCACGACAC CCAG
31. MICA frag1 M3-1.3 rv	CCCAGCCTGACGCCAGCTCAGTGTGATATTCCAGGGATA
32. MICA frag2 M3-1.1 fw	CTGAGCTGGCGTCAGGCTGGGGTATCTTTGAGCCACGACAC CCAG
33. MICA frag1 M6-1.1 rv	CCTCTGCTCCTCTCCTGCGCAAATCCTGGTGGCCACCCAGGT
34. MICA frag2 M6-1.1 fw	TGCGCAGGAGAGGAGCAGAGGTTCACCTGCTACATGGAACA C
35. MICA frag1 M6-1.2 rv	CCTCTGCTCCGCTCCTTGGCAAATCCTGGTGGCCACCCAGGT
36. MICA frag2 M6-1.2 fw	TGCCAAGGAGCGGAGCAGAGGTTCACCTGCTACATGGAACA C
37. MICA frag1 M6-1.3 rv	CCTCGCCTCCTCTCCTTGGCAAATCCTGGTGGCCACCCAGGT
38. MICA frag2 M6-1.3 fw	TGCCAAGGAGAGGAGGCGAGGTTCACCTGCTACATGGAACA C

39. MICA frag1 M6-1.4 rv	CGCCTGCTCCTCTCCTTGGCAAATCCTGGTGGCCACCCAGGT
40. MICA frag2 M6-1.4 fw	TGCCAAGGAGAGGAGCAGGCGTTCACCTGCTACATGGAACAC
41. MICA frag2 rv	CAATGTATCTTATCATGTCTGGATCCTAGGCGCCCTCAGTGGAGCCAGTG
42. MICA frag1 fused M rv	GGTGTCGTGGCTCAAAGATACCCCAGCCTGACGCCAGCTCAGTGTGATATTCCA
43. MICA rv	GCTGTGTTCCATGTAGCAGGTGAACCTCGCCTCCTCTCCTTGGCAAATCCTGGTGGCCAC
44. RSV MICA07 C250A frag1 rv	CCTCTGCTCCTCTCCTTGTGCAATCCTGGTGGCCACCCAGGTC
45. RSV MICA07 C250A frag2 fw	CCAGGATTGCACAAGGAGAGGAGCAGAGGTTCACCTGCTACATGGAACAC
46. RSV MICA07 C250S frag1 rv	GAACCTCTGCTCCTCTCCTTGGCTAATCCTGGTGGCCACCCAGGTCTG
47. RSV MICA07 C250S frag2 fw	CCAGGATTAGCCAAGGAGAGGAGCAGAGGTTCACCTGCTACATGGAACAC
48. RSV MICB frag1 fw	ATGCAGGCAGACTGCCTGCAGAAACTACAGCGATATCTGAAATCCGGGGTGGCC
49. RSV MICB frag2 rv	CTGGCCGCCTGGCTGTAGAGTCTAGGCGCCCTCAGTGGAACCAGTG
50. RSV MICA 6aa to A frag1 rv	CCTGGTGGCCACCCAAGCCGCTGCGGCACCAGCCCCATCAGGCAG
51. RSV MICA 6aa to A frag2 fw	GCGGCTTGGGTGGCCACCAGGATTTGCCAAGGAGAGGAGCAGAGG
54. RSV MICB C190S frag1 rv	GGTGATGTTGCCCTCTGAGACCTCGCTGCTGGTGAC
55. RSV MICB C190S frag2 fw	AGCAGCGAGGTCTCAGAGGGCAACATCACCGTGACATGCAGGGCTTCCAG
56. RSV MICB C190A frag1 rv	GCCCTCTGAGACCTCGCTTGCGGTGAC
57. RSV MICB C190A frag2 fw	GCAAGCGAGGTCTCAGAGGGCAACATCACCGTGACATGCAGG
58. RSV MICA 6aa frag1 rv	GGCCACCCAGGTCTGGTAGGTTCCATTCCCATC
59. RSV MICA 6aa frag2 fw	ACCTACCAGACCTGGGTGGCCACCAGGATTTGCCAAGGAGAGGAG
60. RSV MICA07 M3-1 6Ala reps rv	GAAAATAATAATAACAAAAATAGCAGCAGCAGCAGCAGCAACAGCAGAAACATGG
61. RSV MICA07 M3-1 6Ala reps fw	GCTGCTGCTGCTGCTGCTATTTTTGTTATTATTATTTTCTATGTCCGTTGTTGTAAG
62. RSV MICA07 M6-1 6Ala reps rv	GAAAATAATAATAACAAAAATAGCAGCAGCAGCAGCAGCAACAGCAGAAACATGG
63. RSV MICA07 M6-1 6Ala reps fw	CTGCTGCTGCTGCTATTTTTGTTATTATTATTTTCTATGTCCGTTGTTGTAAGAAGAAAACATC
64. RSV MICA07 9Ala reps rv	GAAAATAATAATAACAAAAATAGCAGCAGCAGCAGCAGCAGCAGCAACAGCAGAAACATG
65. RSV MICA07 9Ala reps fw	GCTGCTGCTGCTGCTGCTGCTGCTATTTTTGTTATTATTATTTTCTATGTCCGTTGTTGTAAG

68. RSV MICA08 C250A rv	CCTCTGCTCCTCTCCTCGTGCAATCCTGGTGGC
69. RSV MICA08 C250A fw	GATTGCACGAGGAGAGGAGCAGAGGTTCACCTGCTACATGGAACAC
70. RSV MICA08 fw	CTGCAGGAACTACGGCGATATCTAGAATCCGGCGTAGTC
71. RSV MICA08 rv	CAATGTATCTTATCATGTCTGGATCCTACAACAACGGACATAG
72. RSV MICA08 Fused M F1 rv	CGTGGCTCAAAGATACCCCAGCCTGACGCCAGGTC
73. RSV MICA08 Fused M F2 fw	GTCAGGCTGGGGTATCTTTGAGCCACGACACCCAGCAGTGGGGGGATGTC
74. RSV MICA08 Fused M F2 rv	CATGTAGCAGGTGAACCTAGCCTCCTCTCC
75. RSV MICA08 Fused M F3 fw	GAGGCTAGGTTCACCTGCTACATGGAACACAGCGGGAATCACAGCACT
76. RSV MICA08 C250S rv	CTCCTCTCCTCGCGAAATCCTGGTGGC
77. RSV MICA08 C250S fw	GGATTTCGCGAGGAGAGGAGCAGAGGTTCACCTGCTACATG
78. RSV MIC SalI fw	TGGGCTGCAGGTCGACGCGGCATGGGGCTGGGCCCGGTCTTCCTG
79. RSV MIC A375 fw	ATGGGGCTGGGCCCGGTCTTCCTGCTTCTG
80. RSV MIC A375 rv	CTAGGCGCCCTCAGTGGAGCCAGTGGACCC
83. RSV vector fw	CGCCATTTGACCATTCACCAC
84. RSV vector rv	GCATTCTAGTTGTGGTTTGTCC

6.1.14 Expression vectors

pFUSE vector (InvivoGen, San, Diego, CA, USA).

RSV.5 neo vector (previously kindly provided by Thomas Spies. Originally constructed by Long et al., 1991. *Hum.Immunology*. Aug; 31(4):229-35.).

6.2 Methods

6.2.1 Mice

MICA transgenic mice (MICAgen mice) were generated as previously described (Kim et al, 2020). Shortly, MICAgen mice harbour a 23.4 kb genomic fragment comprising the entire human MICA*007 gene. MICAgen mice have been continuously backcrossed with C57BL/6J mice for more than 20 years at Zentrale Forschungseinrichtung (local animal facility University Hospital Frankfurt am Main, Germany). All animals were maintained under specific pathogen-free conditions. Animal experiments were approved by the local authorities (Regierungspräsidium Darmstadt, Germany) and performed in full compliance with the respective national guidelines.

6.2.2 Animal experiments

MICAgen transgenic mice were used for all mouse experiments in this thesis. Before each experiment, inoculated cells were analysed for MICA surface expression by flow cytometry and were also tested for mycoplasma. Endotoxins from laboratory-produced BAMO3 and IgG2a were removed by Triton assay and tested for endotoxin with LAL assay.

6.2.3 BAMO3 therapeutic delivery

3 x 10^4 RMA-MICA*007 cells (in matrigel 1:1) were inoculated subcutaneously into the right flank of MICAgen mice. Subsequently, mice were monitored for tumor growth and body weight every two days. When the tumors reached a defined threshold size of 6 mm, antibodies BAMO3 and IgG2a control were administered intravenously (caudal vein), two times per week over the total period of 3 weeks. When the tumor size reached 14 mm, mice were sacrificed by heart puncture and tumors were harvested for further FACS analysis. Heart puncture was performed in animals anesthetized with Ketamine/Xylazine (intraperitoneal administration). Blood collected by heart puncture was used to isolate mouse serum. The animal experiment was repeated two times. BAMO3 and IgG2a control were produced in the laboratory of Prof. Alexander Steinle.

6.2.4 19E9-PBD and 19E9-PBD in combination with PD-1 therapeutic delivery

1 x10^4 B16F10-MICA*001 cells, 3 x10^4 RMA-MICA*007 cells or 1 x10^5 MC38-MICA*004 cells (in matrigel 1:1), respectively, were inoculated subcutaneously into the right flank of MICAgen mice. Subsequently, mice were monitored for tumor growth and body weight every two days. When the tumors reached a defined threshold size of 6 mm (day 11 or 12), therapeutic antibodies were administered intravenously (caudal vein). Treatment dosages are listed in the Table 1-3 and Figure 32. When tumor size reached 14 mm, mice were sacrificed by heart puncture and tumors and tumor-draining lymph nodes were harvested for further FACS analysis. Heart puncture was performed in animals anesthetized with Ketamine/Xylazine (intraperitoneal administration). Blood collected by heart puncture was used to isolate mouse serum. Each of these animal experiments were performed once. The experimental antibodies, B16F10-MICA*001 and MC38-MICA*004 transduced cells were kindly provided by Innate Pharma, France.

6.2.5 Triton endotoxin removal assay and LAL endotoxin assay

Before the animal experiment, removal of endotoxin from mAb BAMO3 and IgG2a was performed by phase separation using Triton-114 (according to Aida et al., 1990). Shortly, an antibody solution was treated with Triton-114 (1 % v/v) and incubated on ice for 15 minutes. The solution was then warmed to 37°C for 15 minutes. Upon the incubation step and centrifugation

step at 13000 rpm for 1 minute at 37°C, two phases were formed. The upper endotoxin-free phase was removed and transferred to a new clean 1,5 ml tube. The solution was then filtered using a 0.2 µm filter. ToxinSensor™ Chromogenic LAL Endotoxin Assay confirmed endotoxin removal.

6.2.6 Cells

Cells were cultured in the appropriate media, passaged 2-3 times per week, and regularly tested for mycoplasma. Cells were kept in an incubator under following conditions: 37°C and 5% CO2. All cells and their culture media used in this thesis are listed in the Chapter 6.1.7.

6.2.7 Flow cytometry

Cells were stained in a 96-well plate. Approximately 2 x 10^5 cells per well were washed twice with FACS buffer (PBS, 2% FCS, 2 mM EDTA, 0.01 % sodium azide) and stained with primary antibody or conjugated antibody at a concentration either recommended by a manufacturer or determined in our laboratory by titration. Cells were incubated for 30 minutes at 4°C in dark. After first antibody staining, cells were washed 3 times with FACS buffer. Cells were stained with a secondary antibody for 20 minutes at 4°C in dark. Following secondary staining, cells were washed twice with FACS buffer. Centrifugation between washing steps was performed with 1600 rpm for 3 minutes at 4°C. Flow cytometry analyses were performed using a FACS Canto II and data analysed using FlowJo (Tree Star, Ashland, OH). The specific fluorescence intensity (SFI) was calculated by subtracting out the median fluorescence intensity (MFI) of the isotype control staining from the MFI of the antibody staining of interest.

6.2.8 Isolation of tumor cells and tumor-infiltrating lymphocytes (TILs)

Freshly isolated tumors and tumor draining lymph nodes were washed in ice-cold PBS. Single – cell suspensions were obtained by passing the minced tissue through a 40 µm cell strainer. TILs were enriched from the tumor cell suspension by gradient centrifugation using Ficoll-Paque Plus. After washing step with ice - cold PBS, TIL and tumor cells were resuspended in ice-cold FACS buffer. Cells were subsequently stained and analysed by flow cytometry in a 96-well plate.

6.2.9 Isolation of mouse splenocytes

Spleen was stored shortly in cold PBS from the time of harvest until the start of the experiment. To obtain a single-cell suspension, the spleen was homogenized by pushing through a 40-µm cell strainer using a syringe plunger. The strainer was washed with cold PBS and this step was repeated twice. Subsequently, the splenocytes were centrifuged (482 g for 10 min at

4°C) and incubated with BD Pharm Lyse Buffer for 3 minutes at room temperature (RT). BD Pharm Lyse Buffer was diluted in sterile cell culture grade water in ratio 1:10. Cell suspension was run through a 40-µm cell strainer before being washed with PBS and centrifuged again (482 g for 10 min at 4°C). The supernatant was discarded and the splenocytes were resuspended in an appropriate volume of FACS buffer.

6.2.10 Isolation of mouse serum

Mouse blood samples were collected by cardiac puncture and transferred in a capillary blood tube (Microvette®500 K3 EDTA) at RT. Subsequently, the tubes were centrifuged (2000 g for 5 min at RT) and the upper phase (serum) was collected in a 1,5 ml microtube. Serum was used for ELISA for detection of sMICA levels.

6.2.11 Sandwich ELISA

Concentration of soluble MICA/B (sMICA/B) in cell culture supernatants or mice sera were determined by modifications of a previously reported MICA/B specific sandwich-ELISA (Salih et al., 2002; Salih et al., 2003; Welte et al., 2003). The MICA-specific mAb AMO1 (5 µg/ml) or the MICB-specific mAb BMO2 (5 µg/ml) was immobilized to ELISA plate (High Binding, F, Sarstedt), and incubated overnight at 4°C. Next day, following the blocking step with loading 15% BSA in PBS, plates were washed five times with ELISA washing buffer (PBS, 0.05 % Tween 20). Cell culture supernatants and mice sera were diluted at appropriate dilution rates prior adding to the plate. After incubation at 37°C for 1 hour, the plate was washed again five times and the capture antibody was loaded – bound sMICA or sMICB was detected by biotinylated anti MICA/B mAb BAMO1 or BAMO3 (1 µg/ml), respectively, followed by horseradish peroxidase (HRP) – conjugated streptavidin (1:4000). The plate was washed six times before adding TMB Peroxidase substrate (KLP, Gaithersburg, MD). HRP activity was stopped by adding 1 M phosphoric acid. The absorbance was measured at 450 nm on a Multiskan™ FC Microplate Photometer.

6.2.12 Immunoblotting

Cells were counted and washed with PBS before being lysed with lysis buffer (NP-40 lysis buffer (50 mM Tris–HCl pH 8.0, 150 mM NaCl, and 1% NP-40) containing the Complete Protease Inhibitor Cocktail) for 30 minutes on ice. When necessary, samples were subjected to PNGaseF or Endoglycosidase H digestion according to the manufacturer's instructions. SDS loading buffer containing β-Mercaptoethanol was used for reducing conditions and SDS loading buffer without β-Mercaptoethanol for non-reducing conditions for 5 minutes at 95°C. Cellular lysates were fractionated by sodium dodecyl sulfate-polyacrylamide gel electrophoresis (SDS-PAGE) in a Mini-PROTEAN Tetra Cell (Bio-Rad, Munich, Germany). Proteins were transferred to polyvinylidene

difluoride (PVDF) membranes by semi-dry blotting. Membranes were blocked in 5% milk powder dissolved in TBST (containing 0,05% Tween-20) overnight at 4°C. Membranes were subsequently incubated in primary antibody prepared in 5% milk and incubated at RT for 1 hour, followed by membrane washing with TBST. Membrane was incubated with secondary antibody, prepared in 5% milk, for 1 hour at RT and after washing, the membrane was developed by HRP-juice PLUS. Membranes were stripped with ReBlot Plus Mild Antibody Stripping Solution.

6.2.13 Co-immunoprecipitation

To assess the physical interaction between MICA mutations and ERp5 or ADAM10, B16F10 cells were counted and washed with ice-cold PBS followed by surface biotinylation (EZ-Link Sulfo - NHS-LC-LC-Biotin) for 30 minutes at 4°C. Then, the cells were lysed in 1% NP-40 buffer (containing Complete Protease Inhibitors (Roche). Cell lysates were incubated with anti-MICA/B antibody 6D4 overnight at 4°C. Next day, Ultralink immobilized protein A/G plus beads were added and incubated for 2 hours at RT. This mixture was then washed with IP buffer (25 mM Tris, 150 mM NaCl, pH 7.2). For elution of the immune complex, the samples were incubated with SDS Laemmli buffer (reducing or non-reducing) for 5 minutes at 95°C and the supernatant collected after centrifugation. The sample was then analyzed by SDS PAGE as described above. The PVDF membrane was incubated with HRP-Streptavidin, BAMO1, and ERp5 antibody, respectively. Secondary antibodies were goat anti-mouse-HRP or goat anti-rabbit-HRP, respectively. To distinguish ERp5 and MICA by molecular mass, we did not digest the protein sample with PNGase F.

6.2.14 RNA extraction, Dnase digestion and cDNA synthesis

RNA was isolated from frozen cells. Thawed cells were centrifuged (400 g for 3 min at RT) and washed twice with PBS. The pellet was subsequently resuspended in peqGOLD TriFast and incubated for 3 minutes at RT. After the incubation step, chloroform was added to the mixture until homogenized and incubated additional 3 minutes at RT. After centrifugation (12000 rpm for 15 minutes at 4°C), the upper aqueous phase was transferred to a 1, 5 ml tube. Isopropanol was added and the solution was incubated for 10 minutes at RT. After centrifugation (12000 rpm for 10 minutes at 4°C), the RNA pellet was washed with 75 % ethanol. The tube was centrifuged again (7500 rpm for 5 minutes at 4°C), the supernatant was discarded, and pellet was left to air-dry. The dry pellet was resuspended in RNA-free water (30-50 µl). RNA concentration was measured by a nanophotometer. The RNA was stored at – 80°C before use. To obtain pure RNA, DNA digestion is required. For DNA digestion, 1µg of RNA was incubated with DNase buffer and DNase for 30-45 minutes at 37°C. Subsequently, DNase stop solution was added and the mixture was incubated for 5 minutes at 65°C and quickly placed on ice for cooling. The obtained pure

RNA was afterwards used for cDNA synthesis. To the pure RNA were added these following reagents: dNTPs (10 mM), random primers (100 ng/ml) and RNase free water. In case of the amplification of the MICA cDNA from A375 cells, the MICA-specific primers were used. This mixture was incubated for 5 minutes at 65°C and subsequently immediately placed on ice. The 5x M-MLV-Buffer and RNasin (40 U/µl) were added and incubated for 2 minutes at RT. The sample was placed on ice afterwards. The cDNA was synthesized as follows:

Priming	25°C	10 min
Synthesis	42°C	50 min
Reverse Transcriptase inactivation	70°C	15 min
Store	4°C	hold

cDNA was stored at -20°C until further use.

6.2.15 Cloning

All kits and enzymes were used according to the manufacturer's protocols. The primers used for polymerase chain reaction (PCR) are listed in the Chapter 6.1.14. Plasmids were shipped out to be sequenced in SeqLab, Göttingen, Germany.

6.2.16 Generation of inserts and overlap extension PCR cloning

Inserts were generated by PCR using Phusion DNA polymerase. Primers were designed in Clone Manager 9 and purchased from Sigma-Aldrich. The correct PCR products were subsequently detected and verified by agarose gel electrophoresis where the bands with correct size were excised and purified using QIAquick gel extraction kit. These PCR products were then used for a subsequent PCR where two fragments of the desired inserts were fused together. The primers for two fragments of the desired insert were designed in a way that would create an overlap of approximately 20-25 base pairs between forward and reverse primer of two fragments. After this PCR step, the above-mentioned steps of gel-electrophoresis and gel extraction and purification were performed again. Fused fragments were used in an overlap extension PCR (according to Bryksin and Matsumura, 2010). The insert was PCR-amplified with the chimeric primers so that the PCR product has overlapping regions of approximately 20-25 base pairs with the vector. Overlap PCR products were directly used for transformation in *E.coli*.

6.2.17 Bacterial transformation in *E.coli*

100 µl of chemically competent bacteria were thawed on ice until the last ice crystals disappeared. Then, 50 µl of cells were gently mixed with 5 µl of purified plasmid DNA (overlap PCR products) and incubated on ice for 30 minutes. After heat shock at 42°C for exactly 30 seconds, the sample was incubated on ice for 5 minutes. 250 µl of SOB medium (RT) was subsequently added to the sample and placed for incubation at 37°C for 60 minutes. Following this step, the sample was spread on the LB plates supplemented with the appropriate antibiotics. The plates were incubated at 37°C overnight. The grown single-cell colonies of bacteria were harvested and used for inoculation of liquid cultures in LB medium or 2X YT medium supplemented with appropriate antibiotics. The liquid cultures were cultured at 37°C while shaking vigorously (250rpm) for at least 5-6 hours. After the incubation, plasmid DNA was isolated by NucleoSpin Plasmid Easy Pure kit according to the manufacturer´s protocol. Before stable transfection in eukaryotic cells, plasmid DNA was isolated from larger cultures of 500 ml by Plasmid Maxi kit according to manufacturer´s protocol.

6.2.18 Vector digestion and de-phosphorylation

Vectors of interest were digested with the appropriate restriction enzymes in order to linearize the plasmid before stable transfection in eukaryotic cells. Verification of the digestion was done by agarose gel electrophoresis and subsequent excision and purification with QIAquick gel extraction kit.

6.2.19 Plasmid DNA purification

Plasmid DNA isolated by the plasmid Maxi kit was stored at -20°C. Before purification it was digested and de-phosphorylated. These steps were followed by purification before stable transfection was performed. 3M Sodium Acetate was added to the plasmid DNA together with 100 % Ethanol. This mixture was incubated at -20°C for 60 minutes or alternatively at – 80°C for 30 minutes. Samples were subsequently centrifuged at 15 000 rpm for 15 minutes at 4°C and the DNA pellet was washed with 70 % Ethanol (stored at -20°C). After centrifugation step (15 000 rpm for 15 minutes at 4°C), the pellet was air dried and resuspended in appropriate volume of RNase free water.

6.2.20 Transient transfection with PEI

293 F cells (0.5 x 10^6 /ml) were cultured in a 6-well plate one day prior to the transfection. For transfection 1 µg of plasmid DNA was mixed with 3 µg of PEI in 100 µl of cell culture medium (without supplements). The transfection mixture was then incubated at RT for 15-30 minutes

before it was pipetted directly to the cells in 6-well plate. Cells and their supernatant were analysed after 24-96 hours of incubation.

6.2.21 Transient transfection with Applifect

COS7 cells (0.5 x 10^6 /well) were cultured in a 6-well plate one day prior to the transfection. 2 µg of plasmid DNA were added to 100 µl of culture medium (without supplements). 6 µl of Applifect was mixed in another 1,5 ml tube with 100 µl of culture medium (without supplements). These mixtures were incubated for 5 minutes at RT. After the incubation, the two solutions were combined and incubated again for 25 minutes at RT. The transfection mixture was then subsequently pipetted to the cells. COS7 cells and the supernatant were analysed after 24-48 hours.

6.2.22 Stable transfection with Lipofectamine

B16F10 cells (1x10^5 cells) were cultured in a 24-well plate one day prior to the transfection. On the day of the transfection, 500 ng of plasmid DNA was added in 100 µl of culture medium (without supplements) and mixed gently. Subsequently, 0.5 µl of PLUS™ Reagent was added to the diluted DNA and incubated for 10 minutes at RT. Lipofectamine LTX Reagent (1.25 µl) was added directly to the same tube, followed by 30-minute incubation at RT. The transfection mixture was then pipetted to the cells. The cells were incubated for 24 hours before they were passaged at an 1:10 ratio. The antibiotic G418 was added one day after passaging. First clones started to appear after 21 days. These clones were tested for expression of the desired surface protein by flow cytometry.

6.2.23 Stable transfection by electroporation

RMA and C1R cells were stably transfected by electroporation. Cells were washed twice with PBS before being counted. 15-18 µg of plasmid DNA (diluted in 20 µl of medium without supplements) was added to 4 x 10^6 RMA cells or 1 x 10^7 C1R cells (in 500 µl of medium without supplements) that were placed in a 4 mm cuvette. The cuvette with the mixture of cells and plasmid DNA was pulsed (250V and 950 µF) in Gene Pulser Xcell electroporation system, incubated for 10 minutes at RT before cells were cultured in a 6-well plate, and incubated for additional 48 hours at 37°C. After 48-hour incubation, G418 was added to the cells. 36 hours later (for RMA cells) or 96 hours later (for C1R cells) the cells were transferred to a 96-well plate (U-bottom) and cultured for approximately 3 weeks before first cell clones appeared and were tested for surface expression of a desired protein by flow cytometry.

6.2.24 Cytotoxicity assay

Cytotoxicity assay was performed with CytoTox 96 ® Non-Radioactive Cytotoxicity Assay kit according to the protocol of the manufacturer. Briefly, effector (E) human NKL cells were cultured with target (T) cells in E:T ratio 8:1, 4:1 and 2:1 in a 96-well plate (U-bottom) for 4 hours. LDH-release was measured by Multiskan™ FC Microplate Photometer at 450 nm. Equation used to determine % cytotoxicity:

$$\%\ cytotoxicity = \frac{\text{Experimental} - \text{Effector spontaneous} - \text{Target spontaneous}}{\text{Target maximum} - \text{Target spontaneous}}\ x\ 100$$

6.2.25 BAMO3 shedding inhibition *in vitro*

1 x 10^6 cells were seeded in a 6-well plate in 1 ml of culture medium with all necessary supplements. BAMO3 or IgG2a control were added to the designated wells at concentrations ranging from 0.1 µg/ml to 30 µg/ml. Broad-spectrum metalloprotease inhibitor BB94 (Batimastat) was used as a control (5µM). After 24 hour-incubation at 37°C and 5% CO_2, the cells and supernatants were harvested and analysed for MICA expression (by flow cytometry) and soluble MICA concentration (by ELISA), respectively.

6.2.26 Shedding induction with PMA and Ionimycin *in vitro*

1 x 10^6 cells were seeded in a 6-well plate in 1 ml of culture medium with all necessary supplements. PMA (100 ng/ml) and ionomycin (2µM) were added to the designated wells. Broad-spectrum metalloprotease inhibitor BB94 was used as a control (5µM). After 2 hours of incubation at 37°C and 5% CO2, the cells and supernatants were harvested and analysed for MICA expression (by flow cytometry) and soluble MICA concentration (by ELISA), respectively.

6.2.27 Statistical analysis

Average tumor volume of MICAgen mice was assessed using Two-way ANOVA + Sidak's multiple comparisons test. Statistical significance for differences in tumor growth rate was assessed with One-way ANOVA. Unpaired t-test was used elsewhere and indicated in the figure descriptions. Statistical significance for differences in survival was assessed using Log-rank (Mantel-Cox) test. *P < 0.05; **P < 0.01; ***P < 0.001; ****P < 0.0001. GraphPad Prism 7.0 was used for all statistical analyses.

7 Results

7.1 BAMO3 inhibits proteolytic shedding of MICA by tumor cells in a dose-dependent and cell-specific manner.

Previously, several studies have demonstrated that the NKG2D-ligand MICA is released from the surface of tumor cells via proteolytic shedding by ADAM metalloproteases, thereby compromising NKG2D-mediated elimination of cancer cells (Salih et al., 2002, Waldhauer et al., 2008, Kaiser et al., 2007, Liu et al., 2010). Moreover, other studies showed obstruction of the NKG2D-NKG2D ligand interaction on cytotoxic lymphocytes due to tumor-derived sMICA chronic binding (Groh et al., 2002; Raffghello et al., 2004; Luo et al., 2020). Therefore, preventing MICA proteolytic shedding from tumor cells appears to be a meaningful strategy to inhibit tumor growth by strengthening the MICA - NKG2D interaction and thereby enabling anti-tumor immune responses mediated by NKG2D-expressing cytotoxic lymphocytes. Several clinical trials attempted to treat cancer patients by administering of broad-spectrum metalloprotease inhibitors to block action of metalloproteases such as MMPs or ADAMs. However, these attempts were unsuccessful due to severe side effects on patient's health and well-being or lack of efficacy of these agents (Sparano et al., 2004; Manello et al., 2005; Goffin et al., 2005). The reason of such cytotoxic effects of these inhibitors lies in the fact that metalloproteinases are involved in many biological processes in humans (embryonic development, cell-cell interaction, signalling...etc) under physiological conditions (Giebeler & Zingrino, 2016). Hence, there is an urging need to develop alternative ways of cancer treatment that lead to MICA shedding inhibition from tumors.

Our findings show that BAMO3 inhibits shedding of MICA from several mouse and human cell lines *in vitro* (Figure 3-4). With increasing concentration of BAMO3 added to the MICA-expressing cells, we observed substantial decrease of soluble MICA. Already at very low concentrations (0.1 µg/ml – 1 µg/ml) BAMO3 mAb efficaciously inhibits MICA shedding, while MICA shedding was almost entirely blocked in the presence of 10 µg/ml BAMO3. With regard to the MICA and MICB expression on the cell surface after BAMO3 treatment, different results were observed across different cell types. In case of some cells, such as B16F10-MICA*007 and RMA-MICA*007 cells (after BAMO3 treatment), no significant increase in MICA surface expression was detectable using mAb AMO1 as compared to the control treatment (Figure 3). However, some cells (such as A375, C1R-MICB*002 and B16F10-MICB*002) showed higher MICA/B expression after BAMO3 treatment when compared to IgG2a treatment (Figure 3 E-H and Figure 4 B).

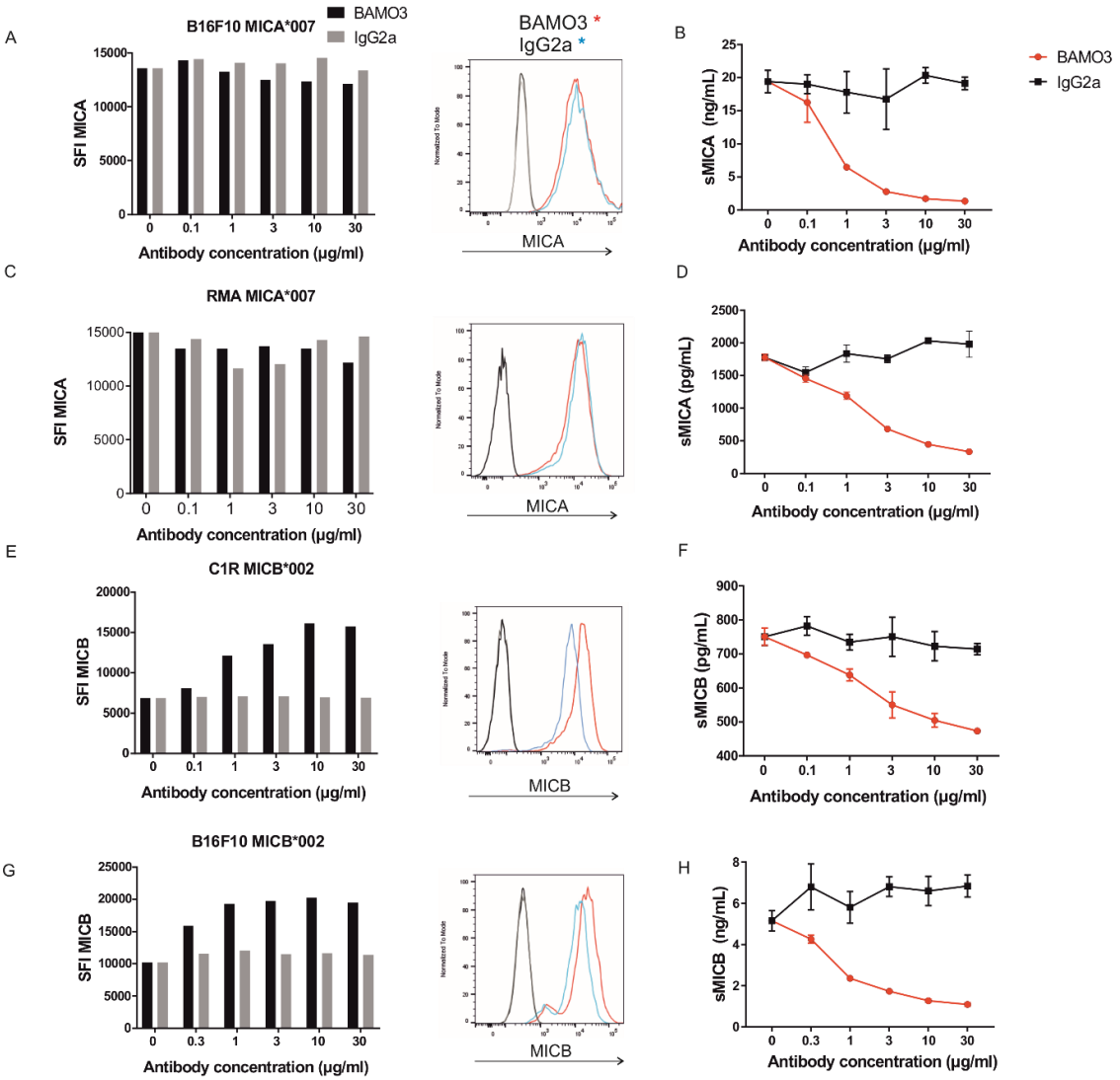

Figure 3. BAMO3 treatment inhibits MICA/B shedding and variously affects surface MICA and MICB expression. B16F10-MICA07 cells (A-B), RMA-MICA*007 cells (C-D), C1R-MICB*002 cells (E-F) and B16F10-MICB*002 (G-H) were treated with BAMO3 mAb or an IgG2a control. After 24 hours, surface MICA/B expression (in SFI) and levels of soluble MICA/B (sMICA/B) and were determined by flow cytometry and ELISA, respectively. SFI= specific fluorescence intensity.

Next, the aim was to investigate further the cause behind the observation that MICA surface expression is differentially affected upon BAMO3-mediated MICA shedding inhibition. First, the question was whether the increase of surface MICA/B expression after BAMO3 treatment depends on the cell type. For this, the human melanoma cell line A375 was treated with BAMO3 and IgG2a and tested for shedding inhibition of MICA and MICB and their surface expression on A375 cells. As shown in Figure 4 A, A375 cells express on their surface both MICA and MICB using MICA and MICB-specific monoclonal antibodies AMO1 and BMO2, respectively. After 24-hour incubation with BAMO3 mAb, a substantial increase of MICA and also MICB expression was observed on the surface of A375 cells as well as shedding inhibition of MICA and

MICB (Figure 4 B-C). In summary, MICA/B-specific mAb BAMO3 efficiently inhibits proteolytic shedding of MICA and MICB in a dose-dependent manner among many cancer cell lines and its effect on MICA/B surface expression depends on the type of cells.

The second raised question was whether the increase in MICA on the surface of A375 depends on the type of MICA allele. The MICA cDNA from the A375 cell line was cloned and transfected into the mouse melanoma B16F10 cells using Lipofectamine and into the human lymphoma C1R cells via electroporation. After successful stable transfection, these cells were subjected to BAMO3 treatment and analysed for surface MICA expression as well as MICA shedding inhibition. Strikingly, a considerable increase of MICA expression after BAMO3 treatment was observed on the surface of human C1R cells but not on mouse B16F10 cells (Figure 5). Therefore, this phenomenon depends on the respective cells rather than on the type of MICA allele.

Apparently, tumors escape from an NKG2D-mediated cancer immunosurveillance by sabotaging the NKG2D/NKG2DL system in various ways. A prevalent escape mechanism constitutes the proteolytic shedding of NKG2DL by tumor cells through metalloproteases as reported by previous studies for the human NKG2DL MICA/B that are broadly expressed by various tumors, but not by the corresponding non-malignant tissues (Groh et al., 1998). Hence, inhibition of NKG2DL-MICA/B shedding by BAMO3 may represent a promising novel immunotherapeutic approach for treating human cancer.

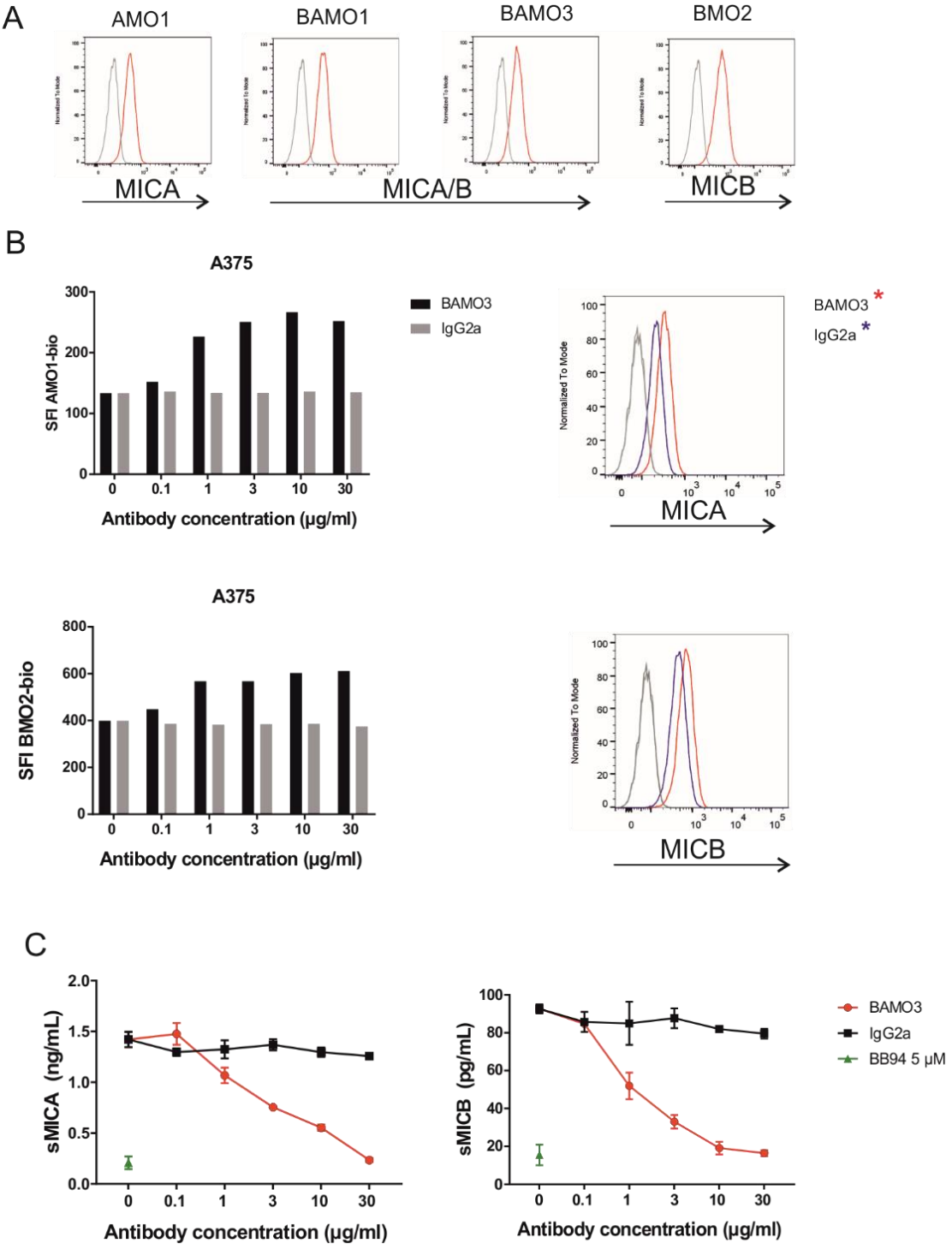

Figure 4. BAMO3 treatment increased MICA and MICB expression on the A375 human melanoma cell line *in vitro.* A.) MICA and MICB expression on A375 cells. AMO1 is anti-MICA mAb, BAMO1 and BAMO3 are MICA/B specific, BMO2 is anti-MICB mAb. B.) Surface expression of MICA and MICB on A375 cells after BAMO3 treatment. 24-hour incubation. Surface expression was determined with flow cytometry. SFI= Specific fluorescence intensity C.) Levels of soluble MICA (sMICA) shed from A375 cells after BAMO3 treatment. 24-hour incubation. sMICA levels were determined with ELISA. BB94= metalloprotease inhibitor. Samples diluted 1:5. Coating antibody. AMO1 (5 µg/mL), Capture antibody BAMO1-bio (1 µg/mL), Secondary antibody SA-HRP (1:4000). For MICB ELISA: coating antibody BAMO1 (5 µg/mL), samples undiluted, Capture antibody BMO2-bio (1 µg/mL), Secondary antibody SA-HRP (1:4000).

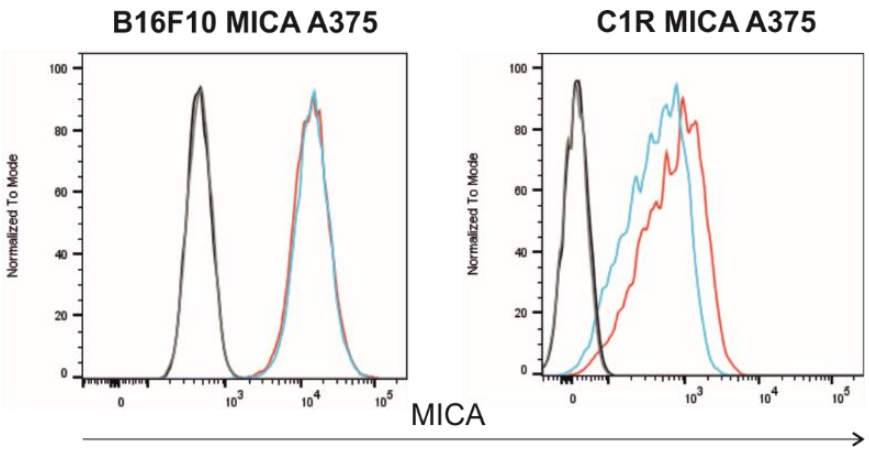

Figure 5. BAMO3 treatment increased MICA expression on C1R MICA A375 cells but not on B16F10 MICA A375. B16F10 MICA A375 (left) and C1R MICA A375 (right) cells were treated with BAMO3 and IgG2a. After 24-hour incubation MICA surface expression was determined by flow cytometry. Red coloured histograms represent BAMO3 treated sample (30 µg/mL), blue coloured histograms represent IgG2a treated sample (30 µg/mL). Gray and black color indicate isotype control used for flow cytometry staining.

7.2 Epitope mapping of monoclonal antibody BAMO3

The MICA/B-specific monoclonal antibody (mAb) BAMO3 is a mouse IgG2a antibody that was generated in this laboratory previously. Briefly, BAMO3 mAb was raised by immunizing BALB/c mice with a mixture of P815-MICA*001, P815-MICA*004, and P815-MICB*001 transfectants. Screening of supernatants of splenic hybridoma cells with MIC-transfectants led to the identification of the BAMO3-producing hybridoma. BAMO3 mAb was purified by affinity chromatography on a protein A-Sepharose column and shown to bind to both MICA and MICB. The Ig-like α3 domain of MICA (see Figure 6) and MICB was described as an epitope for mAb BAMO3 using hybrids of various NKG2D ligands tested for BAMO3 binding (Salih et al., 2002). However, the exact epitope of BAMO3 binding to MICA was not defined.

Therefore, this thesis aimed to map the epitope of BAMO3 to concrete amino acids that are critical for binding of the mAb BAMO3 to MICA and MICB glycoproteins. For this purpose, amino acids pointing out of the structure of α3 MICA domain were selected as potential binding sites for mAb BAMO3. Crystal structure of MICA (Li et al., 2001) is publicly available in the database Uniprot (https://www.uniprot.org) (Figure 6).

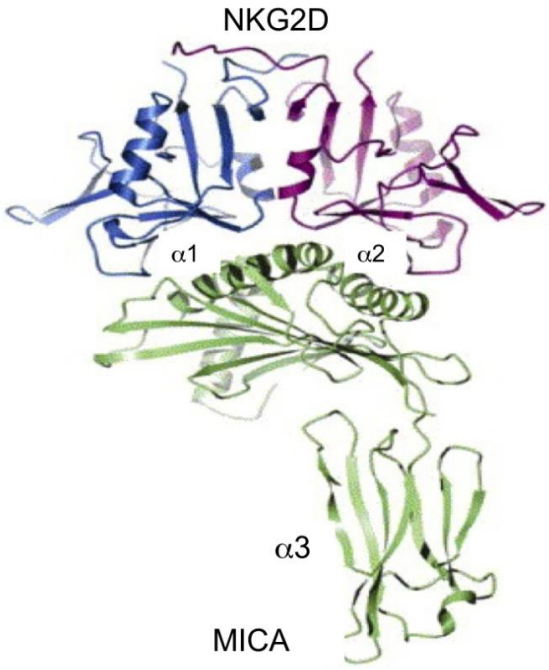

Figure 6. Crystal structure of the MICA/NKG2D complex (Li et al., 2001). The MICA structure consists of three domains: the MHC class-I like α1α2 superdomain where the NKG2D receptor binds and the membrane-proximal α3 domain (green) (taken from uniprot.org).

MICA*007 mutants with a stretch of amino acids (Figure 7 - Table) mutated to alanine were generated. First, different MICA mutants were cloned in pFUSE vector (see Chapter 6.1.14). Subsequently, the MICA mutants were transiently transfected in 293F cells and cell culture supernatants of these transfectants were screened for BAMO3 binding by ELISA. Figure 7 depicts the supernatants from cultures transiently transfected with Mutation 3 and Mutation 6 not binding BAMO3. As a control, the MICA/B-specific mAb BAMO1 with a known epitope in the α1/2 domain of MICA was utilized to show that MICA glycoproteins were present in our experimental samples.

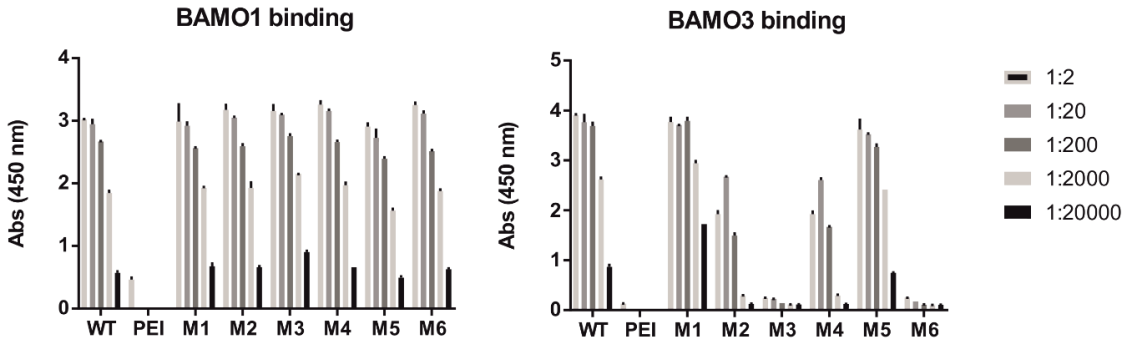

M1	M2	M3	M4	M5	M6
Met 185 Ala	Thr 201 Ala	Arg 217 Ala	Gln 228 Ala	Arg 248 Ala	Gln 251 Ala
Asn 187 Ala	Arg 203 Ala	Gln 218 Ala	Asp 232 Ala	Cys 250 Ala	Glu 253 Ala
Thr 189 Ala	Ser 205 Ala	Asp 219 Ala	Asp 236 Ala		Gln 255 Ala
Glu 192 Ala	Asn 211 Ala	Ser 222 Ala	Asn 238 Ala		Arg 256 Ala
Ser 194 Ala	Thr 213 Ala	Ser 224 Ala			Glu 262 Ala
Glu 195 Ala		His 225 Ala			Asn 266 Ala
Asn 197 Ala		His 226 Ala			His 267 Ala
					Thr 269 Ala

Figure 7. Mutants M3 and M6 do not bind mAb BAMO3. 293F cells were transiently transfected with MICA mutations cloned in pFuse vector. All listed amino acids were mutated to alanine (Ala). 24 hours after transfection, supernatants were collected and binding capacity of MICA mutations to BAMO3 and BAMO1 was determined with ELISA. BAMO1 was used as a control for the presence of MICA mutants in the experimental samples. The transfection reagent PEI only was used as a negative control. Abs (Absorbance). Legends show different dilutions of samples used for ELISA.

As mutants M3 and M6 comprised 7 and 8 mutated amino acids, respectively, each mutation was split into two different ones (Mutation 3 to M3.1 and M3.2 and Mutation 6 to M6.1 and M6.1, respectively) as shown in Figure 8. Again, ELISA of 293F supernatants was performed with the same protocol as with the previous MICA mutants to assess BAMO3 binding. Mutants M3.1 and M6.1 did not bind BAMO3 (Figure 8).

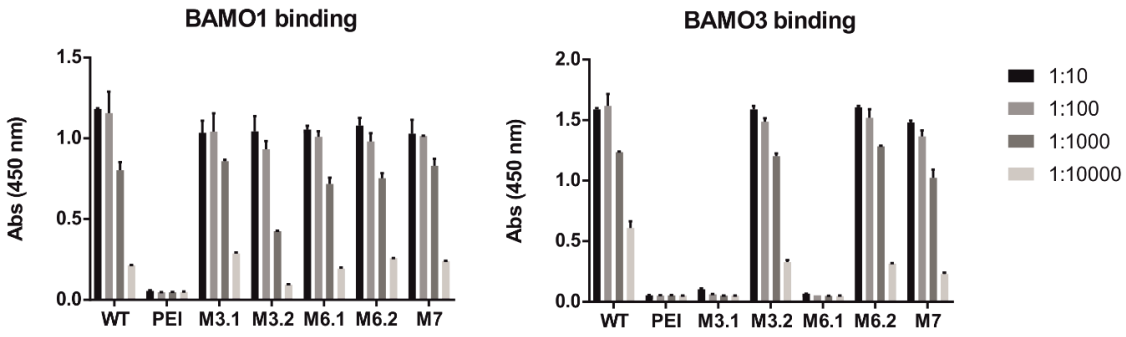

M3.1	M3.2	M6.1	M6.2	M7
Arg 217 Ala	Ser 222 Ala	Gln 251 Ala	Glu 262 Ala	Asn 238 Ala
Gln 218 Ala	Ser 224 Ala	Glu 253 Ala	Asn 266 Ala	Arg 248 Ala
Asp 219 Ala	His 225 Ala	Gln 255 Ala	His 267 Ala	
	His 226 Ala	Arg 256 Ala	Thr 269 Ala	

Figure 8. Mutants M3.1 and M6.1 do not bind mAb BAMO3. 293F cells were transiently transfected with MICA mutants cloned in pFuse vector. All listed amino acids were mutated to alanine (Ala). 24 hours after transfection, supernatants were collected and binding capacity of MICA mutants to BAMO3 and BAMO1 was determined with ELISA. BAMO1 was used as a control for the presence of MICA mutants in the experimental samples. BAMO1 has a known epitope in α1/α2 domain of MICA. PEI is a transfection reagent and was used as a negative control. Abs (Absorbance).

The mutants M3.1 and M6.1 contain 3 and 4 amino acids mutated to alanine, respectively. To determine the specific single amino acids that are critically important for BAMO3 binding, single amino acid mutants were generated (Figure 9). These experiments concluded that amino acids responsible for BAMO3 binding to MICA are aspartic acid (Asp) 219 and glutamine (Gln) 255 (Figure 9).

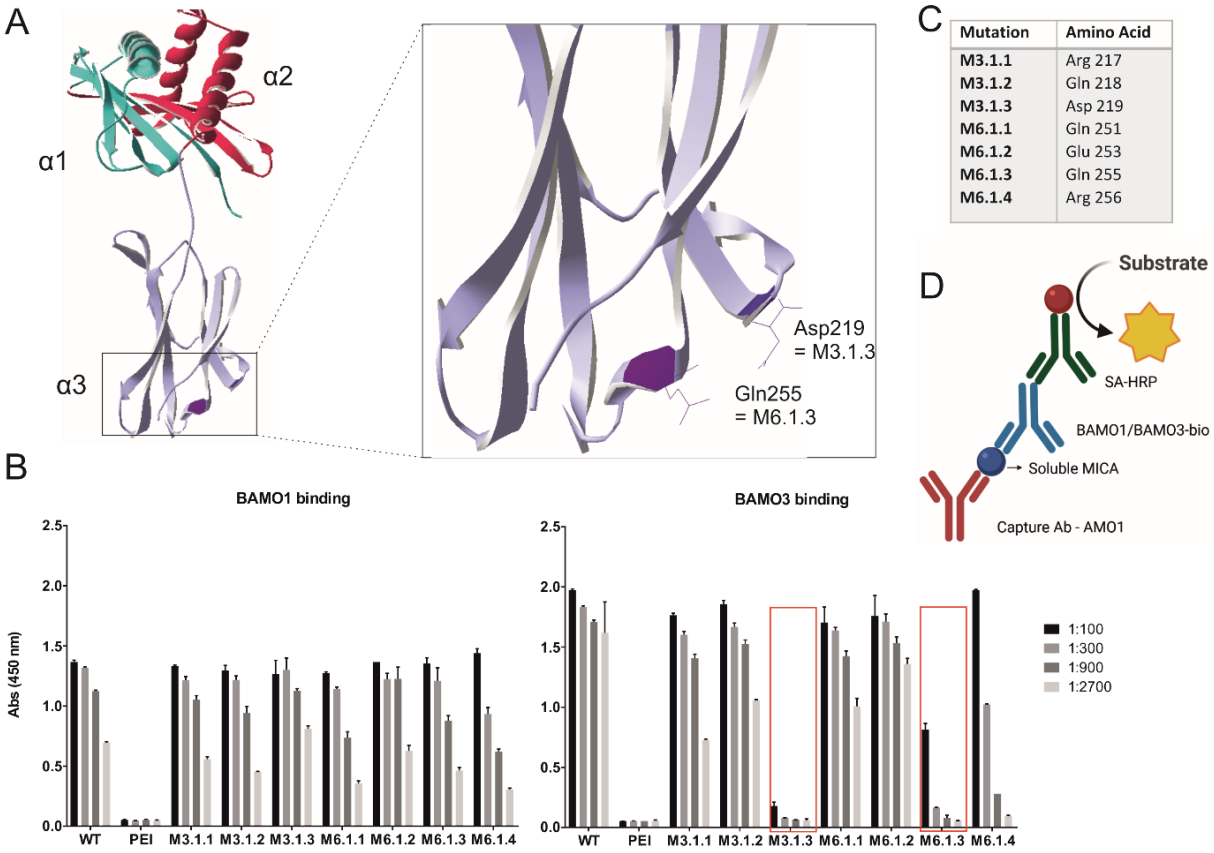

Figure 9. Characterization of the BAMO3 epitope using single amino acid mutants. Aspartic acid (Asp) 219 and glutamine (Gln) 255 are single amino acids crucial for BAMO3 binding and therefore represent the epitope of BAMO3 binding to MICA molecules. (A) Crystal structure of the MICA molecule with highlighted amino acids critical for binding of BAMO3 (Asp219Ala = M3.1.3; Gln255Ala = M6.1.3). (B) Binding of BAMO3 antibody to MICA*007 mutants detected by sandwich ELISA. Several dilutions of supernatants of 293F cells transiently transfected with MICA mutants and WT (wild type) in pFUSE vector were analyzed by sandwich ELISA after 48 hours of culture in fresh medium. The MICA/B-specific antibody BAMO1 (with a known epitope in α1/α2 superdomain) was used as a positive control. Transfecting reagent PEI only was used as a negative control (PEI). (C) List of the MICA amino acids mutated to alanine. (D) ELISA scheme. Created in BioRender.com

For additional experiments with these MICA mutants, they were first cloned into the full length MICA*007 allele into the RSV.5 vector. Both MICA shedding and MICA surface expression of mutants M3.1.3 and M6.1.3 in transiently transfected COS7 cells was assessed. No major alterations of these mutants in MICA cell surface expression (Figure 10) nor any difference in their shedding from the cell surface in comparison to the non-mutated wild type (WT) allele MICA*007 was observed (Figure 11).

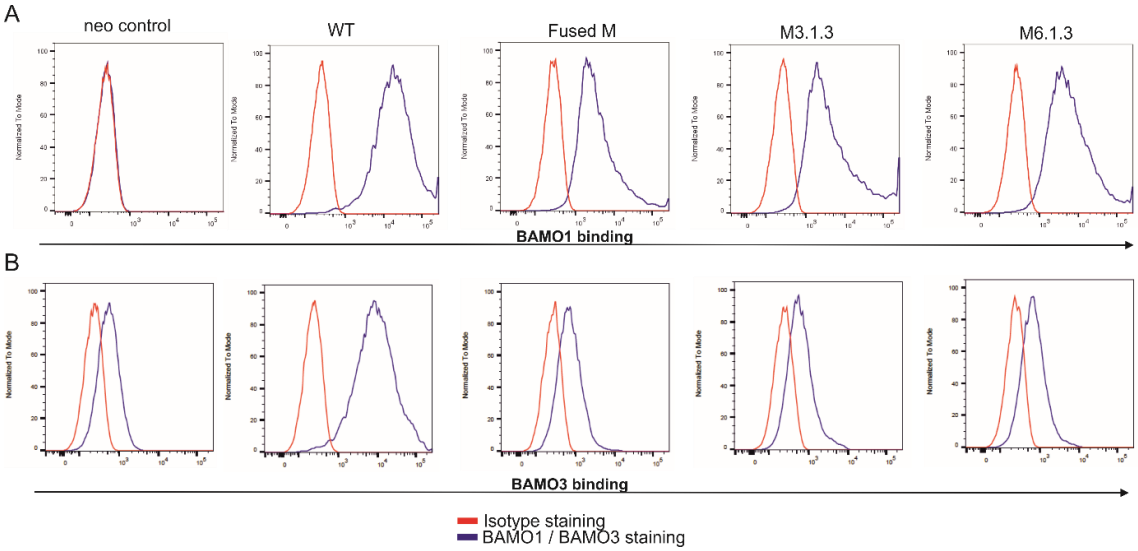

Figure 10. **Surface expression of MICA mutants.** MICA mutants M3.1.3, M6.1.3 and the combined mutant (=fused M) cloned into the RSV.5 neo vector were transiently transfected into COS7 cells and analyzed by flow cytometry for BAMO1 (A) and BAMO3 (B) binding, respectively. Neo = RSV.5 neo control. WT = wildtype MICA*007 (no mutation).

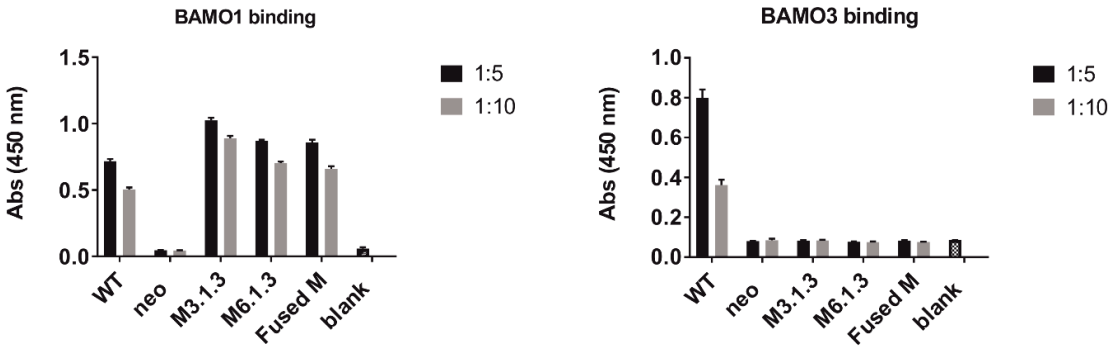

Figure 11. **Shedding of MICA mutants.** MICA mutants M3.1.3, M6.1.3 and the combined mutant (=fused M) cloned into the RSV.5 neo vector were transiently transfected into COS7 cells and supernatants analyzed for ELISA using BAMO1 (left) and BAMO3 (right). Neo = RSV.5 neo control. WT = wildtype MICA*007 (no mutation). Blank = negative control. Abs = Absorbance.

Additionally, binding of the MICA mutants to human NKG2D was tested by flow cytometry. Of note, any interference with NKG2D binding was not expected because NKG2D binds the α1α2 superdomain of MICA which is independent of the α3 domain (Figure 6). In accordance with these expectations, no differences were found when these mutated MICA alleles were compared to the native WT MICA*007 for NKG2D binding (Figure 12). Similarly, the mutations did not interfere with cytotoxicity by the human NK cell line NKL, which predominantly kills via NKG2D (Figure 13).

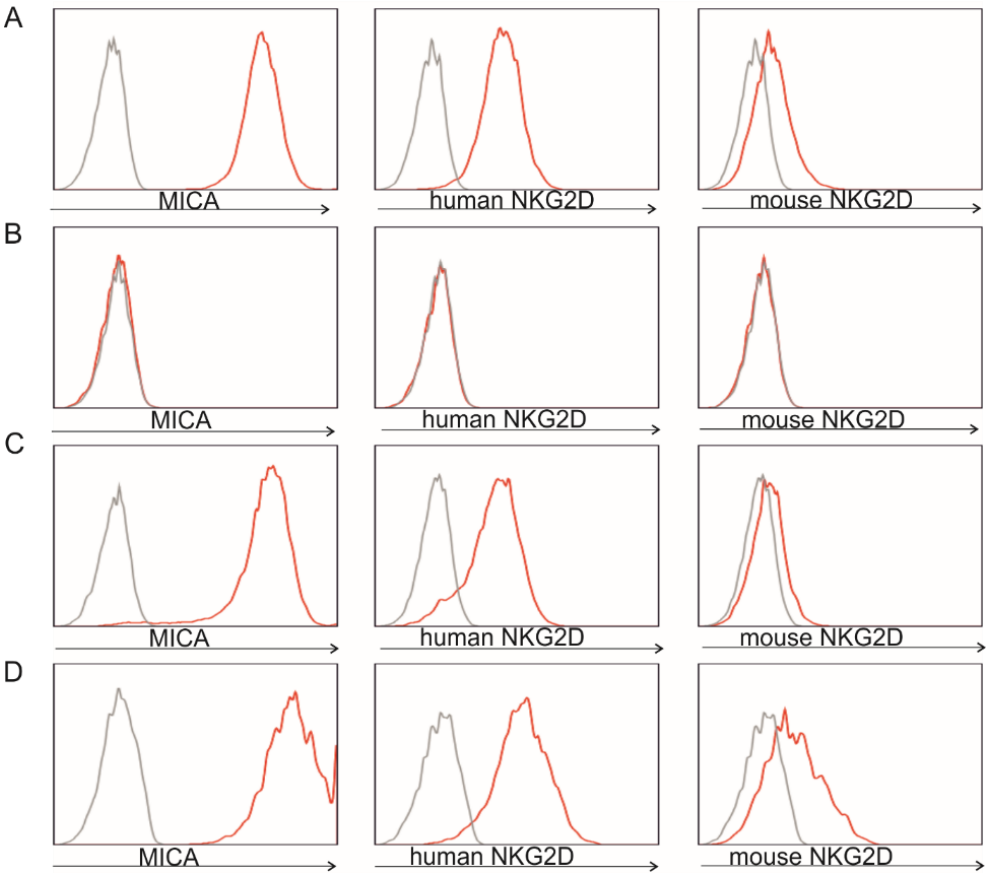

Figure 12. **NKG2D binding to mutants MICA*007 M3.1 and M6.1 is preserved.** RMA cells were transfected with wildtype MICA*007 (positive control) (A), RSV.5 only (negative control) (B), MICA*007 M3.1 (C) and MICA*007 M6.1 (D). Cells were selected with G418 antibiotics at least for one month before flow cytometry experiments. MICA surface expression was assessed with BAMO1 mAb. Binding of NKG2D was determined by incubation of the transfectants with soluble mouse and human NKG2D tetramers and analysed by flow cytometry. Human and mouse NKG2D tetramers were produced in our laboratory.

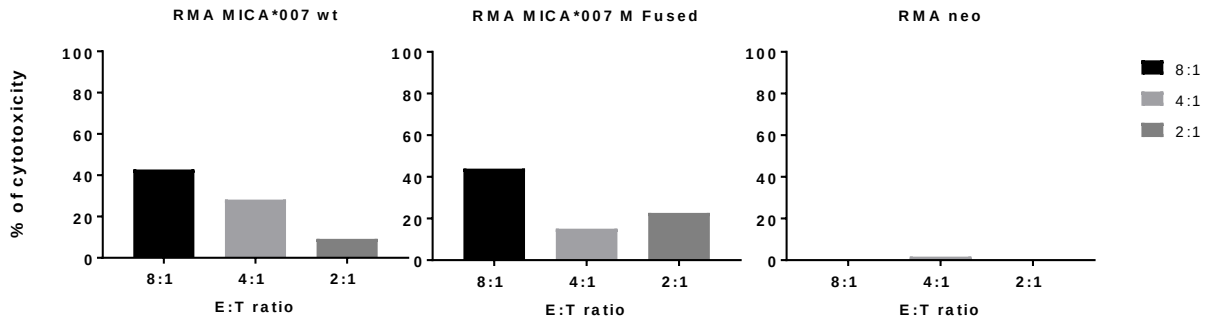

Figure 13. Cytotoxicity of NKL cells is not affected by the BAMO3 epitope MICA mutant. NKL cells were co-cultured with RMA cells transfected with MICA*007 (positive control), MICA*007 Fused M (M3.1.3 + M6.1.3) or RSV.5 neo only (negative control) for 4 hours. Percentage of cytotoxicity by effector cells at different effector (E) toward target cells (T) rations was measured by an LDH-release assay.

In addition, the BAMO3 epitope was confirmed in another MICA*008 allele which is prevalent in Caucasians indicating that BAMO3 has the same epitope among several MICA alleles (Figure 14).

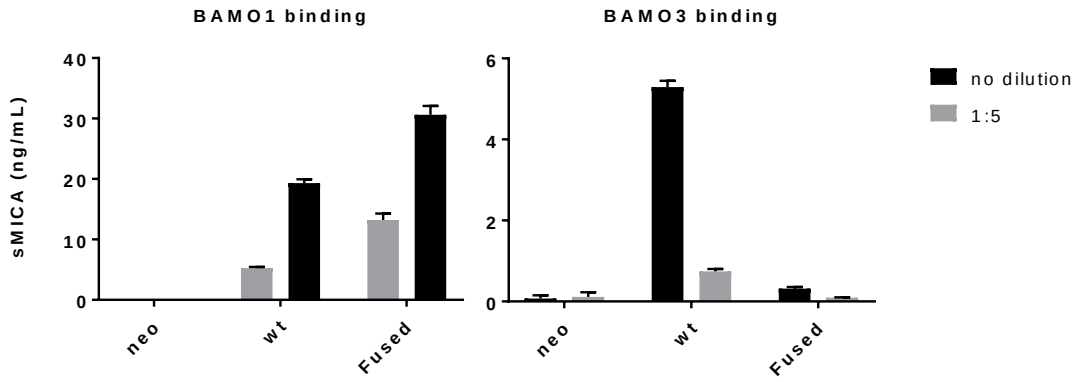

Figure 14. BAMO3 epitope is identical among different MICA alleles. ELISA experiment showing binding of sMICA to BAMO1 and BAMO3, respectively, in supernatants of COS7 cells transiently transfected with wildtype MICA*008 (wt) or MICA*008 mutated at Asp219 and Gln255 (Fused). Transfections with vector RSV.5 neo (neo) served as negative control.

7.3 The amino acid sequence of mAb BAMO3

In order to determine the sequence of BAMO3 mAb heavy and light chain, the mRNA from the hybridoma cell line secreting BAMO3 was isolated and subsequently cDNA was prepared. In the first round of PCR, the antibody genes of different heavy and light chains were amplified using Mouse IgG Library Primer Set #1 (Figure 15 A). These primers are specifically designed to amplify mouse rearranged IgG variable domain coding regions. Amplified DNA was sent out for sequencing. The obtained sequences were compared with sequences existing in the online database Vbase2 (http://www.vbase2.org/vbscAb.php) and those with meaningful sequence were selected for further PCR. The final sequences and their translation to the amino acid sequence are shown in the Figure 15 B. To confirm that this heavy and light chain are indeed functional and bind to MICA, they were cloned into the pFUSE vector (hBAMO3) and transiently transfected 293T cells. After 48 hours, the collected supernatant was used to test binding of hBAMO3 to transiently transfected COS7 cells expressing MICA*007 by flow cytometry. Binding of hBAMO3 to ectopically expressed MICA was comparable to the original mAb BAMO3 (Figure 15 C).

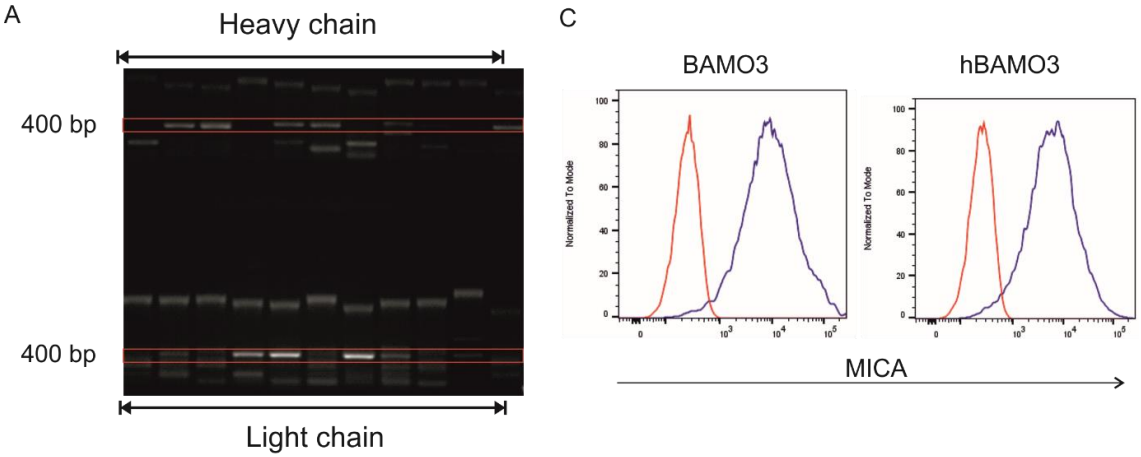

B **Sequence of light chain:**

GATATCCAGATGACACAGACTACATCCTCCCTGTCTGCCTCTCTGGGAGACAGAGTCACCATCAGTTGCAGTG
CAAGTCAGGGCATTAGCAATTATTTAAACTGGTATCAGCAGAAACCAGATGGAACTATTAAACTCCTGATCCA
ATACACATCAATTTTACACTCAGGAGTCCCATCCAGGTTCAGTGGCAGTGGGTCTGGGACAGAATATTCTCTCA
CCATCAGCAACCTGGAACCTGAAGATATTGCCACTTATTTTTGTCAGCAGTATAGTAAGTTTCCTCGGACGTTC
GGTGGAGGCACCAAGCTGGAAATCAAACGGGCTGAT

Translation of light chain (Amino Acid Sequence in FASTA format):

DIQMTQTTSSLSASLGDRVTISCSASQGISNYLNWYQQKPDGTIKLLIQYTSILHSGVPSRFSGSGSGTEYSLTISNLEP
EDIATYFCQQYSKFPRTFGGGTKLEIK

Sequence of heavy chain:

CAGATCCAGTTGGTGCAGTCTGGACCTGAGCTGAAGAAGCCTGGAGAGACAGTCAAGATCTCCTGCAAGGCT
TTCGGGTATACCTTCACAAACTATGGAATGAACTGGGTGAAGCAGGCTCCAGGAAAGGGTATAAAGTGGATG
GGCTGGATAAACACCTACACTGGAGAGCCAACATATGCTGATGACTTCAAGGGACGGTTTGCCTTCTCTTTGG
AAACCTCTGCCAGCACTGCCTATTTGCAGATCAACCACCTCAAAAATGAGGACACGGCTACATATTTCTGTGCA
AGAAACTATGGTAACTACCTTTTTGATTACTGGGGCCAAGGCACCACTCTCACAGTCTCCTCA

Translation of heavy chain (Amino Acid Sequence in FASTA format):

QIQLVQSGPELKKPGETVKISCKAFGYTFTNYGMNWVKQAPGKGIKWMGWINTYTGEPTYADDFKGRFAFSLETS
ASTAYLQINHLKNEDTATYFCARNYGNYLFDYWGQGTTLTVSS

Figure 15. BAMO3 mAb sequence. A.) Bands visualisation after the first PCR. Size of excised band was 400 bp (red). B.) Sequence and translation of variable domain of heavy and light chain of BAMO3 mAb. C.) Binding of hBAMO3 to COS7 cells transiently transfected with wildtype MICA*007 in RSV.5 neo vector. COS7 cells were stained with BAMO3 and hBAMO3 and analysed by flow cytometry. Red color – isotype control. Blue color – MICA staining.

7.4 Length of alanine repeats in the transmembrane domain of MICA does not affect MICA shedding inhibition

At position 319 in the transmembrane region of MICA, there is a polymorphism among different MICA alleles with regard of alanine repeats (Figure 16 A-B). While MICA*007 allele has four alanines at this position, other MICA alleles have two, five, six or even nine alanines, respectively. Therefore, the first question was whether the length of the alanine repeats might directly correlate with MICA shedding intensity. Hence, MICA*007 variants with 6 and 9 alanine

repeats were generated and their shedding capacity and surface expression were tested. The results revealed no interference of the alanine repeats either with MICA surface expression (Figure 16 C) or MICA shedding capacity (Figure 16 D) in comparison to wildtype MICA*007. The second question was whether BAMO3-mediated shedding inhibition could be affected by the length of alanine repeats at position 319. Therefore, B16F10 MICA*007 6A and 9A cell were treated with BAMO3 mAb. After 24 hours, collected cells were analyzed by flow cytometry and cell culture supernatant was analyzed by ELISA. The results showed that the length of the alanine repeats in transmembrane domain of MICA (at position 319) did not alter the ability of BAMO3 mAb to inhibit shedding of MICA. The length of alanine repeats did not affect MICA surface expression after BAMO3 treatment, either (Figure 16 C-D).

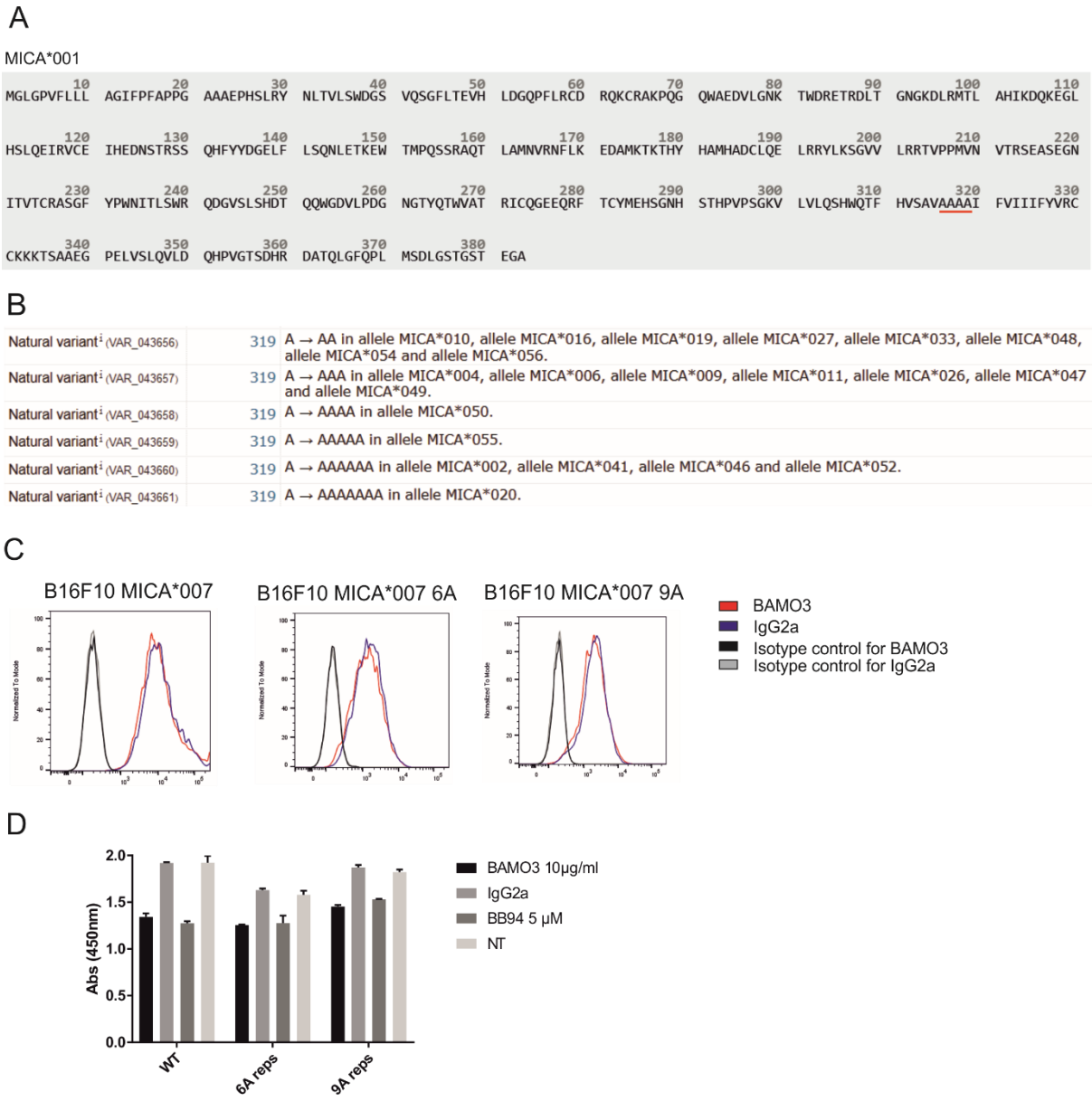

Figure 16. Length of alanine repeats at position 319 in transmembrane region of MICA does not alter BAMO3 shedding MICA inhibition capacity. A.) Amino acid sequence of MICA*001

allele obtained from uniprot.org. Position 319 is underscored (red color). MICA*001 allele contains four Alanine at position 319. B.) Length of alanine repeats differs among MICA alleles. C.) Surface expression of MICA*007, MICA*007 with 6 alanine repeats (6A) and 9 alanine repeats (9A) after BAMO3 treatment. Determined by flow cytometry. D.) ELISA result showing shedding of MICA*007, MICA*007 6A and 9A after BAMO3 treatment. Values are shown as absorbance (450 nm). BB94 = metalloprotease inhibitor (positive control). NT= no treatment.

7.5 Mutation of Cysteine 250 in the MICA α3 domain alleviates MICA shedding

As mentioned earlier, the domain structure of MICA/B consists of three extracellular domains, the α1α2 MHC class I-like superdomain and the Ig-like α3 domain. The α3 domain contains a cysteine at position 250 (Figure 17 A-B), which does not appear to form intramolecular disulfide bonds with any cysteine partner. Similarly, cysteine 190 in MICB does not appear to form a disulfide bond, either (15 C-D). To determine a potential importance for surface expression and shedding of MICA molecules, these cysteines were subjected to various tests. COS7 cells were transiently and B16F10 stably transfected with wildtype MICA*007 or MICA*007 mutants Cys250Ala and Cys250Ser, respectively, and their surface expression assessed by flow cytometry. No interference with MICA surface expression was observed and the expression of the MICA mutants was even higher in comparison to the wild type (WT) MICA (Figure 18 A, D). In immunoblotting analysis of the whole cell lysates, the bands for soluble MICA (sMICA) (33 kDa) of the Cys250Ala sample were of lower intensity than in WT MICA. Surface MICA has a molecular weight approximately 47 kDa (Figure 18 C). Supernatants from the cell supernatants were harvested and used to determine levels of sMICA by ELISA. Significantly decreased levels of sMICA in the culture supernatants were observed when compared to WT MICA*007 (Figure 18 B, E). Taken together, the alanine mutation of Cys250 caused a reduced shedding of MICA.

A

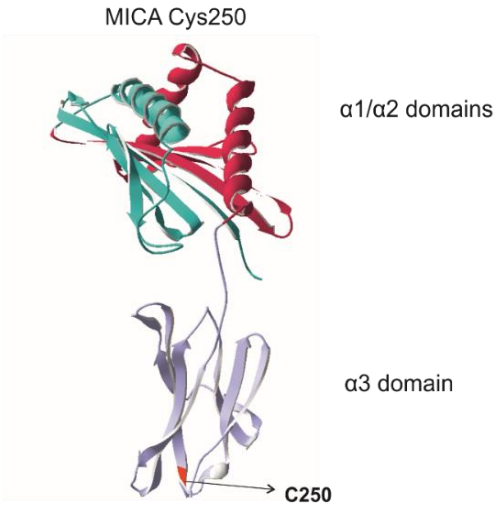

B

MGLGPVFLLLAGIFPFAPPGAAAEPHSLRYNLTVLSWDGSVQSGFLAEVHLDGQPFLRYDRQKCRAKPQGQWAED
VLGNKTWDRETRDLTGNGKDLRMTLAHIKDQKEGLHSLQEIRVCEIHEDNSTRSSQHFYYDGELFLSQNVETEEWT
VPQSSRAQTLAMNVRNFLKEDAMKTKTHYHAMHADCLQELRRYLESSVVLRRTVPPMVNVTRSEASEGNITVTCR
ASSFYPRNITLTWRQDGVSLSHDTQQWGDVLPDGNGTYQTWVATRICQGEEQRFTCYMEHSGNHSTHPVPSGK
VLVLQSHWQTFHVSAVAAAAAAAAAAIFVIIIFYVCCCKKKTSAAEGPELVSLQVLDQHPVGTSDHRDATQLGFQPL
MSDLGSTGSTEGA

C

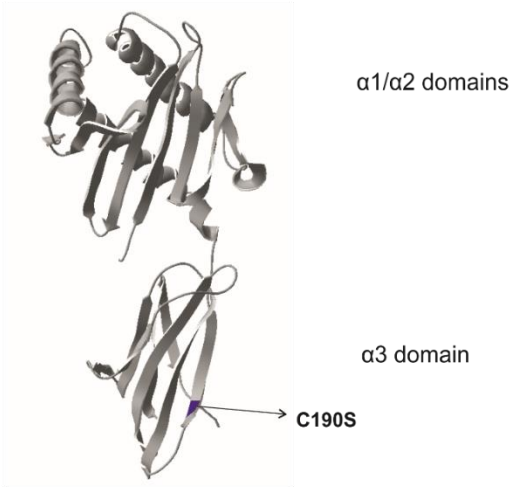

D

MGLGRVLLFLAVAFPFAPPAAAAEPHSLRYNLMVLSQDGSVQSGFLAEGHLDGQPFLRYDRQKRRAKPQGQWAE
NVLGAKTWDTETEDLTENGQDLRRTLTHIKDQKGGLHSLQEIRVCEIHEDSSTRGSRHFYYDGELFLSQNLETQESTV
PQSSRAQTLAMNVTNFWKEDAMKTKTHYRAMQADCLQKLQRYLKSGVAIRRTVPPMVNVTCSEVSEGNITVTCR
ASSFYPRNITLTWRQDGVSLSHNTQQWGDVLPDGNGTYQTWVATRIRQGEEQRFTCYMEHSGNHGTHPVPSGK
ALVLQSQRTDFPYVSAAMPCFVIIIILCVPCCKKKTSAAEGPELVSLQVLDQHPVGTGDHRDAAQLGFQPLMSATGS
TGSTEGT

Figure 17. **Location of cysteine 250 in MICA and cysteine 190 in MICB.** Cysteine 250 in MICA A) crystal structure and B) in amino acid sequence (highlighted in yellow). C) Cysteine 190 in MICB crystal structure and D) in amino acid sequence (highlighted in yellow); (source uniprot.org). Sequence of α3 domain is underlined.

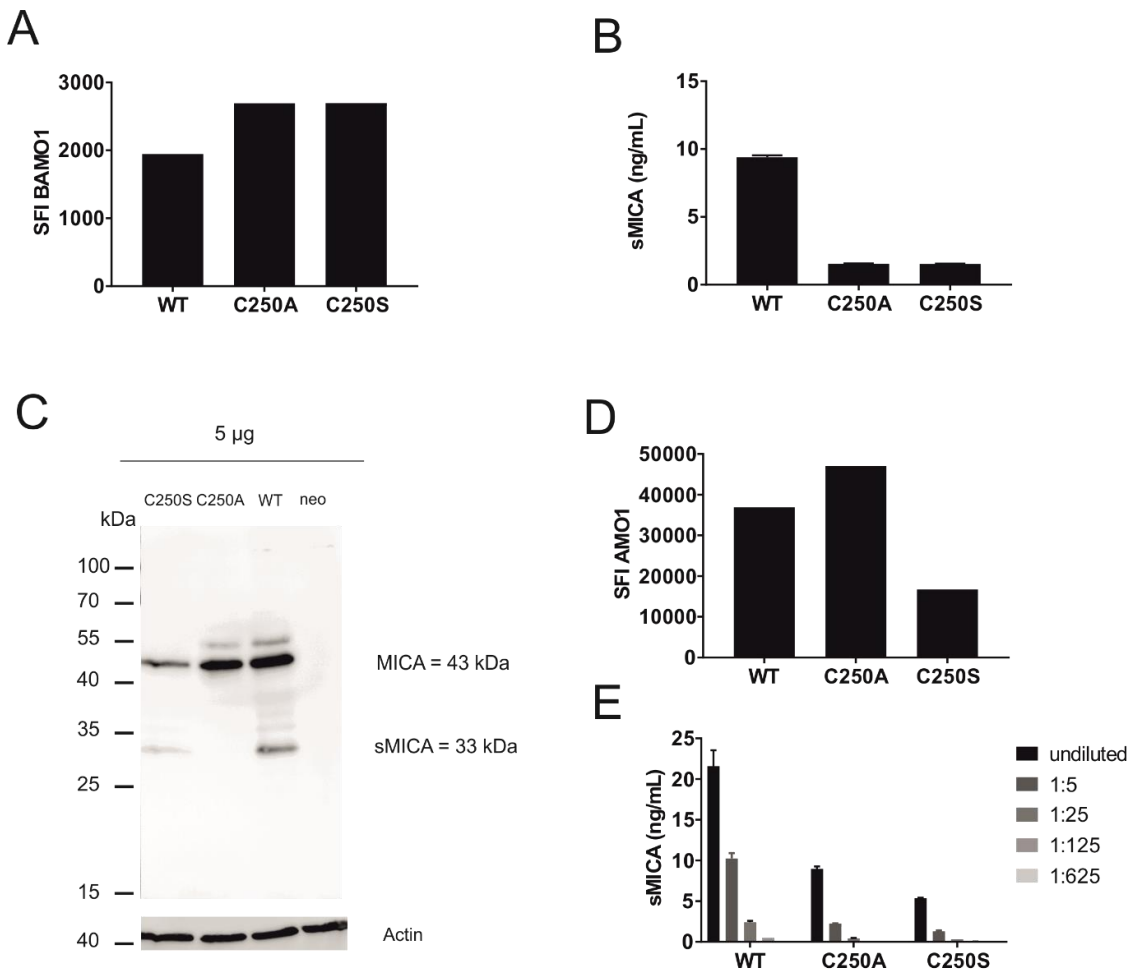

Figure 18. Mutation of cysteine 250 in the α3 domain of MICA results in decreased shedding. A.) Surface expression of MICA*007 and MICA*007 C250A and C250S Mut on COS7 cells (transiently transfected). B.) ELISA result showing soluble MICA in cell culture supernatants of COS7 cells expressing MICA*007 (WT) and MICA*007 C250A and C250S. C.) Western Blot showing MICA (43kDa) and soluble MICA (33kDa) in the whole cell lysate of B16F10 cells stably expressing MICA*007 (WT) and MICA*007 C250A and C250S. D.) Surface expression (in SFI AMO1) of MICA*007, MICA*007 C250A and C250S on B16F10 stable transfectants. SFI=specific fluorescence intensity. E.) ELISA result showing soluble MICA (sMICA, ng/mL) in cell culture supernatants of stable transfectants B16F10 MICA*007 (WT), MICA*007 C250A and C250S.

7.5.1 ADAM10 stimulator ionomycin does not induce shedding of MICA*007 C250A mutation

As the decreased shedding of mutated MICA Cysteine 250 to Alanine was observed (Figure 18), the capacity to enhance MICA shedding after stimulation with well-established agents PMA and ionomycin was tested. PMA is a known activator of protein kinase C and is able to stimulate ADAM17 metalloprotease mediated shedding (Horiuchi et al., 2007). Ionomycin is a calcium ionophore and its stimulatory effects on ADAM10 have been published previously (Le Gall et al., 2009). Figure 19 shows that ionomycin stimulation did not significantly increase release of soluble MICA from B16F10 cells transfected with MICA C250A, but PMA stimulation led to a significant increase in MICA shedding (Figure 19 A). This observation suggested that cysteine 250 in MICA might be an important amino acid for ADAM10-mediated shedding, as ionomycin is an ADAM10 metalloprotease stimulator.

7.5.2 Mutation in Cysteine 250 to Alanine caused lower surface expression of ADAM10

Next, surface expression of ADAM10 and MICA was assessed by flow cytometry. The results show lower levels of ADAM10 on the surface of cells expressing Mut MICA*007 C250A when compared to WT MICA*007 (Figure 19 B). Furthermore, higher expression of surface MICA C250A was observed on the surface of stably transfected B16F10 cells (Figure 19 C).

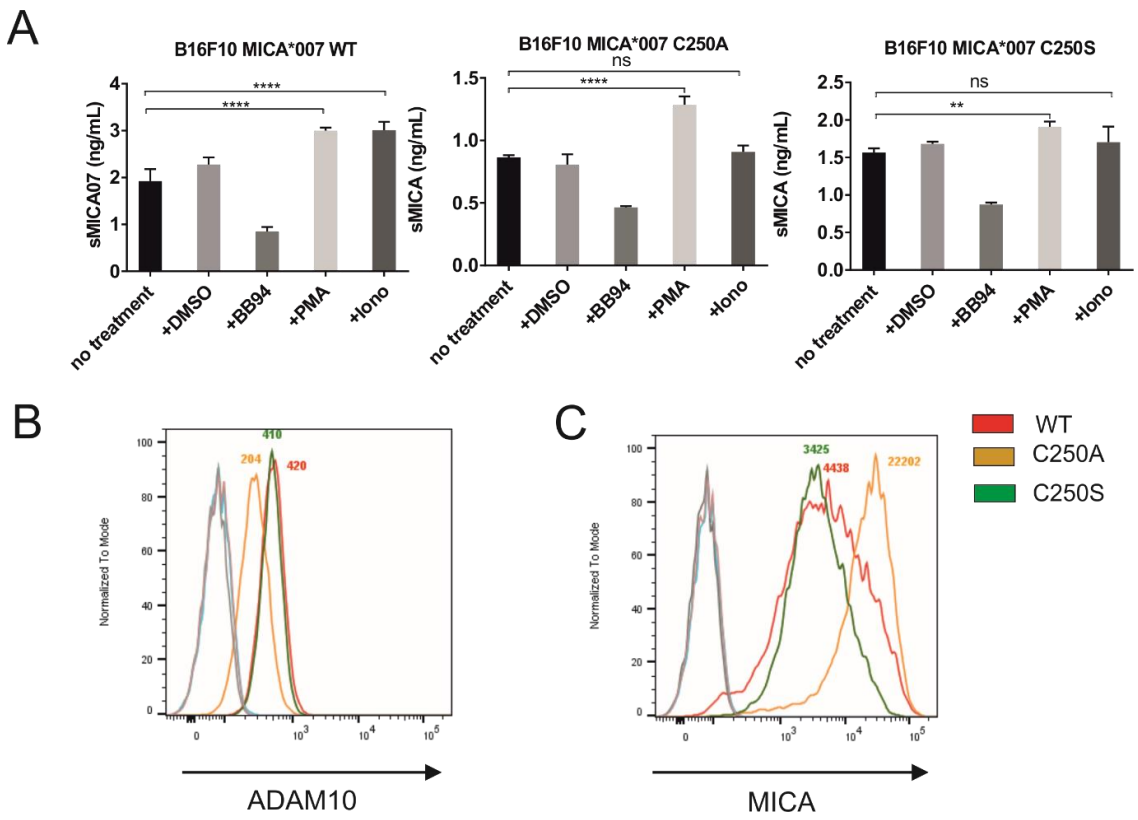

Figure 19. Mutation in C250 is critical for ADAM10 surface expression and MICA shedding. A.) ELISA results showing levels of soluble MICA (ng/ml) after 2 hours of stimulation with PMA and ionomycin. One-way ANOVA and Dunnett´s multiple comparisons test. Flow cytometry showing surface expression of ADAM10 (B) and MICA (C) after PMA and ionomycin stimulation. Displayed values depict SFI (specific fluorescence intensity).

7.5.3 ADAM10 is not retained intracellularly in the endoplasmic reticulum (ER)

As the flow cytometry results demonstrated lower expression of ADAM10 on the surface of B16F10 MICA C250A and C250S mutants (Figure 19 B), the mechanism behind this observed phenomenon was elucidated. The possibility that ADAM10 is retained intracellularly in the C250A and C250S mutants was predicted. To resolve this hypothesis, the whole cell lysates extracted from B16F10 MICA07 C250A and C250S cells were treated with Endoglycosidase H to monitor protein trafficking. Endoglycosidase H is an enzyme able to cleave asparagine-linked high mannose oligosaccharides and can be used to monitor post-translational modifications occurring in the Golgi body. Proteins that are intracellularly retained in the endoplasmic reticulum (ER) are called EndoH sensitive and mature proteins able to traffic to the surface of the cell and past the Golgi apparatus are referred to as EndoH resistant. Treatment with EndoH revealed that ADAM10 in B16F10 MICA*007 C250A cells was resistant to digestion and has probably undergone a post-translational modification in the Golgi body and therefore is not

retained in the ER (Figure 20 A). Furthermore, the western blot analysis showed a less amount of total mature ADAM10 protein in our C250A mutant sample than in the WT MICA sample. As mentioned previously, another important molecule involved in MICA shedding is ERp5. When ERp5 binds MICA, it causes a conformational change of MICA and the potential binding site for metalloproteases is uncovered. For this reason, the attention was focused on assessing the expression state of ERp5. Immunoblotting analysis revealed similar levels of ERp5 in whole cell lysates of mutated and wildtype MICA*007 (Figure 20 B). Ultimately, a lower amount of mature ADAM10 was detected in samples with C250A mutation and no differences in ERp5 protein content were revealed.

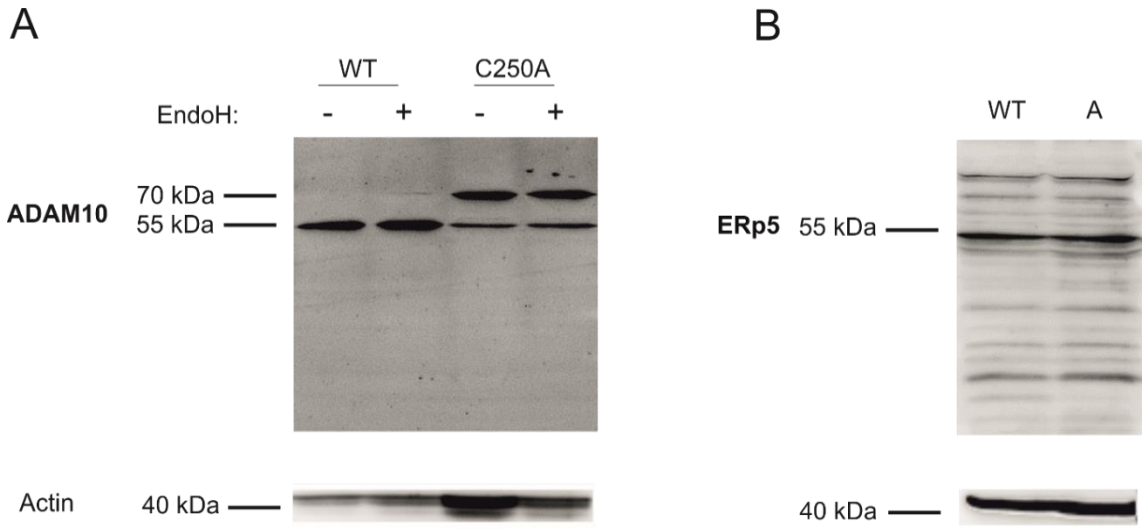

Figure 20. ADAM10 is not retained intracellularly in the endoplasmic reticulum (ER). Western blot showing total ADAM10 (A) and ERp5 (B) protein content in B16F10 cells expressing MICA*007 (WT) and MICA*007 C250A. Cells were lysed with NP-40 buffer and samples (20 µg) were digested with Endoglycosidase H (EndoH) according to the manufacturer´s protocol. Mature ADAM10 molecular mass is 55 kDa. ERp5 molecular mass is 50 kDa.

7.5.4 Mutation in Cysteine 250 reduced interaction with ADAM10 but not with ERp5

Next, the interaction between mutated MICA C250A and ERp5 was studied. As can be seen in Figure 21 C, no interference in MICA C250A and ERp5 interaction was detected. Therefore, the attention was turned to another potential protein involved in MICA shedding - ADAM10. Previous results suggested decreased shedding intensity together with decreased surface expression of MICA. Since the ionomycin shedding stimulation via ADAM10 was not significant, the protein-protein interaction between MICA C250A and ADAM10 was studied. Ultimately, the immunoprecipitation analysis revealed a weaker physical interaction between MICA C250A and ADAM10 (Figure 21 B).

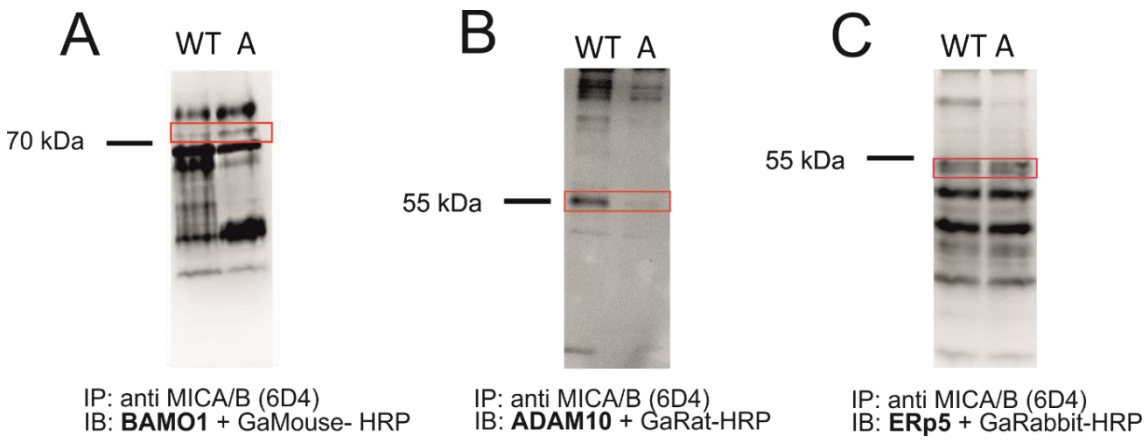

Figure 21. Mutation in Cysteine 250 to Alanine in MICA*007 affects physical interaction with metalloprotease ADAM10 but not with ERp5. B16F10 cells expressing MICA*007 (WT) and MICA*007 C250A (A) were lysed in NP-40 lysis buffer and proteins were precipitated with anti-MICA mAb 6D4. Membranes were subsequently blotted with either A.) BAMO1 antibody, B) ADAM10 antibody and C) ERp5 antibody. Molecular weight of MICA = 68 kDa. Molecular weight of ADAM10 = 55 kDa. Molecular weight of ERp5 = 50 kDa.

7.6 BAMO3 therapeutic delivery delays growth of mouse MICA-positive lymphoma and improves overall survival of MICAgen mice

Because there is already the evidence on BAMO3 shedding inhibition of MICA, the therapeutic efficacy of this monoclonal antibody was tested in MICA transgenic mice (MICAgen) inoculated with MICA-expressing tumor cells. MICAgen transgenic mice have been previously generated in our laboratory (Kim et al.,2020) containing a 23.4 kb *Xba*I/*Sal*I fragment isolated from a cosmid comprising the entire human MICA gene (position 31,393,601 to 31,417,018 on Chr6p21 according to GRCh38.p12). MICAgen mice are the ideal mouse model used in our studies because of several useful properties, including lack of MICA immunogenicity. This mouse strain expresses only very low levels of MICA in their gastrointestinal tract, mimicking the physiological state in humans. The hypothesis on a therapeutic efficacy of BAMO3 was built on several preliminary results. First, MICA shedding was observed in many cancerous cell lines, and it has been suggested as a cancer biomarker in cancer patients. This fact is further supported by numerous studies showing elevated levels of soluble MICA in patients' sera with different types of oncological diseases (Salih et al., 2002; Holdenrieder et al., 2006) and its negative impact on overall survival of these patients. MICA shedding is an interesting target for cancer studies and therefore, it may be beneficial to inhibit MICA shedding in cancer patients, e.g., by BAMO3.

In this experiment, the RMA-MICA*007 mouse lymphoma was utilized (Figure 22). RMA-MICA*007 transfectants, an established, aggressive cell line model, were previously generated

in our lab by electroporation. MICAgen mice were subcutaneously inoculated in their right flank with RMA-MICA*007 cells and observed for their weight and tumor growth size every two days. Once the tumor reached a palpable size of 6 mm (~108 mm^3), MICAgen mice were randomized, and the antibody treatment was initiated. The BAMO3 mAb or an irrelevant isotype control IgG2a were injected intravenously into the lateral tail (caudal) vein and the treatment was repeated 6 times over the period of 3 weeks. During this time, the body weight of MICAgen mice was continuously controlled to ensure safety of the treatment. When the tumor size reached the threshold of 14 mm (~1300 mm^3), the mice were sacrificed, and the tumor tissue was harvested for further analysis (Figure 22).

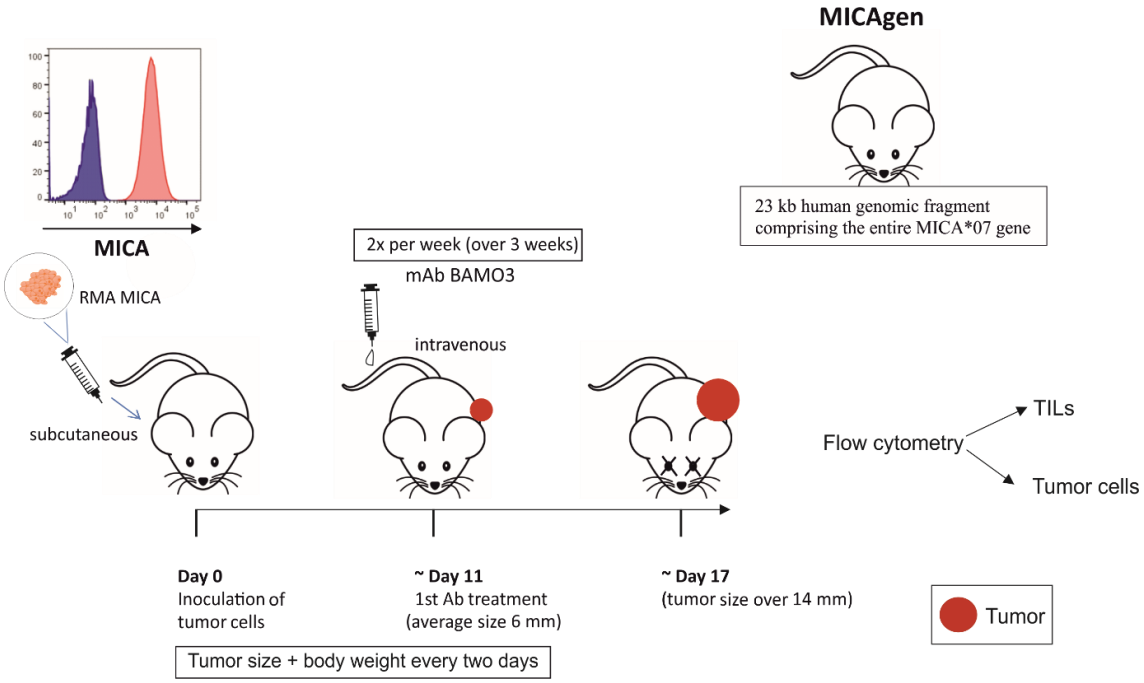

Figure 22. Scheme of therapeutic BAMO3 treatment. 3x10^4 RMA-MICA cells were inoculated subcutaneously into the right flank of MICAgen mice. When tumors reached a palpable size, BAMO3 (or isotype control) was injected intravenously twice a week for 3 weeks. Mice were sacrificed when tumors exceeded 14 mm and were then subjected to flow cytometry analysis. TILs = tumor-infiltrating lymphocytes.

Strikingly, BAMO3 mAb therapy remarkably controlled the growth of RMA-MICA tumors (Figure 23 A-B). Furthermore, longer overall survival of MICAgen mice was observed after BAMO3 treatment, in comparison to MICAgen mice treated with the isotype control antibody (Figure 23 C). Importantly, flow cytometric analysis revealed significantly increased NKG2D expression on NK cells after BAMO3 treatment (Figure 24 A). Contrastingly, no NKG2D expression on $CD8^+$ T cells was observed (Figure 24 B). While analyzing tumor-infiltrating lymphocytes (TILs), higher, but not statistically significant elevated frequencies of $CD39^+$ $CD8^+$ TILs were detected after IgG2a treatment (Figure 24 C-D). In the literature, expression of CD39 on CD8+ T cells

defines a population of highly exhausted cells (Simoni et al., 2018). Furthermore, co-expression of CD39 together with CD103 on CD8+ T cells was associated with better overall survival of patients with head and neck cancer (Duhen et al., 2018). Together with no expression of NKG2D on $CD8^+$ TILs, their bystander function in our cancer model can be assumed. Moreover, based on the observed results, predominant importance of tumor-infiltrating NK cells in the RMA-MICA tumor elimination, rather than $CD8^+$ TILs, can be presumed.

Next, PD-1 (Programmed death-1) expression on TILs and PD-L1 (programmed death-ligand 1) expression on tumor cells was analyzed. PD-1 is an important inhibitory surface receptor that serves also as a T cell checkpoint. A key role of PD-1 is in regulation of T cell exhaustion. In simple terms, engagement of PD-1 with its ligand PD-L1 activates downstream signaling pathways leading to inhibition of T cell activation (Jiang et al., 2019). The flow cytometry analysis did not reveal any differences in the surface PD-1 expression on TILs between respective treatment groups (Figure 24 E-F). Further analysis demonstrated no differences of MICA or PD-L1 expression on the tumor cells (Figure 25) between BAMO3 and IgG2a treatment groups.

To define levels of soluble MICA in blood of MICAgen mice following BAMO3 therapy, blood was sampled from the treated animals and the serum was subsequently isolated. The ELISA assay was used to determine levels of sMICA in the mouse serum and it was compared between the treatment groups. Surprisingly, the results did not reveal any significant differences in sMICA levels between BAMO3 mAb and IgG2a control group (Figure 26).

In summary, the results have shown therapeutic efficacy of BAMO3 mAb in MICAgen mice. BAMO3 was able to control tumor growth over time and to improve overall survival of MICAgen mice in comparison to IgG2a control treatment. Additionally, BAMO3 treatment resulted in higher expression of NKG2D on tumor-infiltrating NK cells whereas no expression on $CD8^+$ TILs was observed. Furthermore, unexpectedly, our analysis did not reveal any difference in sMICA levels between BAMO3 and IgG2a treatment.

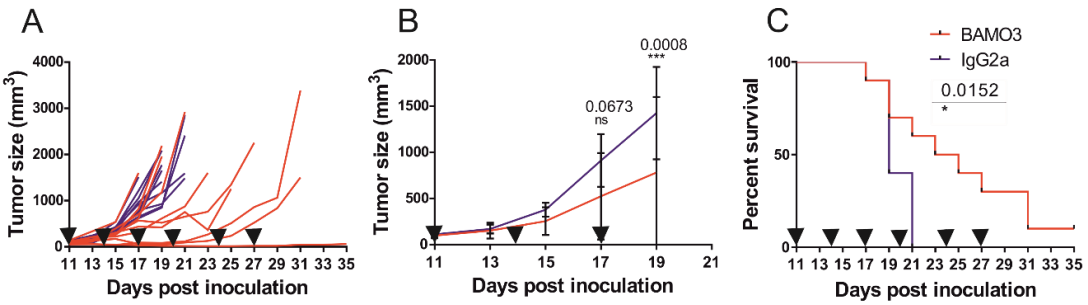

Figure 23. Therapeutic delivery of BAMO3 controlled growth of mouse lymphoma and improved overall survival of MICAgen mice. A.) Tumor growth curves of individual mice inoculated with RMA-MICA cells treated with either BAMO3 or an irrelevant isotype-matched

mAb. B.) Average tumor volume of MICAgen mice assessed between days 11 and 19. 2way Anova + Sidak's multiple comparisons test, C.) Survival curves of BAMO3-treated (red) or isotype-treated mice (blue). (Log-rank test). Arrows indicate days of antibody injection. Mice were sacrificed when tumors exceeded 1300 mm^3. n=10. This mouse experiment was repeated two times. Representative figure of one experiment is shown.

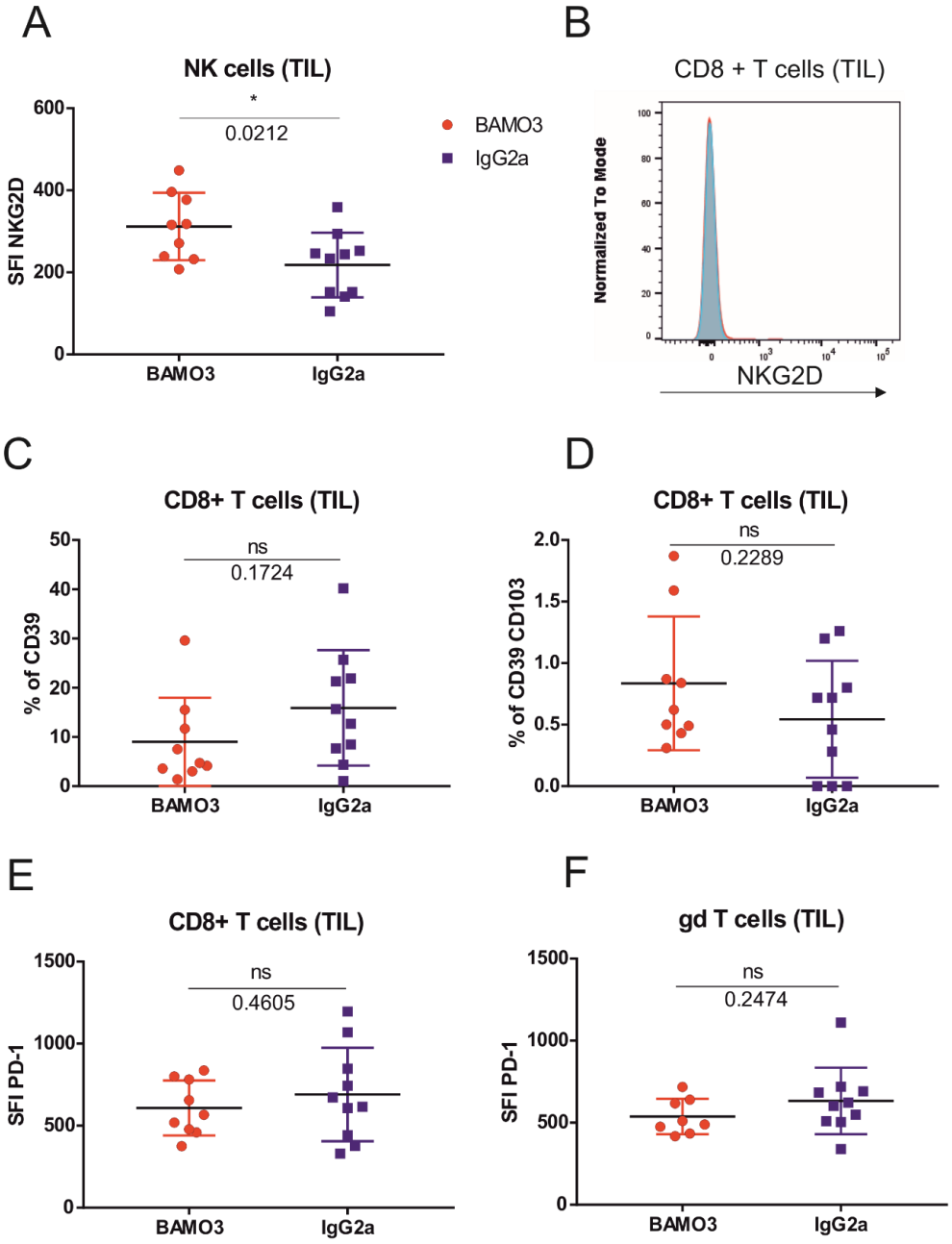

Figure 24. Flow cytometry analysis of tumor-infiltrating lymphocytes (TILs). MICAgen mice bearing RMA-MICA tumors were treated with BAMO3 mAb and an irrelevant isotype control. When tumor size exceeded 1300 mm^3, mice were sacrificed, and tumor tissue was analysed via flow cytometry. A.) NKG2D expression on tumor infiltrating NK cells ($CD45^+$ $CD3^-NKp46^+$). B.) An example showing no NKG2D expression on tumor-infiltrating CD8+ T cells ($CD45^+CD3^+CD8^+$). C.) Frequencies (%) of tumor-infiltrating $CD39^+CD8^+$T cells ($CD45^+CD3^+CD8^+CD39^+$). D.) Frequencies (%) of tumor-infiltrating $CD39^+CD103^+CD8^+$T cells ($CD45^+CD3^+CD8^+CD39^+CD103^+$). E.) PD-1 expression (SFI) on tumor-infiltrating $CD8^+$T cells ($CD45^+CD3^+CD8^+$). F.) PD-1 expression (SFI) on tumor-infiltrating γδ T cells ($CD45^+CD3^+TCR\gamma\delta^+$). Unpaired t-test. SFI= specific fluorescence intensity.

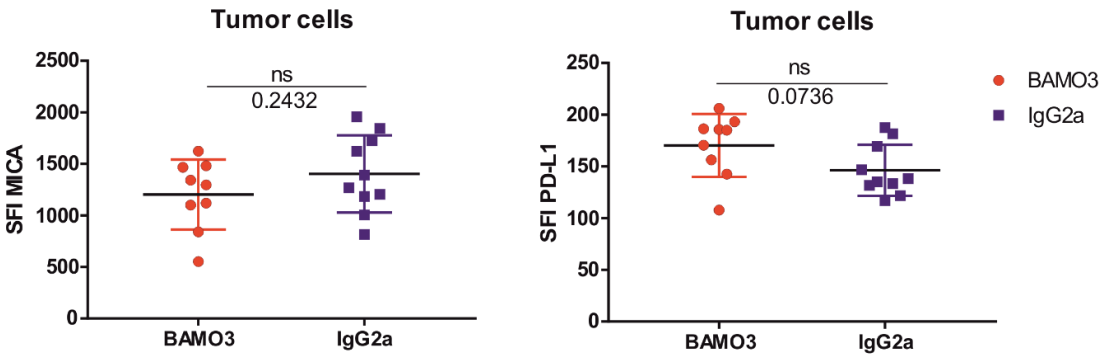

Figure 25. Surface expression of MICA and PD-L1 on RMA tumor cells after BAMO3 treatment. Flow cytometry analysis of tumor cells. MICA (left) and PD-L1 (right) surface expression (SFI) was determined. Samples were harvested when tumor size reached 1300 mm^3. Unpaired t-test ($p < 0.05$). ns= not significant. SFI= specific fluorescence intensity.

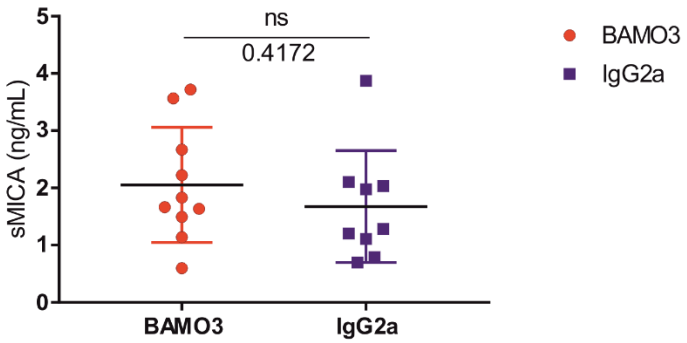

Figure 26. Levels of soluble MICA (sMICA) in mouse serum after BAMO3 treatment. MICAgen mouse serum was isolated from blood that was collected when mice were sacrificed due to tumor size of 1300 mm^3. Levels of sMICA (ng/mL) were determined by MICA-specific sandwich ELISA (AMO1+BAMO1-bio). Statistical analysis: unpaired t-test ($p < 0.05$). BAMO3 group – n=10; IgG2a group – n=9.

7.7 Therapeutic efficacy of mAb 19E9-PBD in treatment of aggressive MICA-expressing tumors

Another focus of this thesis was to evaluate the therapeutic efficacy of an anti-MICA antibody 19E9 conjugated to pyrrolobenzodiazepine (PBD). PBD dimers are highly efficient DNA minor groove cross-linking agents and can be considered as a class of highly potent toxins. Antibody-drug conjugates are able to deliver cytotoxic molecules into cancer cells by tumor specific antibodies via receptor-mediated endocytosis (Panowski et al., 2014). Mechanistically, mAb 19E9 binds to MICA on the surface of a cancer cell. The 19E9-PBD conjugate is subsequently

endocytosed by the cell, where the PBD binds and causes DNA damage, followed by cell death of the cancerous cell. For these experiments, MICAgen mouse model was selected (see above).

The aim of this animal experiment was to explore the therapeutic efficacy of 19E9-PBD conjugated antibody in various established mouse cancer models. First, the potency of 19E9-PBD was tested against B16F10-MICA expressing tumors. Various doses and treatment intervals were compared over the course of the mouse study (Table 1).

Name	Treatment antibody	Dose 1	Dose 2	Dose 3
Group 1	19E9-PBD	1 mg/kg	-	-
Group 2	19E9-PBD	1 mg/kg	1 mg/kg	1 mg/kg
Group 3	19E9-PBD	2 mg/kg	-	-
Group 4	IC-PBD	1 mg/kg	1 mg/kg	1 mg/kg
Group 5	IC-PBD	2 mg/kg	-	-

Table 1. Treatment groups in 19E9-PBD treatment of B16F10-MICA tumors.

The obtained results clearly show the tremendous benefit of 2 mg/ml when administered only one time compared to other doses at various treatment intervals (Figure 27 A-C, 21 A). The mean tumor volume was significantly lower in 19E9-PBD at all doses relative to their respective isotype (IC) controls (Figure 27 B). These observations are also reflected in the growth rate in Figure 28 A which depicts significant benefit of 19E9-PBD (2 mg/ml) over the isotype control (IC) and 19E9-PBD (1 mg/ml) dose as well. Moreover, no therapeutic advantage from administration of 3 doses of 1 mg/ml over 1 dose of 1 mg/ml was observed (Figure 28 A). Overall survival of MICAgen mice was greatly improved as well (Figure 27 C). During the course of the study, the body weight of the animals was carefully monitored as an indicator of 19E9-PBD safety. No weight loss was observed in MICAgen mice for the duration of the study (Figure 28 B), indicating that 19E9-PDB and IC-PBD at all dose levels was safe for the tested animals. When tumor size reached 1300 mm^3, animals were sacrificed and collected tumor tissue was analyzed by flow cytometry.

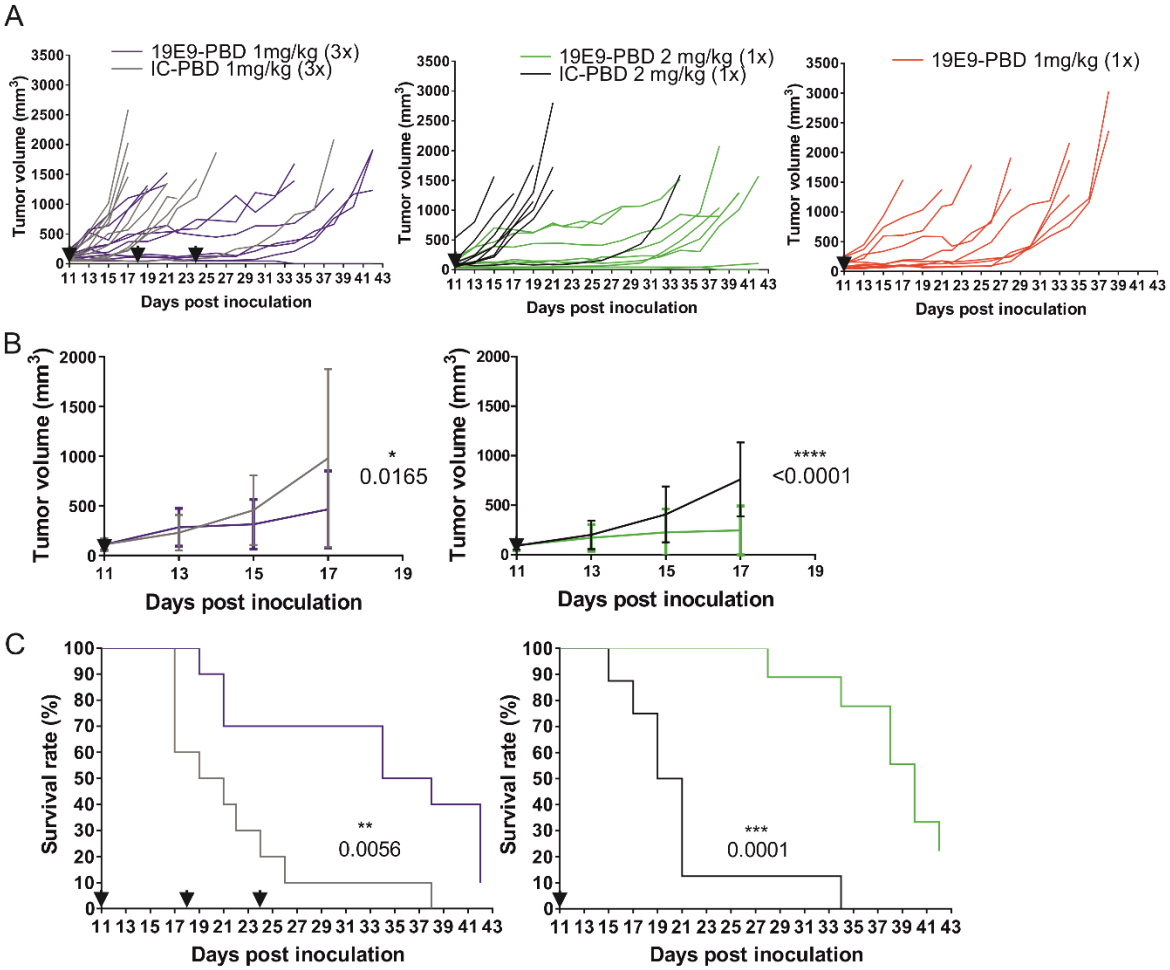

Figure 27. Efficacy of 19E9-PBD in therapy of B16F10 MICA tumors. MICAgen mice were inoculated with 10^4 B16F10-MICA*001 cells and, upon day 11 when tumors reached the defined threshold size were treated with 19E9-PBD or isotype control. Arrows indicate days of injection. A.) Tumor growth (mm^3) of individual mice per group is shown. B.) Average tumor volume (mm^3) per treatment group is shown. Statistical significance for differences in average tumor growth between days 11 and 17 was assessed. (Mean + SEM, Two-way ANOVA + Sidak's multiple comparison test) C.) Survival rate (%) of MICAgen mice (Log-rank test). Treatment at days 11, 18 and 24. When mice were treated only once, the day of treatment was on day 11. Duration of the experiment was up to 42 days.

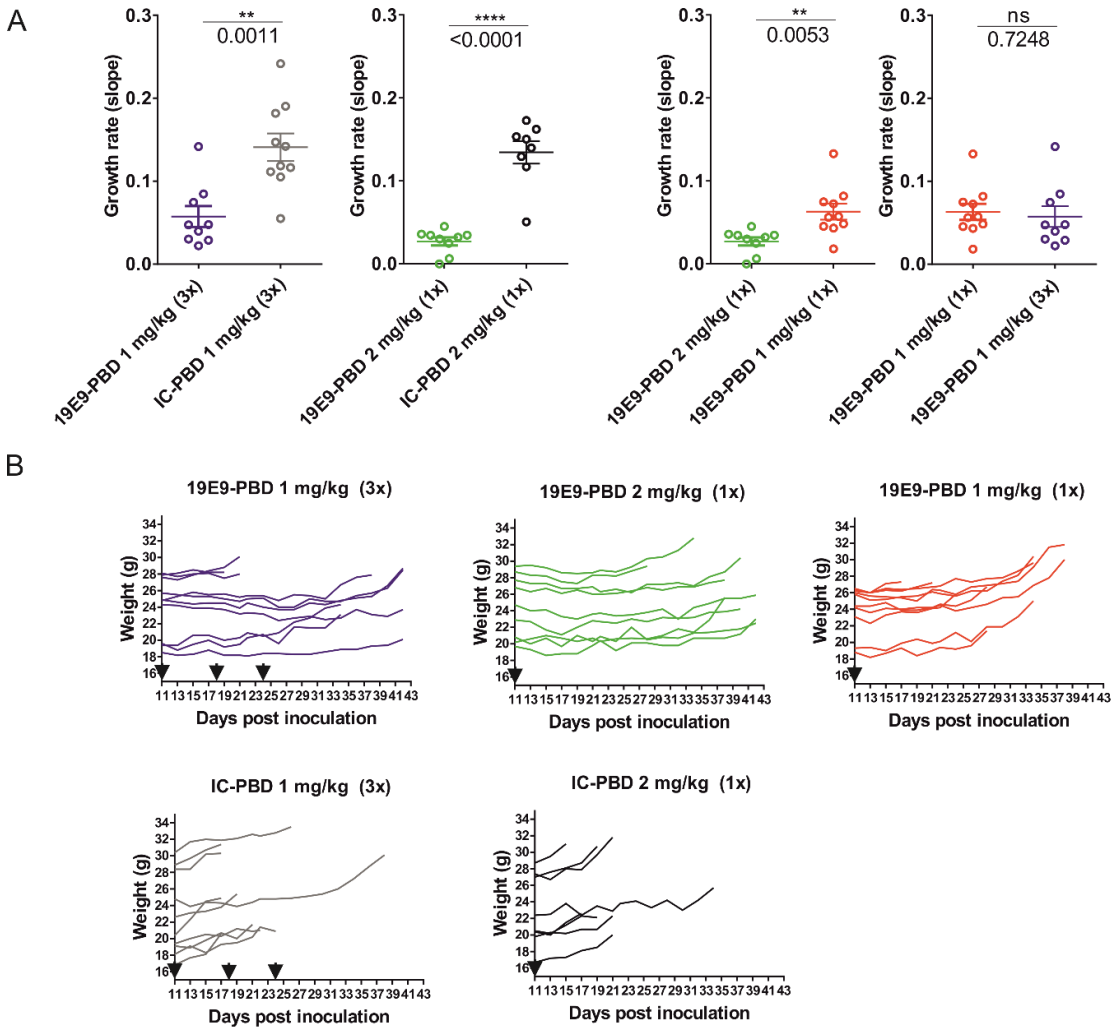

Figure 28. Efficacy of 19E9-PBD in therapy of B16F10 MICA tumors. MICAgen mice were inoculated with 10^4 B16F10-MICA*001 cells and, upon day 11 when tumors reached the defined threshold size, treated either with 19E9-PBD or an isotype control. A.) Tumor growth rate was calculated by log transforming the tumor volume, and the slope of each tumor is calculated individually. Each dot is representing one mouse. Unpaired t-test was used. B.) Body weight (g) of individual mice per group is shown. Body weight was measured every two days. Duration of the experiment was up to 42 days.

Flow cytometry results show a statistically significant decrease of NKG2D expression on γδ TILs (γδ tumor-infiltrating lymphocytes) in the 2 mg/kg (1x) treatment group (Figure 29 A-B). Additionally, a statistically significant decrease of total percentage of γδ T cells (defined as % of $CD3^+$ cells) was shown in the same treatment group (Figure 29 C). Such differences were not observed in other tumor-infiltrating lymphocytes (TILs) studied across all other treatment groups with respect to their isotype controls (Figure 30).

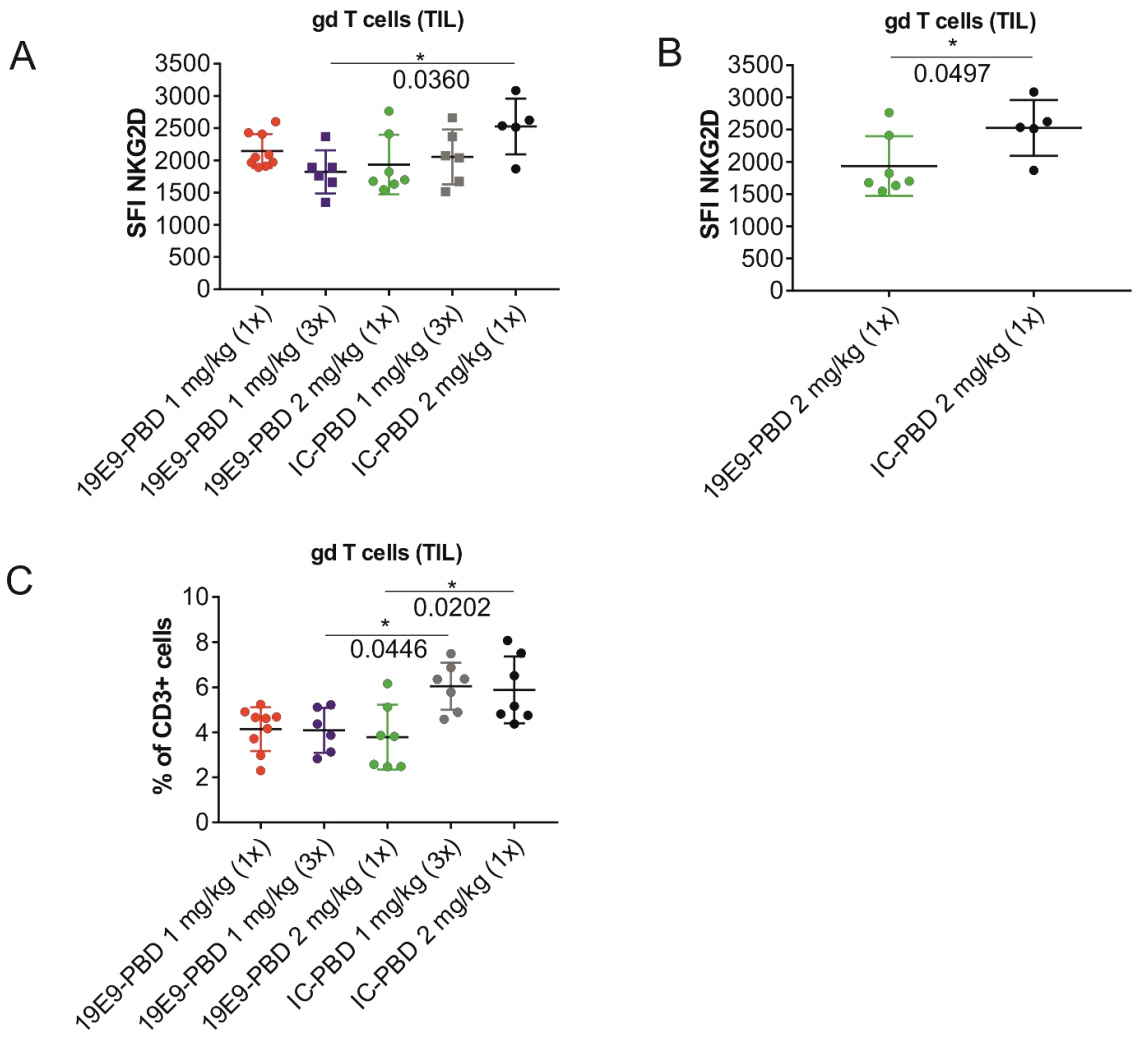

Figure 29. Efficacy of 19E9-PBD in therapy of B16F10 MICA tumors. Flow cytometry analysis of TILs. A.) NKG2D expression (SFI) on γδ TILs. One-way ANOVA statistical analysis. B.) NKG2D expression (SFI) on γδ TILs compared in 2 mg/kg (1x) treatment groups. Unpaired t-test analysis. C.) Percentage of γδ TILs (CD3+ γδ TCR+). One-way ANOVA statistical analysis. SFI=specific fluorescence intensity.

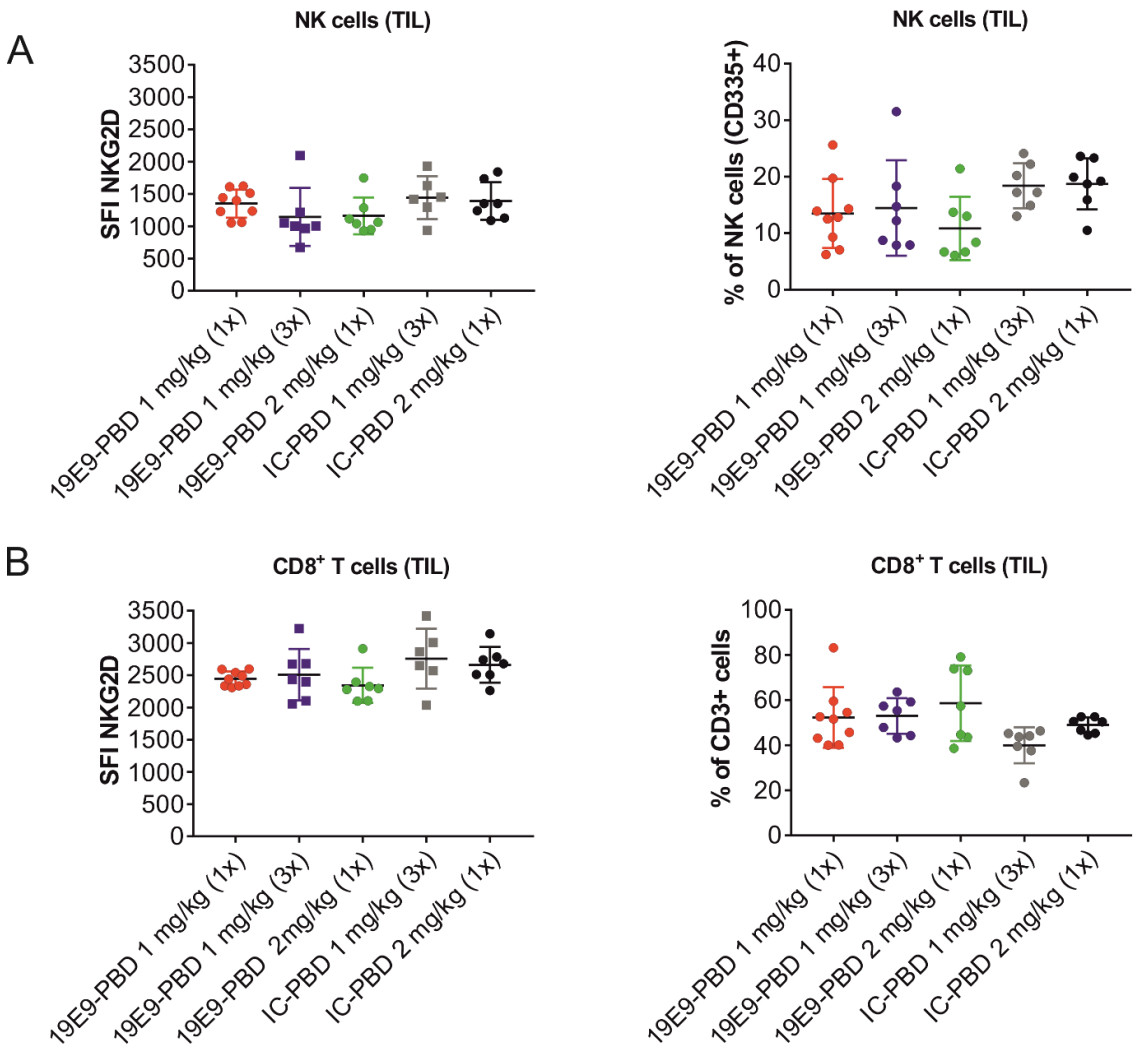

Figure 30. Efficacy of 19E9-PBD in therapy of B16F10 MICA tumors. Flow cytometry analysis of TILs. A.) Left - NKG2D expression (SFI) on NK cells (CD3-CD335+/NKp46+). Right – Frequency (%) of NK cells (CD3-CD335+/NKp46+). B.) Left – NKG2D expression (SFI) on $CD8^+$ T cells (CD3+CD8+). Right – frequency of $CD8^+$ T cells (CD3+CD8+). One-way ANOVA statistical analysis. SFI=specific fluorescence intensity.

Moreover, TILs in tumor draining lymph nodes were also analyzed, as lymph nodes are important peripheral lymphoid organs where antigen and lymphocytes eventually encounter each other. After this encounter, lymphocytes travel to the tumor site where they are required to perform cytotoxicity and clear cancer cells. The flow cytometry results showed no differences in SFI NKG2D on NK cells or percentage of NKG2D+ γδ T cells among all experimental groups (Figure 31).

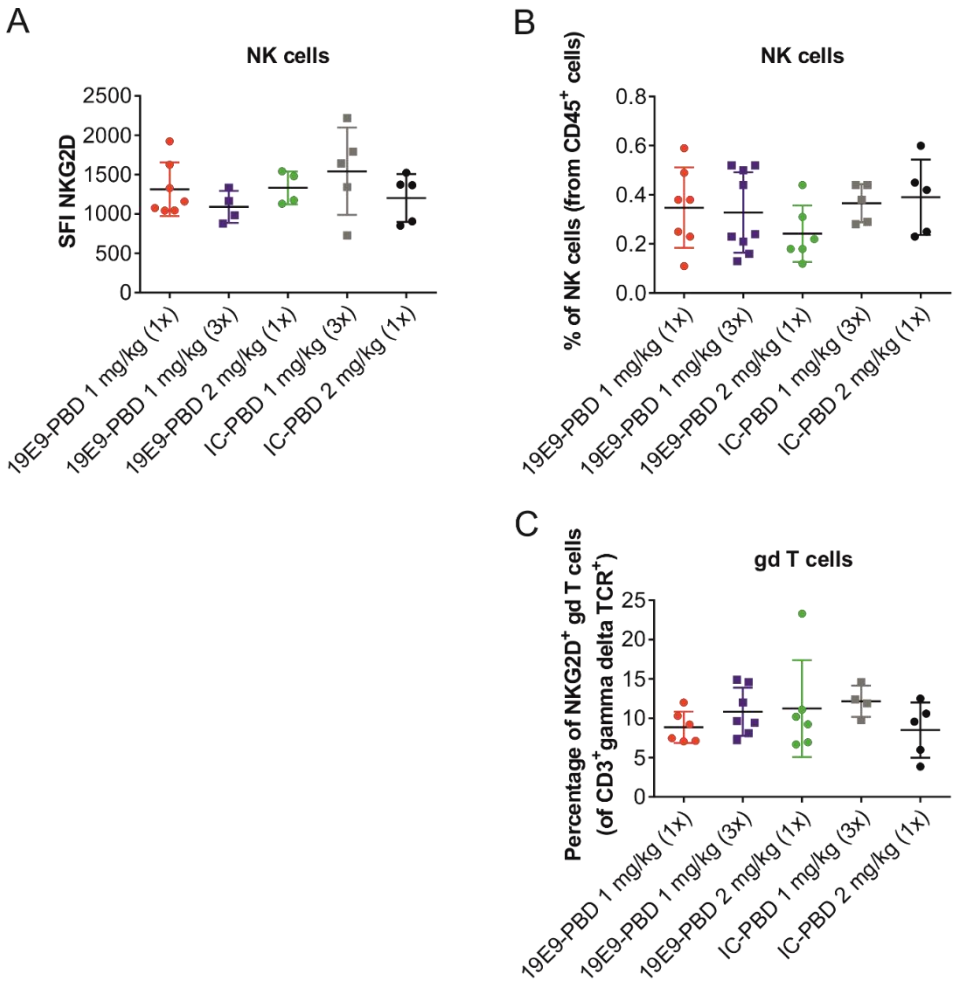

Figure 31. Efficacy of 19E9-PBD in therapy of B16F10 MICA tumors. Flow cytometry analysis of lymphocytes in tumor-draining lymph nodes (TdLN). A.) NKG2D expression (SFI) on NK cells (CD3-CD335+/NKp46+). B.) Frequency of NK cells (CD45+CD3-CD335+/NKp46+). C.) Frequency of γδ T cells (CD3+ γδTCR+). One-way ANOVA statistical analysis performed. SFI=specific fluorescence intensity.

Because 19E9 is an anti-MICA antibody, MICA expression on the B16F10 MICA tumors was studied. Flow cytometry analysis showed that treatment with 19E9-PBD did not alter the expression of surface MICA on tumor cells among all treatment groups (Figure 32 A). Of note, MICA expression on myeloid-derived suppressor cells (MDSCs) in 19E9-PBD treatment groups (both 1 mg/kg (3x) and 2 mg/kg (1x)) was significantly lower than in isotype-treated groups. However, the total percentage of MDSCs was comparable among the treatment groups (Figure 32 B-D).

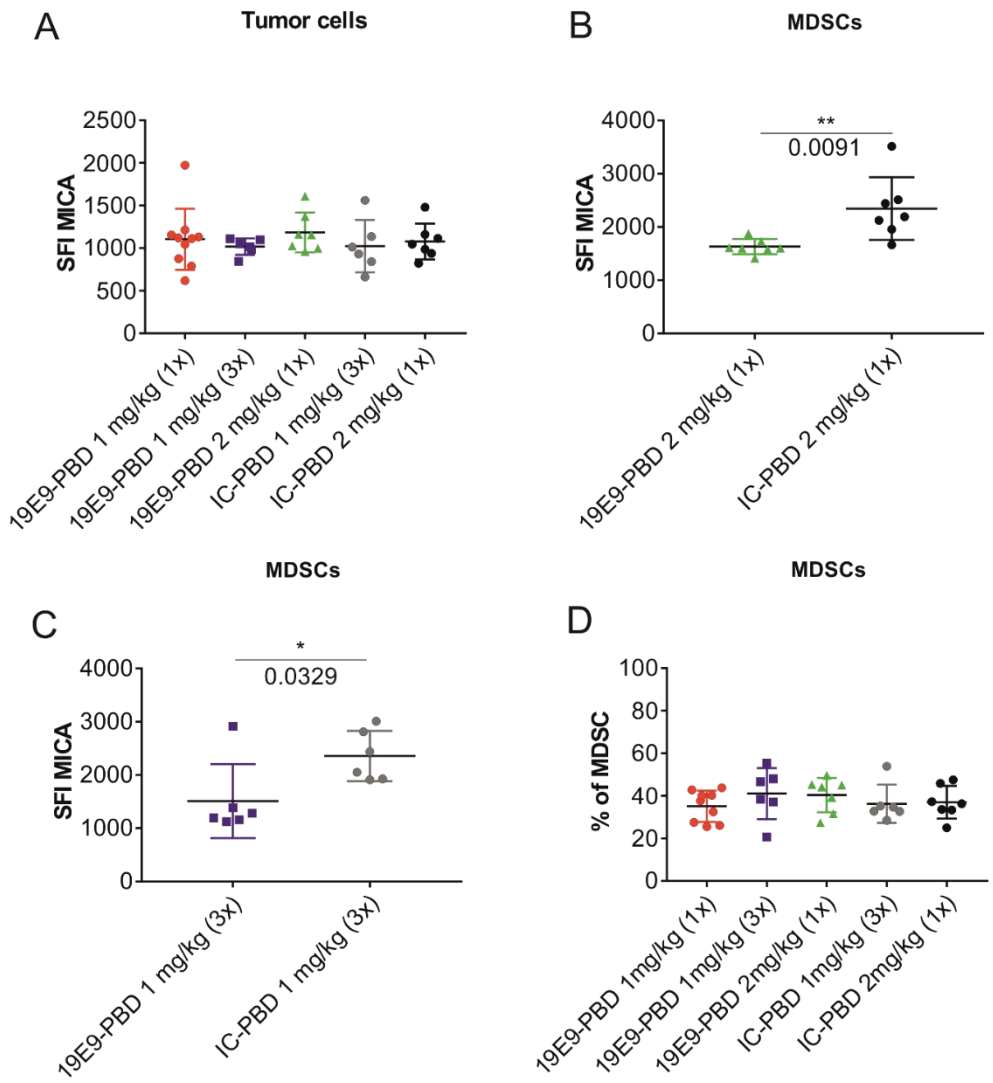

Figure 32. Efficacy of 19E9-PBD in therapy of B16F10 MICA tumors. Flow cytometry of tumor tissue. A.) Surface expression of MICA on tumor cells harvested from MICAgen mice. B.) Comparison of surface expression of MICA on tumor myeloid-derived suppressor cells (MDSCs) between treatment groups 19E9-PBD 2 mg/kg (1x) and the respective isotype control. C.) Comparison of surface expression of MICA on MDSCs between treatment groups 19E9-PBD 1 mg/kg (3x) and the respective isotype control. D.) Frequencies of MDSCs among all treatment groups. MDSCs were defined as $CD3^{-}CD19^{-}CD11b^{+}Gr1^{+}$. Unpaired t-test and One-way ANOVA was performed for statistical analysis.

Taken together, the toxin-conjugated antibody 19E9-PBD significantly delayed the growth of B16F10 MICA tumors and improved the overall survival of MICAgen mice. There were no observed side effects of 19E9-PBD even for higher doses (2 mg/kg). Flow cytometry analysis demonstrated that therapeutic administration of 19E9-PBD shaped TILs and MDSCs.

Based on the recognized better therapeutic effectiveness of the dose of 19E9-PBD 2 mg/kg, an optimized experimental configuration with another cancer model of RMA-MICA was tested (Table 2).

Name	Treatment antibody	Dose 1	Dose 2	Dose 3
Group 1	19E9-PBD	1 mg/kg	1 mg/kg	1 mg/kg
Group 2	19E9-PBD	2 mg/kg	-	-
Group 3	19E9-PBD	2 mg/kg	2 mg/kg	2 mg/kg
Group 4	IC-PBD	2 mg/kg	-	-
Group 5	IC-PBD	2 mg/kg	2 mg/kg	2 mg/kg

Table 2. Treatment groups in 19E9-PBD treatment of RMA-MICA tumors.

Intravenous administration of 19E9-PBD at all tested doses was able to contain the growth of the RMA-MICA lymphoma (Figure 33 A). It should be noted that isotype control eventually caused a decrease in the size of the tumors, as well. The possible causes are elaborated in the discussion chapter. In this study, no weight loss was observed in MICAgen mice and, therefore, the administered dose was concluded to be safe (Figure 33 B).

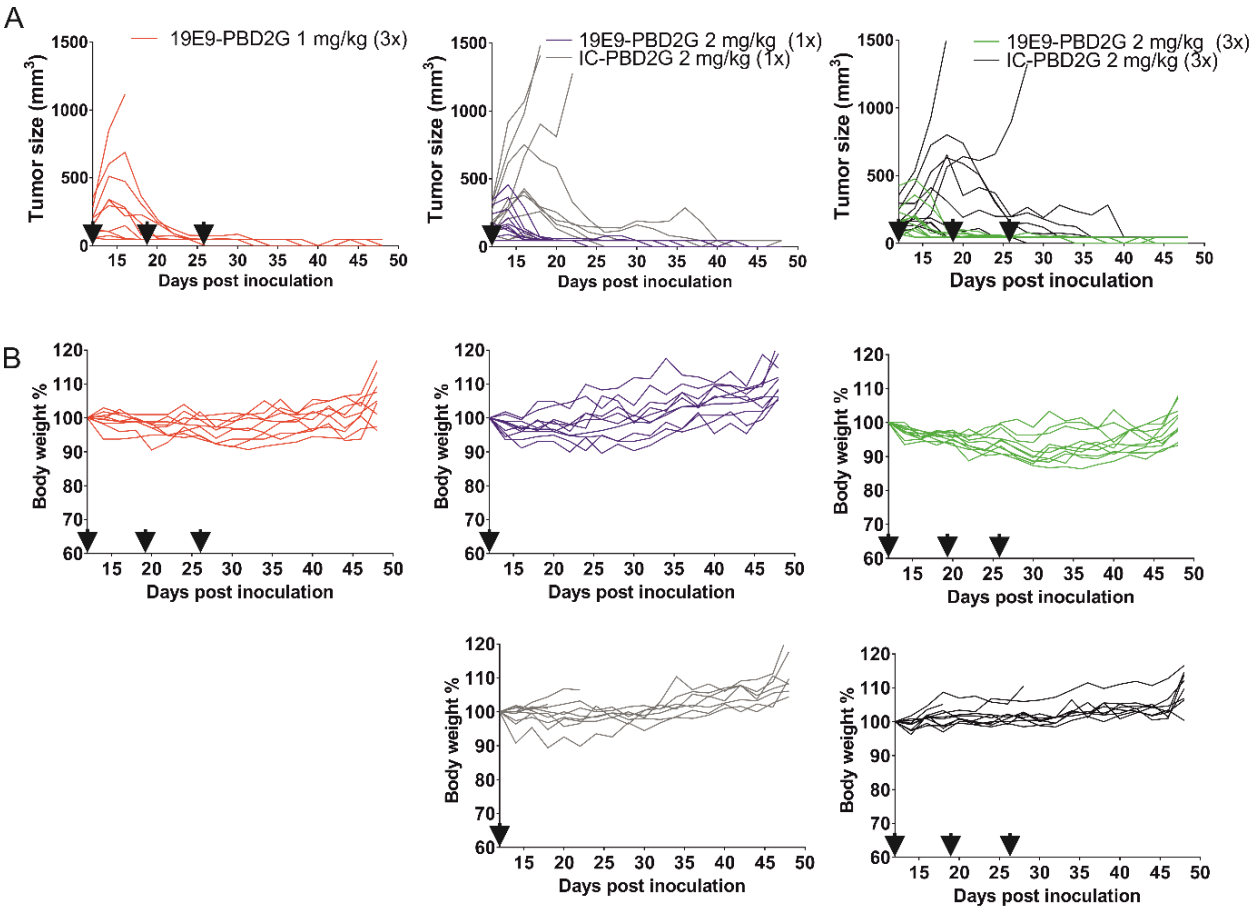

Figure 33. Efficacy of 19E9-PBD in therapy of RMA MICA tumors. MICAgen mice were inoculated s.c. with $3x10^4$ RMA-MICA*07 cells (in matrigel). On day 12, when the tumor cohort had reached the defined threshold, mice were randomized into five treatment groups with ten mice per group with a similar average tumor size. Subsequently, all mice were treated with either 19E9-PBD or IC-PBD (i.v. injection) up to three times. A.) Tumor growth of individual mice is shown. Arrows indicate days of antibody injection. n= 10 mice per group. B.) Body weight of individual tumor-bearing mice is shown. Body weight at day 12 set as 100%. Duration of the experiment was up to 48 days.

Following the initial experiments, higher doses of 19E9-PBD were tested in a MC38-MICA cancer model in MICAgen mice (Table 3). MC38 is an established aggressive cell line derived from C57BL6 murine colon carcinoma. Tumor growth in individual mice was significantly delayed in the 19E9-PBD treated groups; however, unfortunately, a weight loss in MICAgen mice was observed as a result of a too high dosage. Therefore, the experiment was stopped for the well-being of the animals.

Name	Treatment antibody	Dose 1	Dose 2	Dose 3
Group 1	19E9-PBD	7.8 mg/kg	-	-
Group 2	19E9-PBD	7.8 mg/kg	4 mg/kg	-
Group 3	19E9-PBD	3.15 mg/kg	2 mg/kg	2 mg/kg
Group 4	IC-PBD	4,52 mg/kg		
Group 5	IC-PBD	4,52 mg/kg	4 mg/kg	4 mg/kg

Table 3. Treatment groups in 19E9-PBD treatment of MC38-MICA tumors.

Many clinical studies test combinations of different agents, (e.g., checkpoint inhibitors PD-1 in combination with CTLA-4), to improve their individual desired therapeutic efficacy. It has proven to be a useful therapeutic strategy and, therefore, the benefits of 19E9-PBD were evaluated in combination with PD-1 checkpoint inhibitor in the treatment of established B16F10-MICA tumors. MICAgen mice were treated intravenously (caudal tail vein) and the treatment regime is shown in the Figure 34. The objective of this experiment was to ascertain the additional therapeutic effect of the 19E9-PBD antibody on the effectiveness of the PD-1 antibody. Tumor growth analysis revealed that monotherapy (either with PD-1 or with 19E9-PBD) was substantially effective at controlling the tumor growth. In addition, combination therapy showed a tremendous success in inhibiting of the tumor growth compared to the monotherapy or only isotype treated group. However, in the long term, a further effect of 19E9-PBD on the PD-1 antibody was not demonstrated (Figure 34). Tumor growth rate (Figure 34 A) and overall survival analysis (Figure 34 B) showed that there was no significant therapeutic advantage of combinatory therapy when compared to each individual therapy alone (in combination with Isotype control).

In summary, the toxin conjugated anti-MICA antibody 19E9-PBD was safe to deliver in MICAgen mice and substantially controlled the tumor growth of different aggressive murine carcinomas. Hence, it makes it an ideal candidate for further investigations since it can be a useful tool for cancer treatment applications.

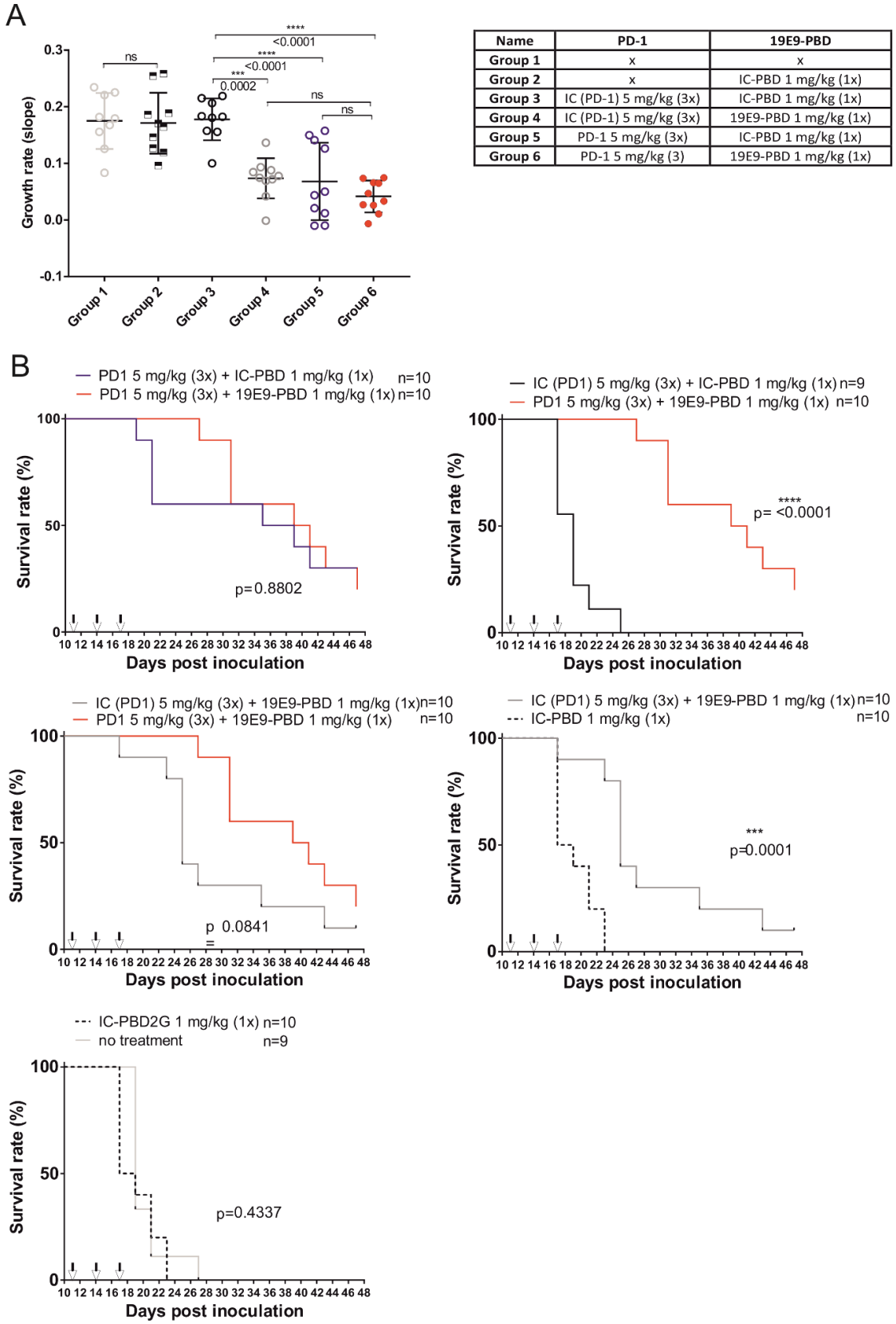

Name	PD-1	19E9-PBD
Group 1	x	x
Group 2	x	IC-PBD 1 mg/kg (1x)
Group 3	IC (PD-1) 5 mg/kg (3x)	IC-PBD 1 mg/kg (1x)
Group 4	IC (PD-1) 5 mg/kg (3x)	19E9-PBD 1 mg/kg (1x)
Group 5	PD-1 5 mg/kg (3x)	IC-PBD 1 mg/kg (1x)
Group 6	PD-1 5 mg/kg (3)	19E9-PBD 1 mg/kg (1x)

Figure 34. Therapeutic efficacy of 19E9-PBD2G in combination with anti-PD1 in treatment of established B16F10-MICA tumors- tumor growth rate. MICAgen mice were inoculated s.c. with 10^4 B16F10-MICA cells (in matrigel). On day 11, when the tumor cohort had reached the defined threshold, mice were randomized into six treatment groups with ten or nine mice per group with a similar average tumor size. Subsequently, all mice were treated intravenously (i.v.)

as stated in the Table (A-right). Statistical significance for differences in tumor growth rate was assessed with One-way ANOVA. Statistical significance for differences in survival was assessed using Log-rank (Mantel-Cox) test. Duration of the experiment was up to 47 days.

8 Discussion

8.1 BAMO3 inhibits proteolytic shedding of MICA by tumor cells in a dose-dependent and cell-specific manner

Monoclonal antibodies are commonly used as a therapeutic tool in patients with a wide variety of diseases from autoimmune disorders to carcinomas (Drewe & Powell, 2002; Boyiadzis & Foon, 2008; Yasunaga 2019). They are used either as monotherapy or in combination with other antibodies or therapeutic agents (Henricks et al., 2015; Corraliza-Gorjón et al., 2017). The aim of this thesis was to describe a monoclonal antibody against MICA/B – i.e., BAMO3 - and test its therapeutic efficacy in a cancer mouse model *in vivo* and *in vitro*. MICA/B is a stress ligand that is ectopically expressed on stressed cells, e.g., on virus- or bacteria-infected cells or on cancerous cells. The expression of MICA/B is strictly regulated and its expression under physiological conditions was reported prevalently in the gastrointestinal tract in humans (Groh et al., 1996). Higher levels of sMICA/B, as a consequence of MICA/B, shedding have been observed in patients with various carcinomas (Holdenrieder et al., 2006). Moreover, high serum sMICA levels negatively correlated with overall survival in cancer patients (Li et al., 2013; Rebmann et al., 2007; Chen et al., 2022). Therefore, these properties mark MICA/B shedding as an interesting candidate for cancer studies. When BAMO3 is applied to MICA/B-expressing cancer cell lines *in vitro*, the concentration of sMICA/B is decreasing with increasing concentrations of BAMO3. The shedding inhibition is very efficient as BAMO3 was able to prevent MICA/B shedding at very low concentrations, as low as 0.1 µg/ml, and at 10 µg/ml the MICA/B shedding was almost completely blocked. BAMO3 is widely applicable as it prevented shedding of different MICA and MICB allelic variants expressed by various cancer cell lines. The epitope of BAMO3 was investigated and mapped to the membrane-proximal site of the MICA α3 domain. Two amino acids were identified as crucial for BAMO3 binding to MICA – aspartic acid 219 (Asp219) and glutamine 255 (Gln255). When these amino acids in MICA*007 were mutated to alanine, BAMO3 did not longer bind to its target MICA. As a control in this experiment, another anti-MICA antibody BAMO1 with a known epitope in the α1/α2 superdomain of MICA was used to confirm the expression of mutant MICA in the experimental samples.

Apart from inhibition of sMICA/B shedding into the cell culture supernatant, the surface expression of MICA/B on cancer cells following BAMO3 treatment was studied. An increased surface expression of MICA/B after mAb BAMO3 treatment in comparison to IgG2a treatment was anticipated (Figure 35). The rationale behind this hypothesis is that decreased MICA/B shedding would lead to an increased expression of MICA/B on the surface of a target cell and

that in turn would trigger a stronger NKG2D-mediated immune response by cytotoxic lymphocyte (Figure 35). As mentioned previously, sMICA is detected in sera of cancer patients and is considered as a cancer marker. Through MICA shedding inhibition and stabilizing of surface bound MICA, we could achieve stronger NKG2DL-NKG2D interaction and thereby tumor control. Flow cytometry analysis showed us that we could achieve increased expression of surface bound MICA on human cells rather than on mouse cells. One of the reasons might be that MICA is a human ligand and we transfected it into mouse cell lines that endogenously do not express MICA on their surface. For example, when A375 cells (human melanoma) were treated with BAMO3, a clear increase of expression of MICA and also of MICB at the cell surface was observed. MICA and MICB are endogenously expressed by A375 cells. However, when the isolated MICA cDNA from these cells was stably transfected into B16F10 cells (mouse melanoma), no increased MICA expression after BAMO3 treatment was observed. Nevertheless, when the A375 MICA cDNA was transfected in C1R human lymphoma cells, increased MICA surface expression upon BAMO3 treatment was observed again. Therefore, these results support the view that BAMO3 increases MICA expression on human cells rather than on mouse cells *in vitro*. Of note, MICB*002 allele behaved differently. An increased MICB*002 expression after BAMO3 treatment on the surface of cancer cells was observed, regardless of their origin (human or mouse). There are several possibilities to explain this phenomenon. Probably the reasons are due to the several differences of MICA and MICB stated across the available literature. It might be the diverse role of ADAM 10 and ADAM 17 in MICA/B shedding or perhaps a position of two amino acids identified as the BAMO3 epitope in MICA and MICB crystal structure. Literature states that MICA and MICB are closely related and share about 91% identity in their coding sequences (Bahram et al., 1994). However, there is evidence showing that although ADAM10 or ADAM17 is required for MICA shedding, both proteases can replace each other. With respect to MICB, ADAM10 appeared to play a minor role, while the downregulation of ADAM17 nearly completely blocked sMICB release. Additionally, MICA shedding was primarily mediated by ADAM17, whereas MICB required both ADAM10 and ADAM17 as downregulation of either one almost completely inhibited MICB shedding (Chitadze et al., 2013). When looking at the crystal structure of MICB and the BAMO3 epitope, the amino acid Gln 255 is placed in a short loop between two antiparallel β-sheets (Figure 36). In the future, options of SPR measurements are to be exploited to study affinity strength of MICA and MICB to BAMO3 and decipher whether there are any differences that would explain this observed phenomenon. Probably, it would be essential to study ERp5 expression and regulation patterns on the surface of these cells to support these ideas.

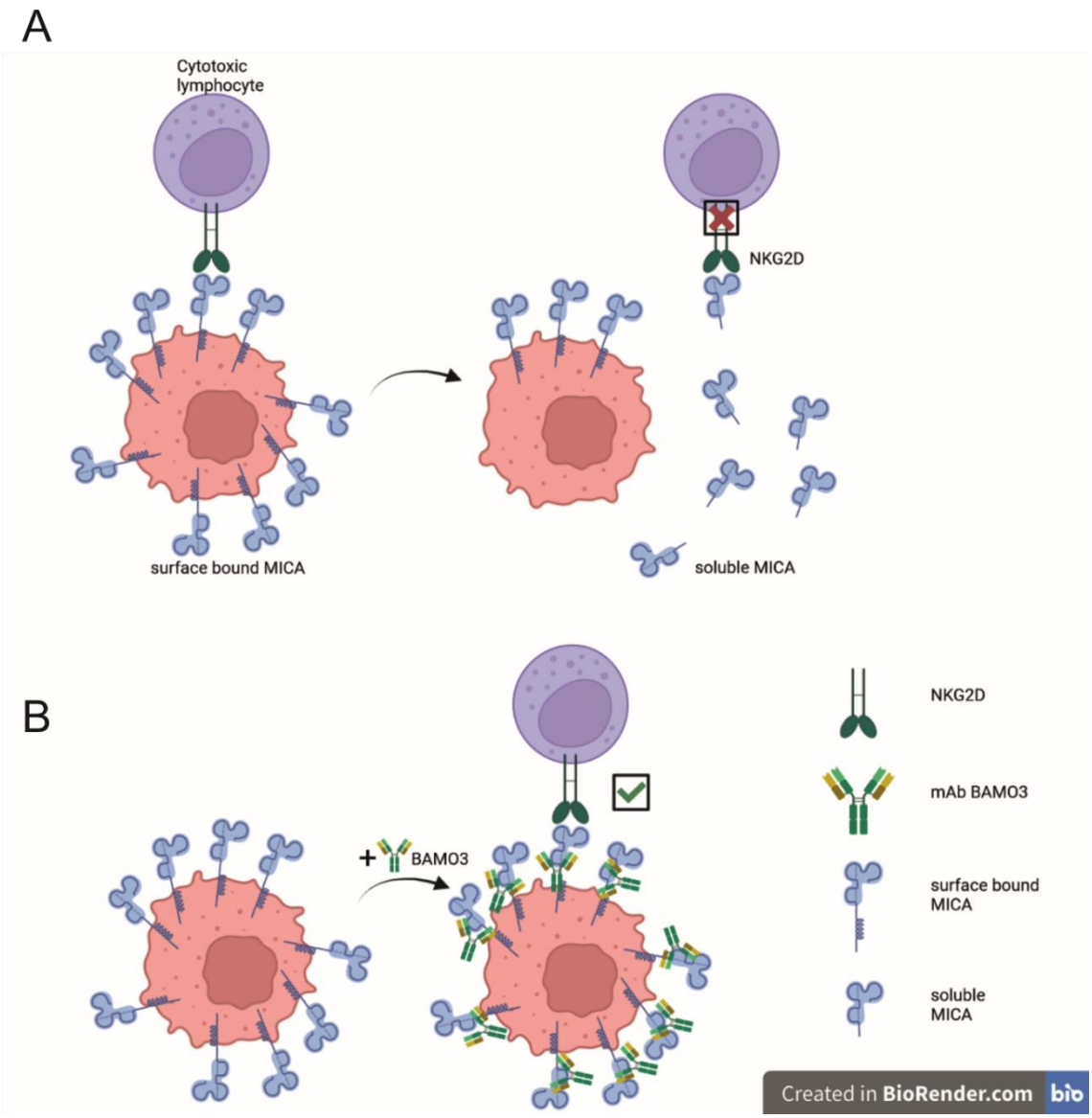

Figure 35. Proposed molecular mechanism of BAMO3 mAb. A.) MICA is shed from the surface of a cancer cell and thereby weakening NKG2DL/NKG2D axis. B.) Administration of BAMO3 leads to inhibition of MICA shedding and simultaneously strengthening of surface bound MICA expression, hence restoring the NKG2D-MICA axis leading to cytotoxicity of cancer cells. Created in BioRender.com

Based on these findings, several hypotheses of molecular mechanism of BAMO3 can be suggested. First of all, the BAMO3 epitope is close to the membrane proximal site where potentially metalloproteases would bind and proteolytically cleave MICA from the cell surface. Therefore, BAMO3 is proposed to act by steric hindrance and hence preventing MICA shedding. Another option that can be considered is the size of BAMO3 and its position when bound to MICA. It is imaginable that just a physical size of BAMO3 could prevent some molecules, such as metalloproteases ADAM10/17 or ERp5 (that are involved in the process of MICA shedding) to engage MICA and by doing so preventing MICA shedding from the surface of a stressed cell.

There is an obvious reason to inhibit MICA and MICB shedding in cancer therapy as it was described as a negative prognostic factor for overall survival of cancer patients (Rebmann et al., 2007; Li et al., 2013). Higher expression of ADAM17 was found in clinical samples from patients with bladder cancer (Pichler et al., 2021). Moreover, other publications described over-expression of ADAM 10 in patients with oral squamous carcinoma (Jones et al., 2013) and ADAM 17 in esophageal squamous cell carcinoma (Liu et al., 2015). Moreover, over-expression of ADAM 17 was found on various cancer cells, such as breast, ovarian and prostate cancer cells (Sinnathamby et al., 2011). Numerous clinical trials attempted to use therapeutic drugs in cancer patients to block metalloproteases' activity to inhibit tumor growth. Unfortunately, these studies had to be terminated because patients experienced severe negative side effects during their treatment and these broad-spectrum metalloprotease inhibitors did not improve the outcome of chemotherapy (Heath et al., 2006; Sparano et al., 2004). The reason behind the negative effects is simple. Metalloproteases have crucial role in shedding of important membrane-associated proteins in a number of physiological processes, such as cell adhesion, migration, cellular signalling, and proteolysis (Giebeler & Zingrino, 2016). However, some recently developed MMP-inhibiting monoclonal antibodies have demonstrated promising antitumor effects in preclinical breast cancer models (Kwon, 2023). As metalloprotease inhibition is not a suitable treatment option, there is a need to develop other means of cancer therapy. Monoclonal antibodies are ideal candidates, and we propose BAMO3 as a suitable therapeutic to be further exploited. Probably best in combination with such MMP-inhibiting monoclonal antibodies.

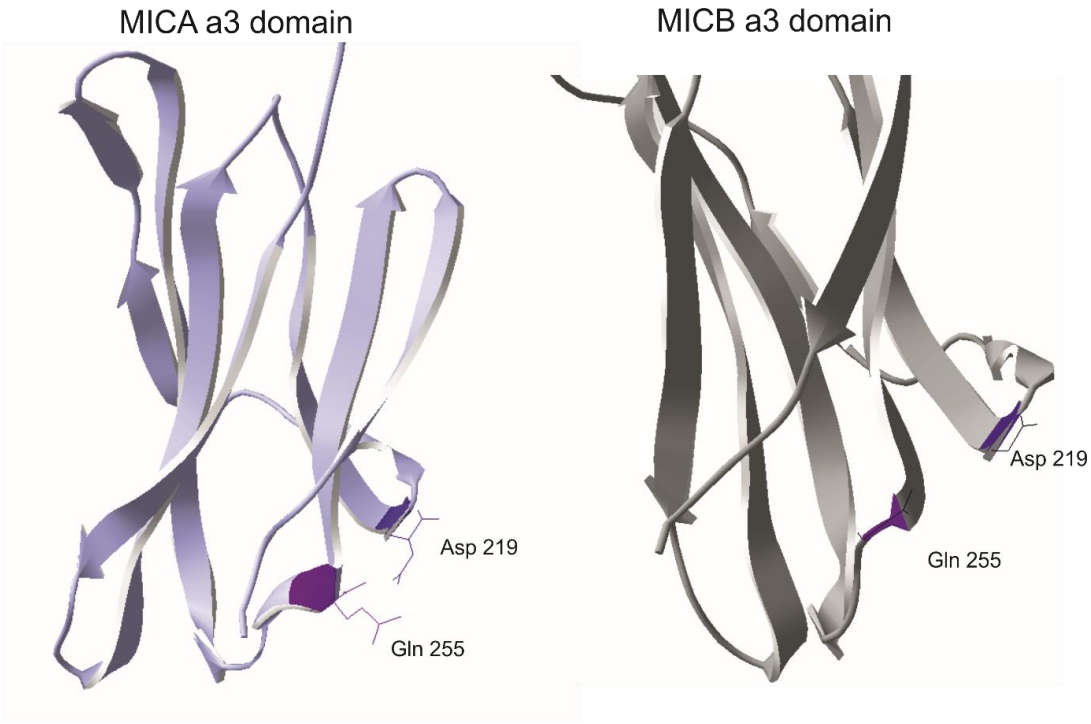

Figure 36. BAMO3 mAb epitope depicted in MICA (Left) and MICB (Right) α3 domain. BAMO3 epitope was mapped to the amino acids Asp 219 and Gln 255.

8.2 Mutation of Cysteine 250 in the MICA α3 domain alleviates MICA shedding

As noted in the previous chapters, MICA and MICB are highly polymorphic and are proteolytically shed from tumor cells by metalloproteases ADAM10 and ADAM17. This result chapter dealt with cysteine 250 in MICA molecule and its impact on MICA shedding. Exchange of Cysteine 250 for alanine or serine in MICA*007 allele resulted in reduced shedding of MICA *in vitro*. Moreover, the ADAM17 stimulant PMA but not the ADAM10 stimulant ionomycin was able to further stimulate Cys250Ala MICA shedding. Therefore, cysteine 250 might be important in the context of MICA shedding by ADAM10 sheddase. Decreased expression of ADAM10 on the cells carrying mutated MICA*007 C250A and C250S was shown. Moreover, these transfectants displayed increased MICA surface expression. Co-immunoprecipitation experiments revealed a weaker physical interaction of MICA*007 C250A and ADAM10 than a physical interaction of WT MICA*007 and ADAM10. Of note, the weaker signal for co-immunoprecipitation could be considered as a direct result of a decreased expression (shown by flow cytometry) and lower total protein content (shown by Western blot). The Western blot analysis revealed a lower total protein content of C250A MICA*007 and digestion with EndoH revealed that ADAM10 in these cells is not intracellularly retained. For this reason, this observation might be proposing that

ADAM10 could be shed from the surface of B16F10 cells. Some studies from 2009 suggested that ADAM10 is likely to be subjected to shedding by other ADAM metalloprotease - ADAM9 (Parkin & Harris, 2009) and ADAM 15 (Tousseyn et al., 2009). Therefore, further experiments to validate this hypothesis are needed, i.e., by ELISA measurement of shed ADAM10 in the supernatant of these cells. Interestingly, mutation of cysteine 190 to alanine or serine in MICB*002 allele did not interfere with shedding ability or their presentation on the surface of COS7 cells. Another publication reported that a 6 amino-acid mutation in the α3 domain of MICA*001 resulted in shedding resistance of MICA (Wang et al., 2009). This mutated site was defined as a binding site for ERp5 – the protein that is involved in mechanism of MICA/B shedding. When this particular mutant was introduced in B16F10 cells in order to reproduce these results, the abovementioned shedding resistance was not observed.

8.3 Length of alanine repeats in the transmembrane domain of MICA does not affect MICA shedding inhibition

Trinucleotide repeat microsatellite polymorphism (GCT)n (encoding for alanine) in the transmembrane domain of MICA were studied in this thesis. Mizuki and colleagues reported on a strong association of six alanine repeats in patients with Behçet disease (Mizuki et al., 1997). Other studies showed the same association in patients with oral squamous cell carcinoma (Liu et al., 2002), gatric cancer (Lo et al., 2004) and ulcerative colitis (Sugimura et al., 2001). Additionally, higher frequencies of MICA allele with 9 alanine repeats were shown in psoriatic arthritis (Gonzales et al., 2001) or type I diabetes (Lee et al., 2000). On the other hands, some studies suggest that MICA alleles with 5 and 9 alanine repeats may be an important protective factor for cancer in Caucasian populations (Ji et al., 2015). Interestingly, such repeats are not observed in MICB alleles. These observations could therefore suggest an important function of alanine repeats in numerous diseases. For this reason, the role of these alanine repeats was studied closer with the connection to sMICA production and shedding inhibition of MICA by BAMO3. The obtained results showed that the cells transfected with a plasmid carrying MICA*007 allele with 6 or 9 alanine repeats did not display greater shedding of sMICA. BAMO3 treatment of these cells did not result in an improved efficacy of MICA shedding inhibition, either. Taken together, length of alanine repeats in the transmembrane domain of MICA does not seem to play a significant role in shedding of MICA from the surface of cancer cells and BAMO3 mAb capacity to inhibit MICA shedding is not affected in any way.

8.4 BAMO3 therapeutic delivery delays growth of mouse MICA-positive lymphoma and improves overall survival of MICAgen mice

Immunotherapy as a research field of medicine is evolving rapidly and monoclonal antibodies (mAbs) have transformed therapy of numerous diseases, including cancer. Since the first FDA approval of mAbs for cancer therapy in 1997 (CD20-targeting rituximab) and in 1998 (HER2-targeting trastuzumab), mAbs became very effective pharmaceutical drugs (Goydel & Rader, 2021). Success of mAb therapy lies in several natural properties of the antibody molecule, such as 1) high specificity and affinity to the antigen, 2) the ability to block or enhance interactions between ligands and receptors and thereby engaging proteins and cells of the immune system to mediate cytotoxicity and 3) long half-life in blood circulation. BAMO3 mAb is an IgG2a mouse antibody that is specific for the α3 domain of MICA/B and is able to inhibit its shedding and thereby stabilizes MICA on the surface of cancer cells *in vitro*. To test therapeutic efficacy of mAb BAMO3 in a mouse tumor model, MICAgen mice inoculated with mouse lymphoma RMA cells expressing MICA*007 were treated with BAMO3. Intravenous delivery of mAb BAMO3 achieved a successful tumor growth control and improved overall survival of MICAgen mice. MICAgen mice reflect the human physiological expression of MICA that is restricted only to some organs of the gastrointestinal tract. This precisely emulates physiological expression of MICA in the human body (Kim et al., 2020). The MICAgen mouse model helped us to test for any negative side effects of this treatment that usually is observed in cancer patients receiving chemotherapy. The MICAgen mouse almost exactly replicates the physiological expression of MICA in humans and therefore it makes it an ideal model to assess potential adverse effects of the BAMO3 mAb. We can confirm that there are no negative side effects during the course of the study were observed and therefore we conclude safety of the BAMO3 mAb. Additionally, to understand the mechanism behind the therapeutic efficacy of BAMO3, tumor-infiltrating lymphocytes (TILs) and their NKG2D expression patterns were studied to elucidate which cytotoxic lymphocytes were responsible for tumor elimination. The results revealed several interesting facts: First, an increased NKG2D expression on tumor-infiltrating NK cells after BAMO3 treatment was observed. In addition, NKG2D expression on tumor-infiltrating $CD8^+$ T cells (TILs) was not found. It is important to mention that mouse $CD8^+$ T cells express NKG2D in state of activation. Moreover, IgG2a treatment led to elevated, but not statistically significant, frequencies of $CD39^+$ $CD8^+$ TILs. In the literature, the expression of CD39 on $CD8^+$ T cells defines a population of highly exhausted cells (Simoni et al., 2018). In colorectal and lung tumors, the absence of CD39 on $CD8^+$ TILs defines populations that lack hallmarks of chronic antigen stimulation at the tumor site, supporting their classification as bystanders. PD-1 (Programmed

death-1) expression on TILs and PD-L1 (programmed death-ligand 1) expression on tumor cells was studied. PD-1 is an important surface receptor that serves also as a T cell checkpoint. Because of all of the above-mentioned expression patterns of TILs in our studies, a prevalent cytotoxic function of NK tumor-infiltrating cells rather than CD8 or γδ T cells was assumed in elimination of RMA tumors in BAMO3 mAb therapy. Moreover, similar levels of sMICA in the sera of mice treated with BAMO3 and Isotype control was found. According to the *in vitro* data, lower sMICA levels in BAMO3 treated mice were expected. However, it is important to point out the fact that the blood was sampled on the day of a great tumor burden when essentially the BAMO3 therapy was failing. Therefore, we might not see the differences here for this reason. Perhaps we would see a difference in sMICA levels on the day 19, according to the tumor growth data when the tumor growth of BAMO3-treated animals was statistically significant lower than the tumor growth of control treated mice.

Multiple lines of evidence were provided that BAMO3 is safe and effective in tumor treatment. Taken together, BAMO3-mediated inhibition of MICA/B shedding by human tumors potentially represents a novel and broadly applicable treatment strategy of human tumors that may be used to complement the immunotherapeutic effects of immune checkpoint blockade.

During the course of these studies, another group published similar data on MICA/B shedding inhibiting antibody 7C6 (Ferrari de Andrade at al., 2018). This publication reported that *in vivo* application of 7C6 antibody resulted in NK cell- mediated tumor immunosurveillance. Further, they showed an increased MICA surface expression on cancer cells after antibody treatment that triggered antibody-dependent cellular cytotoxicity (ADCC) via CD16 on NK cells. Nevertheless, the mouse model used here is a limitation to this study. They used immunodeficient mice to avoid anti – MICA directed xenogeneic immune responses, as MICA is a human and not a mouse ligand. Further studies from 2020 and 2022 of this group showed that *in vivo* delivery of their antibody has resulted in elicitation of NK cell-mediated immune response against tumors that were resistant to cytotoxic T cells (Ferrari de Andrade et al., 2020) and induced macrophage-mediated immunity against acute myeloid leukemia (Alves da Silva et al., 2022). Another publication of this group reported that administration of their antibody triggered NK cell tumor immunity in patients with intrahepatic cholangiocarcinoma (Oliviero et al., 2022). Finally, the group of Wucherpfennig developed a cancer vaccine able to elicit a production of anti-MICA/B antibodies that inhibit MICA/B shedding, increase density of MICA on the surface of tumor cells and thereby are able to inhibit tumor growth by recruiting cytotoxic lymphocytes to the tumor site (Badrinath et al., 2022). Other unpublished data generated in our laboratory suggest a strong NKG2D-dependency in the therapeutic efficacy of BAMO3 treatment.

Intravenous delivery of BAMO3 in NKG2D-deficient mice bearing MICA-expressing tumors did not result in a significant delay of tumor growth or an enhanced mouse survival when compared to control-treated mice. Together with enhanced expression of NKG2D on tumor-infiltrating NK cells (from our RMA-MICA experiments), these observations strongly support the hypothesis that BAMO3 therapeutic efficacy is strongly dependent on the NKG2D/NKG2DL axis. Our unpublished data did not confirm BAMO3 inducement of ADCC, but *in vivo* studies suggest an NKG2D-dependent elimination of tumors in BAMO3 treatment. Another difference in BAMO3 and 7C6 is a different isotype of these two antibodies. 7C6 is IgG1 and BAMO3 is IgG2a. Thereby, molecular mechanism of BAMO3 and 7C6 antibody is suggested to be different in several aspects and can be perhaps used in different clinical applications or even in a combination therapy. In future, to determine whether BAMO3 binds MICA on the surface of cancer cells or MICA on the cells in the tumor microenvironment, and thereby eliciting anti-tumor immune response, we suggest taking advantage of our transfected B16F10 BAMO3-mutated cells that do not longer bind BAMO3. Inoculation of these tumor cells to MICAgen mice followed by BAMO3 treatment would reveal the binding site of BAMO3 *in vivo*. In order to discover which immune cell subsets are responsible for tumor elimination in BAMO3 therapy, depletion of different immune subsets by antibodies can be exploited; for example, depletion of NK cells by anti-NK1.1 antibody. Another alternative is to employ another mouse model that lacks certain immune cells, such as NK cell-deficient mice or T cell deficient mice. In order to further improve the therapeutic efficacy of BAMO3, other agents in combination with BAMO3 mAb could be exploited. For example, certain chemotherapeutics (already used in clinical praxis to treat cancer patients) like Cisplatin, Gemcitabine, Oxiplatin, or 5-fluorouracil are able to increase MICA surface expression on tumor cells (Gasser et al., 2005). An *in vitro* assay showed that repeated exposure to cisplatin resulted in an increased expression of NKG2D ligands, including MICA and MICB, in NSCLC (non-small cell lung cancer) cell lines. As a result, NK cell-cytotoxicity mediated via NKG2D axis was enhanced (Okita et al., 2016). Another therapeutic option that could be used in combination with BAMO3 mAb is newly emerging NKG2D-CAR-transduced NK or T cells. CAR T cells have been FDA approved and are currently used in cancer therapy. New immune therapies using CAR-T/NK cells are still actively being developed for cancer patients that are resistant to conventional therapies. A CAR (chimeric antigen receptor) is a synthetic receptor that enables tumor-specific antigen recognition. Usually, the intracellular signaling domain contains CD3ζ signaling moiety and is often fused to one or more co-stimulatory domains to enhance strength of downstream signaling (Weinkove et al., 2019). NKG2D portion of CAR T/NK cell allows direct targeting of NKG2D ligands. A recent publication from 2021 tested such NK cells and showed that NKG2D-CAR-NK cells exhibited great *in vitro* cytotoxicity against multiple myeloma cells, while showing minimal

activity against healthy cells (Leivas et al., 2021). Currently, there are number of clinical trials using NKG2D-based CAR T, NK or γδ T cells in cancer patients but only CAR T cells have been approved for therapy to this date. Therefore, a combination of such CARs together with BAMO3 mAb could be exploited, especially in solid tumor models where current CAR therapies are often limited (Marofi et al., 2021).

8.5 Therapeutic efficacy of 19E9-PBD in treatment of aggressive MICA-expressing tumors

One of the first toxin-conjugated antibodies used in cancer therapy was reported in 1974 (Chose et al., 1974) and the first antibody-drug conjugate (ADC) was approved by the US Food and Drug Administration (FDA) in 2000. Currently, around 43 ADCs are licensed and marketed, and are used in clinical therapy, over half of which has been added in the past five years (Goydel & Rader, 2021). Toxin-conjugated antibody usually consist of a monoclonal antibody covalently attached to a cytotoxic drug through a linker. This combination provides a greater precise targeting ability together with a specific killing to achieve an accurate and efficient elimination of cancer cells. The antibody used for these experiments is named 19E9-PBD and is specific for the MICA ligand. Therapy with 19E9-PBD showed a tremendously successful control of the tumor growth in all tested mouse tumor models with different therapeutic regimes. Flow cytometry analysis of the first experiment with B16F10-MICA tumor model revealed a decreased NKG2D expression on γδ T cells together with decreased frequencies of γδ T cells in 19E9-PBD treatment group in comparison to isotype-treated group. γδ T cells are defined in the literature as a distinct subset of T cells that upon activation contribute to the first line of defense against foreign infections. γδ T cells play an important role in anti-tumor immunity and there is a lot of evidence that indicates a great promise of γδ T cell-based cancer immunotherapy (reviewed in Liu & Zhang, 2020). Available studies show two ways of tumor recognition by γδ T cells: TCR (T cell receptors) - and NKRs (Natural killer cell receptors) – dependent way (Correia et al., 2013). γδ T cells have the ability to promote anti-tumor responses either directly (production of IFNγ and TNFα) or in indirect ways by facilitating the function of other immune cells, i.e., dendritic cells, B cells and $CD8^+$ T cells (Chitadze et al., 2017; Lafont et al., 2014; Silva-Santos et al., 2019). It is therefore possible that the decreased expression of NKG2D on γδ T lymphocytes after 19E9-PBD therapy might indicate their exhaustion due to their indirect facilitation of the cytotoxicity of other immune subsets. A study of Jamieson et al from 2002 studied different subsets of γδ T lymphocytes and suggested that the expression of NKG2D on γδ T cells was related to previous activation or acquisition of a memory phenotype (Jamieson et al., 2002).

Moreover, the flow cytometry results did not reveal differences in MICA expression on tumor cells between the treatment groups. However, a decreased MICA expression on myeloid-derived suppressor cells (MDSCs) was detected. The tumor microenvironment (TME) is a complex heterogeneous environment consisting of not only tumor cells, but also tumor stroma, tissue-resident and tumor-infiltrating immune cells together with different secreted factors and extracellular matrix proteins. MDSCs are also a part of the TME with a potent T cell-immunosuppressive activity contributing to the immune escape of malignant tumors (Ostrand-Rosenberg & Sinha., 2009). High levels of MDSCs are significantly linked to poor prognosis, tumor progression and immunotherapy responses in patients with breast, colorectal and pulmonary cancers and hematological malignancies (Solito et al., 2011; Yang et al., 2020; Hao et al., 2021). The observed decrease in MICA expression on MDSCs could mean that these cells were targeted by 19E9-PBD antibody and that might have positively contributed to the tumor growth control.

RMA-MICA expressing cells were particularly sensitive to 19E9-PBD treatment; and a reduction of tumor size in Isotype treated groups were observed as well. Hence, this effect might be attributed to the toxin portion of the conjugated therapeutic. This hypothesis is further supported by an *in vitro* experiment that showed cell death after treating cells with Isotype-toxin conjugates (not shown).

Particularly negative side effects of higher doses of 19E9-PBD (7.8 mg/kg) were noticed and were manifested in the form of weight loss of MICAgen mice. Consequently, the experiment was terminated immediately due to animal welfare. Whether the weight loss was due to the high dosage, or the treatment regimen (repeated treatments) is a matter of future studies.

Combination therapy has proven to be a very effective therapeutic strategy in cancer patients. Such therapy is suggested to increase the effectiveness of treatment, prevent the development of drug resistance and reduce the length of treatment (Plana et al., 2022; Mokhtari et al., 2017). The benefit of adding anti-PD1 antibodies to the 19E9-PBD conjugate was investigated. Individual monotherapies were tremendously successful in the inhibition of tumor growth as well as in improving of overall survival of MICAgen mice. The combination of anti – PD-1 antibody with 19E9-PBD was also highly efficacious. However, the addition of anti - PD-1 to 19E9-PBD did not show a significant advantage when compared to the monotherapy. Therefore, other treatment regimens could be further studied with probably different doses of 19E9-PBD that could be supplemented with other immune-checkpoint inhibitors. For example, a report study from 2006 showed decreased levels of sMICA in the sera of melanoma patients treated with CTLA-4 antibody (Jinushi et al., 2006). CTLA-4 (cytotoxic T lymphocyte-associated antigen

4) inhibition is another useful therapeutic strategy that is approved and routinely used in many countries, usually in combination with anti- PD-1 therapy (Seidel et al., 2018).

Taken together, 19E9-PBD conjugated antibody shown to be a very efficacious anti-cancer therapeutic agent and clinical praxis shows us that the effective responses are possible through the various and different anti-tumor mechanisms and immunotherapy may be a key point in future cancer treatments.

References

Alves da Silva PH, Xing S, Kotini AG, Papapetrou EP, Song X, Wucherpfennig KW, Mascarenhas J, Ferrari de Andrade L. MICA/B antibody induces macrophage-mediated immunity against acute myeloid leukemia. Blood. 2022 Jan 13;139(2):205-216. doi: 10.1182/blood.2021011619. PMID: 34359073; PMCID: PMC8777466.

Anfossi N, André P, Guia S, Falk CS, Roetynck S, Stewart CA, Breso V, Frassati C, Reviron D, Middleton D, Romagné F, Ugolini S, Vivier E. Human NK cell education by inhibitory receptors for MHC class I. Immunity. 2006 Aug;25(2):331-42. doi: 10.1016/j.immuni.2006.06.013. Epub 2006 Aug 10. PMID: 16901727.

Arase H, Mocarski ES, Campbell AE, Hill AB, Lanier LL. Direct recognition of cytomegalovirus by activating and inhibitory NK cell receptors. Science. 2002 May 17;296(5571):1323-6. doi: 10.1126/science.1070884. Epub 2002 Apr 11. PMID: 11950999.

Ashiru O, López-Cobo S, Fernández-Messina L, Pontes-Quero S, Pandolfi R, Reyburn HT, Valés-Gómez M. A GPI anchor explains the unique biological features of the common NKG2D-ligand allele MICA*008. Biochem J. 2013 Sep 1;454(2):295-302. doi: 10.1042/BJ20130194. PMID: 23772752.

Bahram S, Bresnahan M, Geraghty DE, Spies T. A second lineage of mammalian major histocompatibility complex class I genes. Proc Natl Acad Sci U S A. 1994 Jul 5;91(14):6259-63. doi: 10.1073/pnas.91.14.6259. PMID: 8022771; PMCID: PMC44180.

Banchereau J, Steinman RM. Dendritic cells and the control of immunity. Nature. 1998 Mar 19;392(6673):245-52. doi: 10.1038/32588. PMID: 9521319.

Banerjee A, Li D, Guo Y, Mahgoub B, Paragas L, Slobin J, Mei Z, Manafi A, Hata A, Li K, Shi L, Westwick J, Slingluff C, Lazear E, Krupnick AS. Retargeting IL-2 Signaling to NKG2D-Expressing Tumor-Infiltrating Leukocytes Improves Adoptive Transfer Immunotherapy. J Immunol. 2021 Jul 1;207(1):333-343. doi: 10.4049/jimmunol.2000926. Epub 2021 Jun 21. PMID: 34155069; PMCID: PMC8688582.

Bartkova J, Horejsí Z, Koed K, Krämer A, Tort F, Zieger K, Guldberg P, Sehested M, Nesland JM, Lukas C, Ørntoft T, Lukas J, Bartek J. DNA damage response as a candidate anti-cancer barrier in early human tumorigenesis. Nature. 2005 Apr 14;434(7035):864-70. doi: 10.1038/nature03482. PMID: 15829956.

Bauer S, Groh V, Wu J, Steinle A, Phillips JH, Lanier LL, Spies T. Activation of NK cells and T cells by NKG2D, a receptor for stress-inducible MICA. Science. 1999 Jul 30;285(5428):727-9. doi: 10.1126/science.285.5428.727. PMID: 10426993.

Baumeister SH, Murad J, Werner L, Daley H, Trebeden-Negre H, Gicobi JK, Schmucker A, Reder J, Sentman CL, Gilham DE, Lehmann FF, Galinsky I, DiPietro H, Cummings K, Munshi NC, Stone RM, Neuberg DS, Soiffer R, Dranoff G, Ritz J, Nikiforow S. Phase I Trial of Autologous CAR T Cells Targeting NKG2D Ligands in Patients with AML/MDS and Multiple Myeloma. Cancer Immunol Res. 2019 Jan;7(1):100-112. doi: 10.1158/2326-6066.CIR-18-0307. Epub 2018 Nov 5. PMID: 30396908; PMCID: PMC7814996.

Bayat Mokhtari R, Homayouni TS, Baluch N, Morgatskaya E, Kumar S, Das B, Yeger H. Combination therapy in combating cancer. Oncotarget. 2017 Jun 6;8(23):38022-38043. doi: 10.18632/oncotarget.16723. PMID: 28410237; PMCID: PMC5514969.

Bernardini G, Gismondi A, Santoni A. Chemokines and NK cells: regulators of development, trafficking and functions. Immunol Lett. 2012 Jul 30;145(1-2):39-46. doi: 10.1016/j.imlet.2012.04.014. PMID: 22698182; PMCID: PMC7112821.

Bléry M, Mrabet-Kraiem M, Morel A, Lhospice F, Bregeon D, Bonnafous C, Gauthier L, Rossi B, Remark R, Cornen S, Anceriz N, Viaud N, Trichard S, Carpentier S, Joulin-Giet A, Grondin G, Liptakova V, Kim Y, Daniel L, Haffner A, Macagno N, Pouyet L, Perrot I, Paturel C, Morel Y, Steinle A, Romagné F, Narni-Mancinelli E, Vivier E. Targeting MICA/B with cytotoxic therapeutic antibodies leads to tumor control [version 2; peer review: 2 approved]. Open Res Eur. 2021 Oct 27;1:107. doi: 10.12688/openreseurope.13314.2. PMID: 35967081; PMCID: PMC7613279.

Borchers MT, Harris NL, Wesselkamper SC, Vitucci M, Cosman D. NKG2D ligands are expressed on stressed human airway epithelial cells. Am J Physiol Lung Cell Mol Physiol. 2006 Aug;291(2):L222-31. doi: 10.1152/ajplung.00327.2005. Epub 2006 Feb 10. PMID: 16473864.

Borregaard N. Neutrophils, from marrow to microbes. Immunity. 2010 Nov 24;33(5):657-70. doi: 10.1016/j.immuni.2010.11.011. PMID: 21094463.

Borrego F, Masilamani M, Marusina AI, Tang X, Coligan JE. The CD94/NKG2 family of receptors: from molecules and cells to clinical relevance. Immunol Res. 2006;35(3):263-78. doi: 10.1385/IR:35:3:263. PMID: 17172651.

Böttcher JP, Bonavita E, Chakravarty P, Blees H, Cabeza-Cabrerizo M, Sammicheli S, Rogers NC, Sahai E, Zelenay S, Reis e Sousa C. NK Cells Stimulate Recruitment of cDC1 into the Tumor Microenvironment Promoting Cancer Immune Control. Cell. 2018 Feb 22;172(5):1022-1037.e14. doi: 10.1016/j.cell.2018.01.004. Epub 2018 Feb 8. PMID: 29429633; PMCID: PMC5847168.

Boutet P, Agüera-González S, Atkinson S, Pennington CJ, Edwards DR, Murphy G, Reyburn HT, Valés-Gómez M. Cutting edge: the metalloproteinase ADAM17/TNF-alpha-converting enzyme regulates proteolytic shedding of the

MHC class I-related chain B protein. J Immunol. 2009 Jan 1;182(1):49-53. doi: 10.4049/jimmunol.182.1.49. PMID: 19109134.

Boyiadzis M, Foon KA. Approved monoclonal antibodies for cancer therapy. Expert Opin Biol Ther. 2008 Aug;8(8):1151-8. doi: 10.1517/14712598.8.8.1151. PMID: 18613766.

Brown A, Kumar S, Tchounwou PB. Cisplatin-Based Chemotherapy of Human Cancers. J Cancer Sci Ther. 2019;11(4):97. Epub 2019 Apr 8. PMID: 32148661; PMCID: PMC7059781.

Brown MG, Dokun AO, Heusel JW, Smith HR, Beckman DL, Blattenberger EA, Dubbelde CE, Stone LR, Scalzo AA, Yokoyama WM. Vital involvement of a natural killer cell activation receptor in resistance to viral infection. Science. 2001 May 4;292(5518):934-7. doi: 10.1126/science.1060042. PMID: 11340207.

Buckle I, Guillerey C. Inhibitory Receptors and Immune Checkpoints Regulating Natural Killer Cell Responses to Cancer. Cancers (Basel). 2021 Aug 24;13(17):4263. doi: 10.3390/cancers13174263. PMID: 34503073; PMCID: PMC8428224.

Burgess SJ, Marusina AI, Pathmanathan I, Borrego F, Coligan JE. IL-21 down-regulates NKG2D/DAP10 expression on human NK and CD8+ T cells. J Immunol. 2006 Feb 1;176(3):1490-7. doi: 10.4049/jimmunol.176.3.1490. PMID: 16424177.

Caligiuri MA. Human natural killer cells. Blood. 2008 Aug 1;112(3):461-9. doi: 10.1182/blood-2007-09-077438. PMID: 18650461; PMCID: PMC2481557.

Carayannopoulos LN, Naidenko OV, Fremont DH, Yokoyama WM. Cutting edge: murine UL16-binding protein-like transcript 1: a newly described transcript encoding a high-affinity ligand for murine NKG2D. J Immunol. 2002 Oct 15;169(8):4079-83. doi: 10.4049/jimmunol.169.8.4079. PMID: 12370332.

Castriconi R, Cantoni C, Della Chiesa M, Vitale M, Marcenaro E, Conte R, Biassoni R, Bottino C, Moretta L, Moretta A. Transforming growth factor beta 1 inhibits expression of NKp30 and NKG2D receptors: consequences for the NK-mediated killing of dendritic cells. Proc Natl Acad Sci U S A. 2003 Apr 1;100(7):4120-5. doi: 10.1073/pnas.0730640100. Epub 2003 Mar 19. PMID: 12646700; PMCID: PMC153058.

Cerboni C, Fionda C, Soriani A, Zingoni A, Doria M, Cippitelli M, Santoni A. The DNA Damage Response: A Common Pathway in the Regulation of NKG2D and DNAM-1 Ligand Expression in Normal, Infected, and Cancer Cells. Front Immunol. 2014 Jan 7;4:508. doi: 10.3389/fimmu.2013.00508. PMID: 24432022; PMCID: PMC3882864.

Cerwenka A, Bakker AB, McClanahan T, Wagner J, Wu J, Phillips JH, Lanier LL. Retinoic acid early inducible genes define a ligand family for the activating NKG2D receptor in mice. Immunity. 2000 Jun;12(6):721-7. doi: 10.1016/s1074-7613(00)80222-8. PMID: 10894171.

Cesana GC, DeRaffele G, Cohen S, Moroziewicz D, Mitcham J, Stoutenburg J, Cheung K, Hesdorffer C, Kim-Schulze S, Kaufman HL. Characterization of CD4+CD25+ regulatory T cells in patients treated with high-dose interleukin-2 for metastatic melanoma or renal cell carcinoma. J Clin Oncol. 2006 Mar 1;24(7):1169-77. doi: 10.1200/JCO.2005.03.6830. PMID: 16505437.

Chan CJ, Smyth MJ, Martinet L. Molecular mechanisms of natural killer cell activation in response to cellular stress. Cell Death Differ. 2014 Jan;21(1):5-14. doi: 10.1038/cdd.2013.26. Epub 2013 Apr 12. PMID: 23579243; PMCID: PMC3857624. (License nr.: 5620160479337)

Chen D, Gyllensten U. MICA polymorphism: biology and importance in cancer. Carcinogenesis. 2014 Dec;35(12):2633-42. doi: 10.1093/carcin/bgu215. Epub 2014 Oct 20. PMID: 25330802.

Chen D, Juko-Pecirep I, Hammer J, Ivansson E, Enroth S, Gustavsson I, Feuk L, Magnusson PK, McKay JD, Wilander E, Gyllensten U. Genome-wide association study of susceptibility loci for cervical cancer. J Natl Cancer Inst. 2013 May 1;105(9):624-33. doi: 10.1093/jnci/djt051. Epub 2013 Mar 12. PMID: 23482656.

Chiossone L, Chaix J, Fuseri N, Roth C, Vivier E, Walzer T. Maturation of mouse NK cells is a 4-stage developmental program. Blood (2009) 113:5488–96. doi:10.1182/blood-2008-10-187179

Chitadze G, Lettau M, Bhat J, Wesch D, Steinle A, Fürst D, Mytilineos J, Kalthoff H, Janssen O, Oberg HH, Kabelitz D. Shedding of endogenous MHC class I-related chain molecules A and B from different human tumor entities: heterogeneous involvement of the "a disintegrin and metalloproteases" 10 and 17. Int J Cancer. 2013 Oct 1;133(7):1557-66. doi: 10.1002/ijc.28174. Epub 2013 Apr 18. PMID: 23526433..

Chuang S.S., Kim M.H., Johnson L.A., Albertsson P., Kitson R.P., Nannmark U., Goldfarb R.H., Mathew P.A. 2B4 stimulation of YT cells induces natural killer cell cytolytic function and invasiveness. Immunology. 2000;100:378–383. doi: 10.1046/j.1365-2567.2000.00031.x

Clément MV, Haddad P, Soulié A, Legros-Maida S, Guillet J, Cesar E, Sasportes M. Involvement of granzyme B and perforin gene expression in the lytic potential of human natural killer cells. Res Immunol. 1990 Jul-Aug;141(6):477-89. doi: 10.1016/0923-2494(90)90017-s. PMID: 2284495.

Cooper MA, Fehniger TA, Turner SC, Chen KS, Ghaheri BA, Ghayur T, Carson WE, Caligiuri MA. Human natural killer cells: a unique innate immunoregulatory role for the CD56(bright) subset. Blood. 2001 May 15;97(10):3146-51. doi: 10.1182/blood.v97.10.3146. PMID: 11342442.

Corraliza-Gorjón I, Somovilla-Crespo B, Santamaria S, Garcia-Sanz JA, Kremer L. New Strategies Using Antibody Combinations to Increase Cancer Treatment Effectiveness. Front Immunol. 2017 Dec 21;8:1804. doi: 10.3389/fimmu.2017.01804. PMID: 29312320; PMCID: PMC5742572.

Cosman D, Müllberg J, Sutherland CL, Chin W, Armitage R, Fanslow W, Kubin M, Chalupny NJ. ULBPs, novel MHC class I-related molecules, bind to CMV glycoprotein UL16 and stimulate NK cytotoxicity through the NKG2D receptor. Immunity. 2001 Feb;14(2):123-33. doi: 10.1016/s1074-7613(01)00095-4. PMID: 11239445.

Cotran RS, Pober JS, Gimbrone MA Jr, Springer TA, Wiebke EA, Gaspari AA, Rosenberg SA, Lotze MT. Endothelial activation during interleukin 2 immunotherapy. A possible mechanism for the vascular leak syndrome. J Immunol. 1988 Mar 15;140(6):1883-8. PMID: 3279124.

Crane CA, Han SJ, Barry JJ, Ahn BJ, Lanier LL, Parsa AT. TGF-beta downregulates the activating receptor NKG2D on NK cells and CD8+ T cells in glioma patients. Neuro Oncol. 2010 Jan;12(1):7-13. doi: 10.1093/neuonc/nop009. Epub 2009 Nov 5. PMID: 20150362; PMCID: PMC2940557.

Curio S, Jonsson G, Marinović S. A summary of current NKG2D-based CAR clinical trials. Immunother Adv. 2021 Aug 13;1(1):ltab018. doi: 10.1093/immadv/ltab018. PMID: 34604863; PMCID: PMC8480431.

Dai Z, Turtle CJ, Booth GC, Riddell SR, Gooley TA, Stevens AM, Spies T, Groh V. Normally occurring NKG2D+CD4+ T cells are immunosuppressive and inversely correlated with disease activity in juvenile-onset lupus. J Exp Med. 2009 Apr 13;206(4):793-805. doi: 10.1084/jem.20081648. Epub 2009 Mar 16. PMID: 19289577; PMCID: PMC2715116.

Devaux PF, Herrmann A, Ohlwein N, Kozlov MM. How lipid flippases can modulate membrane structure. Biochim Biophys Acta 2008;1778: 1591-1600.

Diefenbach A, Colonna M, Koyasu S. Development, differentiation, and diversity of innate lymphoid cells. Immunity. 2014 Sep 18;41(3):354-365. doi: 10.1016/j.immuni.2014.09.005. PMID: 25238093; PMCID: PMC4171710.

Diefenbach A, Jamieson AM, Liu SD, Shastri N, Raulet DH. Ligands for the murine NKG2D receptor: expression by tumor cells and activation of NK cells and macrophages. Nat Immunol. 2000 Aug;1(2):119-26. doi: 10.1038/77793. PMID: 11248803.

Diefenbach A, Raulet DH. Strategies for target cell recognition by natural killer cells. Immunol Rev. 2001 Jun;181:170-84. doi: 10.1034/j.1600-065x.2001.1810114.x. PMID: 11513138.

Diefenbach A, Tomasello E, Lucas M, Jamieson AM, Hsia JK, Vivier E, et al. Selective associations with signaling proteins determine stimulatory versus costimulatory activity of NKG2D. Nat Immunol (2002) 3:1142–9. doi:10.1038/ni858

Drewe E, Powell RJ. Clinically useful monoclonal antibodies in treatment. J Clin Pathol. 2002 Feb;55(2):81-5. doi: 10.1136/jcp.55.2.81. PMID: 11864998; PMCID: PMC1769580.

Easom NJW, Stegmann KA, Swadling L, Pallett LJ, Burton AR, Odera D, Schmidt N, Huang WC, Fusai G, Davidson B, Maini MK. IL-15 Overcomes Hepatocellular Carcinoma-Induced NK Cell Dysfunction. Front Immunol. 2018 May 9;9:1009. doi: 10.3389/fimmu.2018.01009. PMID: 29867983; PMCID: PMC5954038.

Ehrlich LI, Ogasawara K, Hamerman JA, Takaki R, Zingoni A, Allison JP, et al. Engagement of NKG2D by cognate ligand or antibody alone is insufficient to mediate costimulation of human and mouse CD8+ T cells. J Immunol (2005) 174:1922–31. doi:10.4049/jimmunol.174.4.1922

Fauriat C, Long EO, Ljunggren HG, Bryceson YT. Regulation of human NK-cell cytokine and chemokine production by target cell recognition. Blood. 2010 Mar 18;115(11):2167-76. doi: 10.1182/blood-2009-08-238469. Epub 2009 Dec 1. PMID: 19965656; PMCID: PMC2844017.

Ferlazzo G, Moretta L. Dendritic cell editing by natural killer cells. Crit Rev Oncog. 2014;19(1-2):67-75. doi: 10.1615/critrevoncog.2014010827. PMID: 24941374.

Ferlazzo G, Münz C. NK cell compartments and their activation by dendritic cells. J Immunol. 2004 Feb 1;172(3):1333-9. doi: 10.4049/jimmunol.172.3.1333. PMID: 14734707.

Ferlazzo G, Tsang ML, Moretta L, Melioli G, Steinman RM, Münz C. Human dendritic cells activate resting natural killer (NK) cells and are recognized via the NKp30 receptor by activated NK cells. J Exp Med. 2002 Feb 4;195(3):343-51. doi: 10.1084/jem.20011149. PMID: 11828009; PMCID: PMC2193591.

Ferrari de Andrade L, Kumar S, Luoma AM, Ito Y, Alves da Silva PH, Pan D, Pyrdol JW, Yoon CH, Wucherpfennig KW. Inhibition of MICA and MICB Shedding Elicits NK-Cell-Mediated Immunity against Tumors Resistant to Cytotoxic T Cells. Cancer Immunol Res. 2020 Jun;8(6):769-780. doi: 10.1158/2326-6066.CIR-19-0483. Epub 2020 Mar 24. PMID: 32209637; PMCID: PMC7269842.

Ferrari de Andrade L, Tay RE, Pan D, Luoma AM, Ito Y, Badrinath S, Tsoucas D, Franz B, May KF Jr, Harvey CJ, Kobold S, Pyrdol JW, Yoon C, Yuan GC, Hodi FS, Dranoff G, Wucherpfennig KW. Antibody-mediated inhibition of MICA and MICB shedding promotes NK cell-driven tumor immunity. Science. 2018 Mar 30;359(6383):1537-1542. doi: 10.1126/science.aao0505. PMID: 29599246; PMCID: PMC6626532.

Fodil N, Laloux L, Wanner V, Pellet P, Hauptmann G, Mizuki N, Inoko H, Spies T, Theodorou I, Bahram S. Allelic repertoire of the human MHC class I MICA gene. Immunogenetics. 1996;44(5):351-7. doi: 10.1007/BF02602779. PMID: 8781120.

Fröhlich C, Nehammer C, Albrechtsen R, Kronqvist P, Kveiborg M, Sehara-Fujisawa A, Mercurio AM, Wewer UM. ADAM12 produced by tumor cells rather than stromal cells accelerates breast tumor progression. Mol Cancer Res. 2011 Nov;9(11):1449-61. doi: 10.1158/1541-7786.MCR-11-0100. Epub 2011 Aug 29. PMID: 21875931; PMCID: PMC3219818.

Galli SJ, Tsai M. Mast cells in allergy and infection: versatile effector and regulatory cells in innate and adaptive immunity. Eur J Immunol. 2010 Jul;40(7):1843-51. doi: 10.1002/eji.201040559. PMID: 20583030; PMCID: PMC3581154.

Ghasemi R, Lazear E, Wang X, Arefanian S, Zheleznyak A, Carreno BM, Higashikubo R, Gelman AE, Kreisel D, Fremont DH, Krupnick AS. Selective targeting of IL-2 to NKG2D bearing cells for improved immunotherapy. Nat Commun. 2016 Sep 21;7:12878. doi: 10.1038/ncomms12878. PMID: 27650575; PMCID: PMC5036003.

Giebeler N, Zigrino P. A Disintegrin and Metalloprotease (ADAM): Historical Overview of Their Functions. Toxins (Basel). 2016 Apr 23;8(4):122. doi: 10.3390/toxins8040122. PMID: 27120619; PMCID: PMC4848645.

Goffin JR, Anderson IC, Supko JG, Eder JP Jr, Shapiro GI, Lynch TJ, Shipp M, Johnson BE, Skarin AT. Phase I trial of the matrix metalloproteinase inhibitor marimastat combined with carboplatin and paclitaxel in patients with advanced non-small cell lung cancer. Clin Cancer Res. 2005 May 1;11(9):3417-24. doi: 10.1158/1078-0432.CCR-04-2144. PMID: 15867243.

Goto K, Annan DA, Morita T, Li W, Muroyama R, Matsubara Y, Ito S, Nakagawa R, Tanoue Y, Jinushi M, Kato N. Novel chemoimmunotherapeutic strategy for hepatocellular carcinoma based on a genome-wide association study. Sci Rep. 2016 Dec 2;6:38407. doi: 10.1038/srep38407. PMID: 27910927; PMCID: PMC5133582.

Goto K, Kato N. MICA SNPs and the NKG2D system in virus-induced HCC. J Gastroenterol. 2015 Mar;50(3):261-72. doi: 10.1007/s00535-014-1000-9. Epub 2014 Oct 1. PMID: 25270965.

Goydel RS, Rader C. Antibody-based cancer therapy. Oncogene. 2021 May;40(21):3655-3664. doi: 10.1038/s41388-021-01811-8. Epub 2021 May 4. PMID: 33947958; PMCID: PMC8357052.

Greenberg AH, Hudson L, Shen L, Roitt IM. Antibody-dependent cell-mediated cytotoxicity due to a "null" lymphoid cell. Nat New Biol. 1973 Mar 28;242(117):111-3. doi: 10.1038/newbio242111a0. PMID: 4541031.

Groh V, Bahram S, Bauer S, Herman A, Beauchamp M, Spies T. Cell stress-regulated human major histocompatibility complex class I gene expressed in gastrointestinal epithelium. Proc Natl Acad Sci U S A. 1996 Oct 29;93(22):12445-50. doi: 10.1073/pnas.93.22.12445. PMID: 8901601; PMCID: PMC38011.

Groh V, Bruhl A, El-Gabalawy H, Nelson JL, Spies T. Stimulation of T cell autoreactivity by anomalous expression of NKG2D and its MIC ligands in rheumatoid arthritis. Proc Natl Acad Sci U S A. 2003 Aug 5;100(16):9452-7. doi: 10.1073/pnas.1632807100. Epub 2003 Jul 23. PMID: 12878725; PMCID: PMC170939.

Groh V, Rhinehart R, Randolph-Habecker J, Topp MS, Riddell SR, Spies T. Costimulation of CD8alphabeta T cells by NKG2D via engagement by MIC induced on virus-infected cells. Nat Immunol (2001) 2:255–60. doi:10.1038/85321

Groh V, Steinle A, Bauer S, Spies T. Recognition of stress-induced MHC molecules by intestinal epithelial gammadelta T cells. Science. 1998 Mar 13;279(5357):1737-40. doi: 10.1126/science.279.5357.1737. PMID: 9497295.

Guerra N, Pestal K, Juarez T, Beck J, Tkach K, Wang L, Raulet DH. A selective role of NKG2D in inflammatory and autoimmune diseases. Clin Immunol. 2013 Dec;149(3):432-9. doi: 10.1016/j.clim.2013.09.003. Epub 2013 Sep 14. PMID: 24211717; PMCID: PMC3868205.

Guerra N, Tan YX, Joncker NT, Choy A, Gallardo F, Xiong N, Knoblaugh S, Cado D, Greenberg NM, Raulet DH. NKG2D-deficient mice are defective in tumor surveillance in models of spontaneous malignancy. Immunity. 2008 Apr;28(4):571-80. doi: 10.1016/j.immuni.2008.02.016. Erratum in: Immunity. 2008 May;28(5):723. Greenberg, Norman R [corrected to Greenberg, Norman M]. PMID: 18394936; PMCID: PMC3528789.

Guma M, Angulo A, Vilches C, Gomez-Lozano N, Malats N, Lopez-Botet M. Imprint of human cytomegalovirus infection on the NK cell receptor repertoire. Blood (2004) 104:3664–71. 10.1182/blood-2004-05-2058

Gumireddy K, Sun F, Klein-Szanto AJ, Gibbins JM, Gimotty PA, Saunders AJ, Schultz PG, Huang Q. In vivo selection for metastasis promoting genes in the mouse. Proc Natl Acad Sci U S A. 2007 Apr 17;104(16):6696-701. doi: 10.1073/pnas.0701145104. Epub 2007 Apr 9. PMID: 17420453; PMCID: PMC1871848.

Gumperz JE, Miyake S, Yamamura T, Brenner MB. Functionally distinct subsets of CD1d-restricted natural killer T cells revealed by CD1d tetramer staining. J Exp Med. 2002 Mar 4;195(5):625-36. doi: 10.1084/jem.20011786. PMID: 11877485; PMCID: PMC2193772.

Hao Z, Li R, Wang Y, Li S, Hong Z, Han Z. Landscape of Myeloid-derived Suppressor Cell in Tumor Immunotherapy. Biomark Res. 2021 Oct 24;9(1):77. doi: 10.1186/s40364-021-00333-5. Erratum in: Biomark Res. 2022 Feb 7;10(1):7. PMID: 34689842; PMCID: PMC8543853.

Hayakawa, Y., Huntington, N.D., Nutt, S.L. and Smyth, M.J. (2006), Functional subsets of mouse natural killer cells. Immunological Reviews, 214: 47-55. https://doi.org/10.1111/j.1600-065X.2006.00454.x

Henricks LM, Schellens JH, Huitema AD, Beijnen JH. The use of combinations of monoclonal antibodies in clinical oncology. Cancer Treat Rev. 2015 Dec;41(10):859-67. doi: 10.1016/j.ctrv.2015.10.008. Epub 2015 Oct 30. PMID: 26547132.

Ho EL, Heusel JW, Brown MG, Matsumoto K, Scalzo AA, Yokoyama WM. Murine Nkg2d and Cd94 are clustered within the natural killer complex and are expressed independently in natural killer cells. Proc Natl Acad Sci U S A. 1998 May 26;95(11):6320-5. doi: 10.1073/pnas.95.11.6320. PMID: 9600963; PMCID: PMC27675.

Holdenrieder S, Stieber P, Peterfi A, Nagel D, Steinle A, Salih HR. Soluble MICB in malignant diseases: analysis of diagnostic significance and correlation with soluble MICA. Cancer Immunol Immunother. 2006 Dec;55(12):1584-9. doi: 10.1007/s00262-006-0167-1. Epub 2006 Apr 25. PMID: 16636811. **b**

Holdenrieder S, Stieber P, Peterfi A, Nagel D, Steinle A, Salih HR. Soluble MICA in malignant diseases. Int J Cancer. 2006 Feb 1;118(3):684-7. doi: 10.1002/ijc.21382. PMID: 16094621. **a**

Hosomi S, Grootjans J, Huang YH, Kaser A, Blumberg RS. New Insights Into the Regulation of Natural-Killer Group 2 Member D (NKG2D) and NKG2D-Ligands: Endoplasmic Reticulum Stress and CEA-Related Cell Adhesion Molecule 1. Front Immunol. 2018 Jun 18;9:1324. doi: 10.3389/fimmu.2018.01324. PMID: 29973929; PMCID: PMC6020765.

Houchins JP, Yabe T, McSherry C, Bach FH. DNA sequence analysis of NKG2, a family of related cDNA clones encoding type II integral membrane proteins on human natural killer cells. J Exp Med. 1991 Apr 1;173(4):1017-20. doi: 10.1084/jem.173.4.1017. PMID: 2007850; PMCID: PMC2190798.

Huergo-Zapico L, Gonzalez-Rodriguez AP, Contesti J, Gonzalez E, López-Soto A, Fernandez-Guizan A, Acebes-Huerta A, de Los Toyos JR, Lopez-Larrea C, Groh V, Spies T, Gonzalez S. Expression of ERp5 and GRP78 on the membrane of chronic lymphocytic leukemia cells: association with soluble MICA shedding. Cancer Immunol Immunother. 2012 Aug;61(8):1201-10. doi: 10.1007/s00262-011-1195-z. Epub 2012 Jan 4. PMID: 22215138.

Isernhagen A, Schilling D, Monecke S, Shah P, Elsner L, Walter L, Multhoff G, Dressel R. The MICA-129Met/Val dimorphism affects plasma membrane expression and shedding of the NKG2D ligand MICA. Immunogenetics. 2016 Feb;68(2):109-23. doi: 10.1007/s00251-015-0884-8. Epub 2015 Nov 19. PMID: 26585323; PMCID: PMC4728179.

Jamieson AM, Diefenbach A, McMahon CW, Xiong N, Carlyle JR, Raulet DH. The role of the NKG2D immunoreceptor in immune cell activation and natural killing. Immunity. 2002 Jul;17(1):19-29. doi: 10.1016/s1074-7613(02)00333-3. Erratum in: Immunity. 2004 Jun;20(6):799. PMID: 12150888.

Ji M, Wang J, Yuan L, Zhang Y, Zhang J, Dong W, Peng X. MICA polymorphisms and cancer risk: a meta-analysis. Int J Clin Exp Med. 2015 Jan 15;8(1):818-26. PMID: 25785062; PMCID: PMC4358517.

Jiang X, Huang JF, Huo Z, Zhang Q, Jiang Y, Wu X, Li Y, Jiang G, Zeng L, Yan XX, Yu P, Cao R. Elevation of soluble major histocompatibility complex class I related chain A protein in malignant and infectious diseases in Chinese patients. BMC Immunol. 2012 Nov 26;13:62. doi: 10.1186/1471-2172-13-62. PMID: 23181907; PMCID: PMC3552998.

Jiang X, Wang J, Deng X, Xiong F, Ge J, Xiang B, Wu X, Ma J, Zhou M, Li X, Li Y, Li G, Xiong W, Guo C, Zeng Z. Role of the tumor microenvironment in PD-L1/PD-1-mediated tumor immune escape. Mol Cancer. 2019 Jan 15;18(1):10. doi: 10.1186/s12943-018-0928-4. PMID: 30646912; PMCID: PMC6332843.

Jinushi M, Hodi FS, Dranoff G. Therapy-induced antibodies to MHC class I chain-related protein A antagonize immune suppression and stimulate antitumor cytotoxicity. Proc Natl Acad Sci U S A. 2006 Jun 13;103(24):9190-5. doi: 10.1073/pnas.0603503103. Epub 2006 Jun 5. PMID: 16754847; PMCID: PMC1482588.

Jinushi M, Vanneman M, Munshi NC, Tai YT, Prabhala RH, Ritz J, Neuberg D, Anderson KC, Carrasco DR, Dranoff G. MHC class I chain-related protein A antibodies and shedding are associated with the progression of multiple myeloma. Proc Natl Acad Sci U S A. 2008 Jan 29;105(4):1285-90. doi: 10.1073/pnas.0711293105. Epub 2008 Jan 17. PMID: 18202175; PMCID: PMC2234130.

Kaiser BK, Yim D, Chow IT, Gonzalez S, Dai Z, Mann HH, Strong RK, Groh V, Spies T. Disulphide-isomerase-enabled shedding of tumour-associated NKG2D ligands. Nature. 2007 May 24;447(7143):482-6. doi: 10.1038/nature05768. Epub 2007 May 9. PMID: 17495932.

Kärre K, Ljunggren HG, Piontek G, Kiessling R. Selective rejection of H-2-deficient lymphoma variants suggests alternative immune defence strategy. Nature. 1986 Feb 20-26;319(6055):675-8. doi: 10.1038/319675a0. PMID: 3951539.

Kiessling R, Klein E, Wigzell H. “Natural” killer cells in the mouse. I. Cytotoxic cells with specificity for mouse Moloney leukemia cells. Specificity and distribution according to genotype. Eur J Immunol (1975) 5(2):112–7. doi:10.1002/eji.1830050208

Kim Y, Born C, Bléry M, Steinle A. MICAgen Mice Recapitulate the Highly Restricted but Activation-Inducible Expression of the Paradigmatic Human NKG2D Ligand MICA. Front Immunol. 2020 Jun 4;11:960. doi: 10.3389/fimmu.2020.00960. PMID: 32582150; PMCID: PMC7287395.

Kohga K, Takehara T, Tatsumi T, Ishida H, Miyagi T, Hosui A, Hayashi N. Sorafenib inhibits the shedding of major histocompatibility complex class I-related chain A on hepatocellular carcinoma cells by down-regulating a disintegrin and metalloproteinase 9. Hepatology. 2010 Apr;51(4):1264-73. doi: 10.1002/hep.23456. PMID: 20099300.

Kohga K, Takehara T, Tatsumi T, Miyagi T, Ishida H, Ohkawa K, Kanto T, Hiramatsu N, Hayashi N. Anticancer chemotherapy inhibits MHC class I-related chain a ectodomain shedding by downregulating ADAM10 expression in

hepatocellular carcinoma. Cancer Res. 2009 Oct 15;69(20):8050-7. doi: 10.1158/0008-5472.CAN-09-0789. Epub 2009 Oct 13. PMID: 19826051.

Konjević G, Mirjačić Martinović K, Vuletić A, Radenković S. Novel aspects of in vitro IL-2 or IFN-α enhanced NK cytotoxicity of healthy individuals based on NKG2D and CD161 NK cell receptor induction. Biomed Pharmacother. 2010 Dec;64(10):663-71. doi: 10.1016/j.biopha.2010.06.013. Epub 2010 Jul 17. PMID: 20800424.

Krieg S, Ullrich E. Novel immune modulators used in hematology: impact on NK cells. Front Immunol. 2013 Jan 3;3:388. doi: 10.3389/fimmu.2012.00388. PMID: 23316191; PMCID: PMC3539673.

Kwon MJ. Matrix metalloproteinases as therapeutic targets in breast cancer. Front Oncol. 2023 Jan 19;12:1108695. doi: 10.3389/fonc.2022.1108695. PMID: 36741729; PMCID: PMC9897057.

Lafont V, Sanchez F, Laprevotte E, Michaud HA, Gros L, Eliaou JF, Bonnefoy N. Plasticity of γδ T Cells: Impact on the Anti-Tumor Response. Front Immunol. 2014 Dec 8;5:622. doi: 10.3389/fimmu.2014.00622. PMID: 25538706; PMCID: PMC4259167.

Langers I, Renoux VM, Thiry M, Delvenne P, Jacobs N. Natural killer cells: role in local tumor growth and metastasis. Biologics. 2012;6:73-82. doi: 10.2147/BTT.S23976. Epub 2012 Apr 5. PMID: 22532775; PMCID: PMC3333822.

Lanier LL, Corliss BC, Wu J, Leong C, Phillips JH. Immunoreceptor DAP12 bearing a tyrosine-based activation motif is involved in activating NK cells. Nature. 1998 Feb 12;391(6668):703-7. doi: 10.1038/35642. PMID: 9490415.

Lanier LL, Le AM, Civin CI, Loken MR, Phillips JH. The relationship of CD16 (Leu-11) and Leu-19 (NKH-1) antigen expression on human peripheral blood NK cells and cytotoxic T lymphocytes. J Immunol. 1986 Jun 15;136(12):4480-6. PMID: 3086432. **b**

Lanier LL, Le AM, Cwirla S, Federspiel N, Phillips JH. Antigenic, functional, and molecular genetic studies of human natural killer cells and cytotoxic T lymphocytes not restricted by the major histocompatibility complex. Fed Proc. 1986 Nov;45(12):2823-8. PMID: 3095151.

Lanier LL. NK cell recognition. Annu Rev Immunol. 2005;23:225-74. doi: 10.1146/annurev.immunol.23.021704.115526. PMID: 15771571.

Lanier LL. NKG2D Receptor and Its Ligands in Host Defense. Cancer Immunol Res. 2015 Jun;3(6):575-82. doi: 10.1158/2326-6066.CIR-15-0098. PMID: 26041808; PMCID: PMC4457299. (License nr: 1379730-1)

Lanier LL. Up on the tightrope: natural killer cell activation and inhibition. Nat Immunol. 2008 May;9(5):495-502. doi: 10.1038/ni1581. PMID: 18425106; PMCID: PMC2669298.

Lazarova M, Wels WS, Steinle A. Arming cytotoxic lymphocytes for cancer immunotherapy by means of the NKG2D/NKG2D-ligand system. Expert Opin Biol Ther. 2020 Dec;20(12):1491-1501. doi: 10.1080/14712598.2020.1803273. Epub 2020 Aug 31. PMID: 32726145.

Lee K.-M., McNerney M.E., Stepp S.E., Mathew P.A., Schatzle J.D., Bennett M., Kumar V. 2B4 acts as a non-major histocompatibility complex binding inhibitory receptor on mouse natural killer cells. J. Exp. Med. 2004;199:1245–1254. doi: 10.1084/jem.20031989.

Lee YS, Heo W, Nam J, Jeung YH, Bae J. The combination of ionizing radiation and proteasomal inhibition by bortezomib enhances the expression of NKG2D ligands in multiple myeloma cells. J Radiat Res. 2018 May 1;59(3):245-252. doi: 10.1093/jrr/rry005. PMID: 29518205; PMCID: PMC5967576.

Leivas A, Valeri A, Córdoba L, García-Ortiz A, Ortiz A, Sánchez-Vega L, Graña-Castro O, Fernández L, Carreño-Tarragona G, Pérez M, Megías D, Paciello ML, Sánchez-Pina J, Pérez-Martínez A, Lee DA, Powell DJ Jr, Río P, Martínez-López J. NKG2D-CAR-transduced natural killer cells efficiently target multiple myeloma. Blood Cancer J. 2021 Aug 14;11(8):146. doi: 10.1038/s41408-021-00537-w. PMID: 34392311; PMCID: PMC8364555.

Li D, Wu M. Pattern recognition receptors in health and diseases. Signal Transduct Target Ther. 2021 Aug 4;6(1):291. doi: 10.1038/s41392-021-00687-0. PMID: 34344870; PMCID: PMC8333067.

Li P, Willie ST, Bauer S, Morris DL, Spies T, Strong RK. Crystal structure of the MHC class I homolog MIC-A, a gammadelta T cell ligand. Immunity. 1999 May;10(5):577-84. doi: 10.1016/s1074-7613(00)80057-6. PMID: 10367903.

Li SS, Ogbomo H, Mansour MK, Xiang RF, Szabo L, Munro F, Mukherjee P, Mariuzza RA, Amrein M, Vyas JM, Robbins SM, Mody CH. Identification of the fungal ligand triggering cytotoxic PRR-mediated NK cell killing of Cryptococcus and Candida. Nat Commun. 2018 Feb 21;9(1):751. doi: 10.1038/s41467-018-03014-4. PMID: 29467448; PMCID: PMC5821813.

Li Y, Mariuzza RA. Structural basis for recognition of cellular and viral ligands by NK cell receptors. Front Immunol. 2014 Mar 26;5:123. doi: 10.3389/fimmu.2014.00123. PMID: 24723923; PMCID: PMC3972465.

Lichtenthaler SF, Lemberg MK, Fluhrer R. Proteolytic ectodomain shedding of membrane proteins in mammals-hardware, concepts, and recent developments. EMBO J. 2018 Aug 1;37(15):e99456. doi: 10.15252/embj.201899456. Epub 2018 Jul 5. PMID: 29976761; PMCID: PMC6068445.

Lieberman J. The ABCs of granule-mediated cytotoxicity: new weapons in the arsenal. Nat Rev Immunol. 2003 May;3(5):361-70. doi: 10.1038/nri1083. PMID: 12766758.

Ljunggren HG, Kärre K. In search of the “missing self”: MHC molecules and NK cell recognition. Immunol Today 1990;11:237–44.

Long EO. Regulation of immune responses through inhibitory receptors. Annu Rev Immunol. 1999;17:875-904. doi: 10.1146/annurev.immunol.17.1.875. PMID: 10358776.

Lopez-Vazquez A, Rodrigo L, Mina-Blanco A, Martinez-Borra J, Fuentes D, Rodriguez M, et al. Extended human leukocyte antigen haplotype EH18.1 influences progression to hepatocellular carcinoma in patients with hepatitis C virus infection. J Infect Dis. 2004;189:957–63.

Lotze MT, Frana LW, Sharrow SO, Robb RJ, Rosenberg SA. In vivo administration of purified human interleukin 2. I. Half-life and immunologic effects of the Jurkat cell line-derived interleukin 2. J Immunol. 1985 Jan;134(1):157-66. PMID: 3871099.

Maasho K, Opoku-Anane J, Marusina AI, Coligan JE, Borrego F. NKG2D is a costimulatory receptor for human naive CD8+ T cells. J Immunol. 2005 Apr 15;174(8):4480-4. doi: 10.4049/jimmunol.174.8.4480. PMID: 15814668.

Mace EM, Dongre P, Hsu HT, Sinha P, James AM, Mann SS, Forbes LR, Watkin LB, Orange JS. Cell biological steps and checkpoints in accessing NK cell cytotoxicity. Immunol Cell Biol. 2014 Mar;92(3):245-55. doi: 10.1038/icb.2013.96. Epub 2014 Jan 21. PMID: 24445602; PMCID: PMC3960583.

Mandelboim O, Lieberman N, Lev M, Paul L, Arnon TI, Bushkin Y, Davis DM, Strominger JL, Yewdell JW, Porgador A. Recognition of haemagglutinins on virus-infected cells by NKp46 activates lysis by human NK cells. Nature. 2001 Feb 22;409(6823):1055-60. doi: 10.1038/35059110. PMID: 11234016.

Mannello F, Tonti G, Papa S. Matrix metalloproteinase inhibitors as anticancer therapeutics. Curr Cancer Drug Targets. 2005 Jun;5(4):285-98. doi: 10.2174/1568009054064615. PMID: 15975049.

Märklin M, Hagelstein I, Koerner SP, Rothfelder K, Pfluegler MS, Schumacher A, Grosse-Hovest L, Jung G, Salih HR. Bispecific NKG2D-CD3 and NKG2D-CD16 fusion proteins for induction of NK and T cell reactivity against acute myeloid leukemia. J Immunother Cancer. 2019 May 29;7(1):143. doi: 10.1186/s40425-019-0606-0. PMID: 31142382; PMCID: PMC6542021.

Mathew S.O., Kumaresan P.R., Lee J.K., Huynh V.T., Mathew P.A. Mutational analysis of the human 2B4 (CD244)/CD48 interaction: Lys68 and Glu70 in the V domain of 2B4 are critical for CD48 binding and functional activation of NK cells. J. Immunol. 2005;175:1005–1013. doi: 10.4049/jimmunol.175.2.1005.

Mathew S.O., Rao K.K., Kim J.R., Bambard N.D., Mathew P.A. Functional role of human NK cell receptor 2B4 (CD244) isoforms. Eur. J. Immunol. 2009;39:1632–1641. doi: 10.1002/eji.200838733.

Medjouel Khlifi H, Guia S, Vivier E, Narni-Mancinelli E. Role of the ITAM-Bearing Receptors Expressed by Natural Killer Cells in Cancer. Front Immunol. 2022 Jun 10;13:898745. doi: 10.3389/fimmu.2022.898745. PMID: 35757695; PMCID: PMC9231431.

Meresse B, Chen Z, Ciszewski C, Tretiakova M, Bhagat G, Krausz TN, Raulet DH, Lanier LL, Groh V, Spies T, Ebert EC, Green PH, Jabri B. Coordinated induction by IL15 of a TCR-independent NKG2D signaling pathway converts CTL into lymphokine-activated killer cells in celiac disease. Immunity. 2004 Sep;21(3):357-66. doi: 10.1016/j.immuni.2004.06.020. PMID: 15357947.

Mittal R. 2016. Intricate Functions of Matrix Metalloproteinases in Physiological and Pathological Conditions. J Cell Physiol. 2016 Dec;231(12):2599-621. doi: 10.1002/jcp.25430. Epub 2016 Jul 11.

Mizuki N, Ota M, Kimura M, Ohno S, Ando H, Katsuyama Y, Yamazaki M, Watanabe K, Goto K, Nakamura S, Bahram S, Inoko H. Triplet repeat polymorphism in the transmembrane region of the MICA gene: a strong association of six GCT repetitions with Behçet disease. Proc Natl Acad Sci U S A. 1997 Feb 18;94(4):1298-303. doi: 10.1073/pnas.94.4.1298. PMID: 9037047; PMCID: PMC19785.

Mogensen TH. Pathogen recognition and inflammatory signaling in innate immune defenses. Clin Microbiol Rev. 2009 Apr;22(2):240-73, doi: 10.1128/CMR.00046-08. PMID: 19366914; PMCID: PMC2668232.

Morandi B, Bougras G, Muller WA, Ferlazzo G, Münz C. NK cells of human secondary lymphoid tissues enhance T cell polarization via IFN-gamma secretion. Eur J Immunol. 2006 Sep;36(9):2394-400. doi: 10.1002/eji.200636290. PMID: 16917961.

Muntasell A, Magri G, Pende D, Angulo A, López-Botet M. Inhibition of NKG2D expression in NK cells by cytokines secreted in response to human cytomegalovirus infection. Blood. 2010 Jun 24;115(25):5170-9. doi: 10.1182/blood-2009-11-256479. Epub 2010 Apr 14. PMID: 20393128.

Murphy G. 2008. The ADAMs: signalling scissors in the tumour microenvironment. Nat Rev Cancer. 2008 Dec;8(12):929-41. doi: 10.1038/nrc2459.

Murphy, K. M, & Weaver, C. Janeway's immunobiology. 9th ed. New York: Garland Science.2017. ISBN 978-0-8153-4505-3

Murray PJ, Wynn TA. Protective and pathogenic functions of macrophage subsets. Nat Rev Immunol. 2011 Oct 14;11(11):723-37. doi: 10.1038/nri3073. PMID: 21997792; PMCID: PMC3422549.

Narni-Mancinelli E, Gauthier L, Baratin M, Guia S, Fenis A, Deghmane AE, Rossi B, Fourquet P, Escalière B, Kerdiles YM, Ugolini S, Taha MK, Vivier E. Complement factor P is a ligand for the natural killer cell-activating receptor NKp46. Sci Immunol. 2017 Apr 28;2(10):eaam9628. doi: 10.1126/sciimmunol.aam9628. PMID: 28480349; PMCID: PMC5419422.

Nyren-Erickson EK, Jones JM, Srivastava DK, Mallik S. A disintegrin and metalloproteinase-12 (ADAM12): function, roles in disease progression, and clinical implications. Biochim Biophys Acta. 2013 Oct;1830(10):4445-55. doi: 10.1016/j.bbagen.2013.05.011. Epub 2013 May 13. PMID: 23680494; PMCID: PMC3740046.

Okita, R., Maeda, A., Shimizu, K., Nojima, Y., Saisho, S., Nakata, M."Effect of platinum-based chemotherapy on the expression of natural killer group 2 member D ligands, programmed cell death-1 ligand 1 and HLA class I in non-small cell lung cancer". Oncology Reports 42, no. 2 (2019): 839-848. https://doi.org/10.3892/or.2019.7185

Okita, R., Yukawa, T., Nojima, Y. et al. MHC class I chain-related molecule A and B expression is upregulated by cisplatin and associated with good prognosis in patients with non-small cell lung cancer. Cancer Immunol Immunother 65, 499–509 (2016). https://doi.org/10.1007/s00262-016-1814-9

O'Leary JG, Goodarzi M, Drayton DL, von Andrian UH. T cell- and B cell-independent adaptive immunity mediated by natural killer cells. Nat Immunol. 2006 May;7(5):507-16. doi: 10.1038/ni1332. Epub 2006 Apr 16. PMID: 16617337.

Orr MT, Lanier LL. Natural killer cell education and tolerance. Cell. 2010 Sep 17;142(6):847-56. doi: 10.1016/j.cell.2010.08.031. PMID: 20850008; PMCID: PMC2945212.

Ostrand-Rosenberg S, Sinha P. Myeloid-derived suppressor cells: linking inflammation and cancer. J Immunol. 2009 Apr 15;182(8):4499-506. doi: 10.4049/jimmunol.0802740. PMID: 19342621; PMCID: PMC2810498.

Ota M, Katsuyama Y, Mizuki N, Ando H, Furihata K, Ono S, Pivetti-Pezzi P, Tabbara KF, Palimeris GD, Nikbin B, Davatchi F, Chams H, Geng Z, Bahram S, Inoko H. Trinucleotide repeat polymorphism within exon 5 of the MICA gene (MHC class I chain-related gene A): allele frequency data in the nine population groups Japanese, Northern Han, Hui, Uygur, Kazakhstan, Iranian, Saudi Arabian, Greek and Italian. Tissue Antigens. 1997 May;49(5):448-54. doi: 10.1111/j.1399-0039.1997.tb02778.x. PMID: 9174136.

Pallmer K, Oxenius A. Recognition and Regulation of T Cells by NK Cells. Front Immunol. 2016 Jun 24;7:251. doi: 10.3389/fimmu.2016.00251. PMID: 27446081; PMCID: PMC4919350.

Park YP, Choi SC, Kiesler P, Gil-Krzewska A, Borrego F, Weck J, Krzewski K, Coligan JE. Complex regulation of human NKG2D-DAP10 cell surface expression: opposing roles of the γc cytokines and TGF-β1. Blood. 2011 Sep 15;118(11):3019-27. doi: 10.1182/blood-2011-04-346825. Epub 2011 Aug 3. PMID: 21816829; PMCID: PMC3291493.

Parkin E, Harris B. A disintegrin and metalloproteinase (ADAM)-mediated ectodomain shedding of ADAM10. J Neurochem. 2009 Mar;108(6):1464-79. doi: 10.1111/j.1471-4159.2009.05907.x. Epub 2009 Jan 22. PMID: 19183255.

Paust S, Gill HS, Wang BZ, Flynn MP, Moseman EA, Senman B, Szczepanik M, Telenti A, Askenase PW, Compans RW, von Andrian UH. Critical role for the chemokine receptor CXCR6 in NK cell-mediated antigen-specific memory of haptens and viruses. Nat Immunol. 2010 Dec;11(12):1127-35. doi: 10.1038/ni.1953. Epub 2010 Oct 24. PMID: 20972432; PMCID: PMC2982944.

Pena SV, Hanson DA, Carr BA, Goralski TJ, Krensky AM. Processing, subcellular localization, and function of 519 (granulysin), a human late T cell activation molecule with homology to small, lytic, granule proteins. J Immunol. 1997;158:2680–2688

Plana D, Palmer AC, Sorger PK. Independent Drug Action in Combination Therapy: Implications for Precision Oncology. Cancer Discov. 2022 Mar 1;12(3):606-624. doi: 10.1158/2159-8290.CD-21-0212. PMID: 34983746; PMCID: PMC8904281.

Pogge von Strandmann E, Simhadri VR, von Tresckow B, Sasse S, Reiners KS, Hansen HP, Rothe A, Böll B, Simhadri VL, Borchmann P, McKinnon PJ, Hallek M, Engert A. Human leukocyte antigen-B-associated transcript 3 is released from tumor cells and engages the NKp30 receptor on natural killer cells. Immunity. 2007 Dec;27(6):965-74. doi: 10.1016/j.immuni.2007.10.010. Epub 2007 Dec 6. PMID: 18055229.

Prager I, Watzl C. Mechanisms of natural killer cell-mediated cellular cytotoxicity. J Leukoc Biol. 2019 Jun;105(6):1319-1329. doi: 10.1002/JLB.MR0718-269R. Epub 2019 May 20. PMID: 31107565.

Rabinovich B, Li J, Wolfson M, Lawrence W, Beers C, Chalupny J, Hurren R, Greenfield B, Miller R, Cosman D. NKG2D splice variants: a reexamination of adaptor molecule associations. Immunogenetics. 2006 Apr;58(2-3):81-8. doi: 10.1007/s00251-005-0078-x. Epub 2006 Feb 10. PMID: 16470377.

Raulet DH, Gasser S, Gowen BG, Deng W, Jung H. Regulation of ligands for the NKG2D activating receptor. Annu Rev Immunol. 2013;31:413-41. doi: 10.1146/annurev-immunol-032712-095951. Epub 2013 Jan 3. PMID: 23298206; PMCID: PMC4244079.

Raulet DH, Guerra N. Oncogenic stress sensed by the immune system: role of natural killer cell receptors. Nat Rev Immunol. 2009 Aug;9(8):568-80. doi: 10.1038/nri2604. PMID: 19629084; PMCID: PMC3017432.

Raulet DH, Vance RE. Self-tolerance of natural killer cells. Nat Rev Immunol. 2006 Jul;6(7):520-31. doi: 10.1038/nri1863. PMID: 16799471.

Ravetch JV, Lanier LL. Immune inhibitory receptors. Science. 2000 Oct 6;290(5489):84-9. doi: 10.1126/science.290.5489.84. PMID: 11021804.

Raynaud A, Desrumeaux K, Vidard L, Termine E, Baty D, Chames P, Vigne E, Kerfelec B. Anti-NKG2D single domain-based antibodies for the modulation of anti-tumor immune response. Oncoimmunology. 2020 Dec 29;10(1):1854529. doi: 10.1080/2162402X.2020.1854529. PMID: 33457075; PMCID: PMC7781768.

Rebmann V, Schütt P, Brandhorst D, Opalka B, Moritz T, Nowrousian MR, Grosse-Wilde H. Soluble MICA as an independent prognostic factor for the overall survival and progression-free survival of multiple myeloma patients. Clin Immunol. 2007 Apr;123(1):114-20. doi: 10.1016/j.clim.2006.11.007. Epub 2007 Jan 10. PMID: 17218152.

Roberts AI, Lee L, Schwarz E, Groh V, Spies T, Ebert EC, Jabri B. NKG2D receptors induced by IL-15 costimulate CD28-negative effector CTL in the tissue microenvironment. J Immunol. 2001 Nov 15;167(10):5527-30. doi: 10.4049/jimmunol.167.10.5527. PMID: 11698420.

Robertson MJ. Role of chemokines in the biology of natural killer cells. J Leukoc Biol. 2002 Feb;71(2):173-83. PMID: 11818437.

Rosen DB, Araki M, Hamerman JA, Chen T, Yamamura T, Lanier LL. A Structural basis for the association of DAP12 with mouse, but not human, NKG2D. J Immunol. 2004 Aug 15;173(4):2470-8. doi: 10.4049/jimmunol.173.4.2470. PMID: 15294961.

Rosenberg SA. IL-2: the first effective immunotherapy for human cancer. J Immunol. 2014 Jun 15;192(12):5451-8. doi: 10.4049/jimmunol.1490019. PMID: 24907378; PMCID: PMC6293462.

Rothenberg ME, Hogan SP. The eosinophil. Annu Rev Immunol. 2006;24:147-74. doi: 10.1146/annurev.immunol.24.021605.090720. PMID: 16551246.

Salih HR, Antropius H, Gieseke F, Lutz SZ, Kanz L, Rammensee HG, Steinle A. Functional expression and release of ligands for the activating immunoreceptor NKG2D in leukemia. Blood. 2003 Aug 15;102(4):1389-96. doi: 10.1182/blood-2003-01-0019. Epub 2003 Apr 24. PMID: 12714493.

Salih HR, Goehlsdorf D, Steinle A. Release of MICB molecules by tumor cells: mechanism and soluble MICB in sera of cancer patients. Hum Immunol. 2006 Mar;67(3):188-95. doi: 10.1016/j.humimm.2006.02.008. Epub 2006 Mar 29. PMID: 16698441.

Salih HR, Rammensee HG, Steinle A. Cutting edge: down-regulation of MICA on human tumors by proteolytic shedding. J Immunol. 2002 Oct 15;169(8):4098-102. doi: 10.4049/jimmunol.169.8.4098. PMID: 12370336.

Satwani P, Bavishi S, Saha A, Zhao F, Ayello J, van de Ven C, Chu Y, Cairo MS. Upregulation of NKG2D ligands in acute lymphoblastic leukemia and non-Hodgkin lymphoma cells by romidepsin and enhanced in vitro and in vivo natural killer cell cytotoxicity. Cytotherapy. 2014 Oct;16(10):1431-40. doi: 10.1016/j.jcyt.2014.03.008. Epub 2014 May 20. PMID: 24856896.

Scoville SD, Freud AG, Caligiuri MA. Modeling human natural killer cell development in the era of innate lymphoid cells. Front Immunol (2017) 8:360. doi:10.3389/fimmu.2017.00360

Seidel JA, Otsuka A, Kabashima K. Anti-PD-1 and Anti-CTLA-4 Therapies in Cancer: Mechanisms of Action, Efficacy, and Limitations. Front Oncol. 2018 Mar 28;8:86. doi: 10.3389/fonc.2018.00086. PMID: 29644214; PMCID: PMC5883082.

Sentman CL, Meehan KR. NKG2D CARs as cell therapy for cancer. Cancer J. 2014 Mar-Apr;20(2):156-9. doi: 10.1097/PPO.0000000000000029. PMID: 24667963; PMCID: PMC4017323.

Silva-Santos B, Mensurado S, Coffelt SB. γδ T cells: pleiotropic immune effectors with therapeutic potential in cancer. Nat Rev Cancer. 2019 Jul;19(7):392-404. doi: 10.1038/s41568-019-0153-5. PMID: 31209264.

Simoni Y, Newell EW. Dissecting human ILC heterogeneity: more than just three subsets. Immunology. 2018 Mar;153(3):297-303. doi: 10.1111/imm.12862. Epub 2017 Dec 26. PMID: 29140572; PMCID: PMC5795188.

Slavuljica I, Krmpotić A, Jonjić S. Manipulation of NKG2D ligands by cytomegaloviruses: impact on innate and adaptive immune response. Front Immunol. 2011 Dec 28;2:85. doi: 10.3389/fimmu.2011.00085. PMID: 22566874; PMCID: PMC3342069.

Solito S, Falisi E, Diaz-Montero CM, Doni A, Pinton L, Rosato A, Francescato S, Basso G, Zanovello P, Onicescu G, Garrett-Mayer E, Montero AJ, Bronte V, Mandruzzato S. A human promyelocytic-like population is responsible for the immune suppression mediated by myeloid-derived suppressor cells. Blood. 2011 Aug 25;118(8):2254-65. doi: 10.1182/blood-2010-12-325753. Epub 2011 Jul 6. PMID: 21734236; PMCID: PMC3709641.

Sparano JA, Bernardo P, Stephenson P, Gradishar WJ, Ingle JN, Zucker S, Davidson NE. Randomized phase III trial of marimastat versus placebo in patients with metastatic breast cancer who have responding or stable disease after first-line chemotherapy: Eastern Cooperative Oncology Group trial E2196. J Clin Oncol. 2004 Dec 1;22(23):4683-90. doi: 10.1200/JCO.2004.08.054. Erratum in: J Clin Oncol. 2005 Jan 1;23(1):248. PMID: 15570070.

Stanietsky N, Simic H, Arapovic J, Toporik A, Levy O, Novik A, Levine Z, Beiman M, Dassa L, Achdout H, Stern-Ginossar N, Tsukerman P, Jonjic S, Mandelboim O. The interaction of TIGIT with PVR and PVRL2 inhibits human NK cell cytotoxicity. Proc Natl Acad Sci U S A. 2009 Oct 20;106(42):17858-63. doi: 10.1073/pnas.0903474106. Epub 2009 Oct 7. PMID: 19815499; PMCID: PMC2764881.

Steinle A, Li P, Morris DL, Groh V, Lanier LL, Strong RK, Spies T. Interactions of human NKG2D with its ligands MICA, MICB, and homologs of the mouse RAE-1 protein family. Immunogenetics. 2001 May-Jun;53(4):279-87. doi: 10.1007/s002510100325. PMID: 11491531.

Stenger S, Hanson DA, Teitelbaum R, et al. An antimicrobial activity of cytolytic T cells mediated by granulysin. Science. 1998;282:121–125.

Sterner RC, Sterner RM. CAR-T cell therapy: current limitations and potential strategies. Blood Cancer J. 2021 Apr 6;11(4):69. doi: 10.1038/s41408-021-00459-7. PMID: 33824268; PMCID: PMC8024391.

Sun JC, Beilke JN, Lanier LL. Adaptive immune features of natural killer cells. Nature. 2009 Jan 29;457(7229):557-61. doi: 10.1038/nature07665. Epub 2009 Jan 11. Erratum in: Nature. 2009 Feb 26;457(7233):1168. PMID: 19136945; PMCID: PMC2674434.

Takada A, Yoshida S, Kajikawa M, Miyatake Y, Tomaru U, Sakai M, Chiba H, Maenaka K, Kohda D, Fugo K, Kasahara M. Two novel NKG2D ligands of the mouse H60 family with differential expression patterns and binding affinities to NKG2D. J Immunol. 2008 Feb 1;180(3):1678-85. doi: 10.4049/jimmunol.180.3.1678. PMID: 18209064.

Takeda K, Hayakawa Y, Smyth MJ, Kayagaki N, Yamaguchi N, Kakuta S, Iwakura Y, Yagita H, Okumura K. Involvement of tumor necrosis factor-related apoptosis-inducing ligand in surveillance of tumor metastasis by liver natural killer cells. Nat Med. 2001 Jan;7(1):94-100. doi: 10.1038/83416. PMID: 11135622.

Tamaki S, Sanefuzi N, Kawakami M, Aoki K, Imai Y, Yamanaka Y, Yamamoto K, Ishitani A, Hatake K, Kirita T. Association between soluble MICA levels and disease stage IV oral squamous cell carcinoma in Japanese patients. Hum Immunol. 2008 Feb;69(2):88-93. doi: 10.1016/j.humimm.2008.01.010. Epub 2008 Feb 22. PMID: 18361932.

Tolcher AW. The Evolution of Antibody-Drug Conjugates: A Positive Inflexion Point. Am Soc Clin Oncol Educ Book. 2020 Mar;40:1-8. doi: 10.1200/EDBK_281103. PMID: 32223669.

Tomasello E, Bléry M, Vély F, Vivier E. Signaling pathways engaged by NK cell receptors: double concerto for activating receptors, inhibitory receptors and NK cells. Semin Immunol. 2000 Apr;12(2):139-47. doi: 10.1006/smim.2000.0216. Erratum in: Semin Immunol 2000 Aug;12(4):417. PMID: 10764622.

Tong HV, Toan NL, Song LH, Bock CT, Kremsner PG, Velavan TP. Hepatitis B virus-induced hepatocellular carcinoma: functional roles of MICA variants. J Viral Hepat. 2013 Oct;20(10):687-98. doi: 10.1111/jvh.12089. Epub 2013 May 7. PMID: 24010643.

Tousseyn T, Thathiah A, Jorissen E, Raemaekers T, Konietzko U, Reiss K, Maes E, Snellinx A, Serneels L, Nyabi O, Annaert W, Saftig P, Hartmann D, De Strooper B. ADAM10, the rate-limiting protease of regulated intramembrane proteolysis of Notch and other proteins, is processed by ADAMS-9, ADAMS-15, and the gamma-secretase. J Biol Chem. 2009 Apr 24;284(17):11738-47. doi: 10.1074/jbc.M805894200. Epub 2009 Feb 11. PMID: 19213735; PMCID: PMC2670177.

Ullrich E, Koch J, Cerwenka A, Steinle A. New prospects on the NKG2D/NKG2DL system for oncology. Oncoimmunology. 2013 Oct 1;2(10):e26097. doi: 10.4161/onci.26097. Epub 2013 Oct 25. PMID: 24353908; PMCID: PMC3862635.

Vaidya S.V., Mathew P.A. Of mice and men: Different functions of the murine and human 2B4 (CD244) receptor on NK cells. Immunol. Lett. 2006;105:180–184. doi: 10.1016/j.imlet.2006.02.006.

Vales-Gomez M, Reyburn HT, Erskine RA, Strominger J. Differential binding to HLA-C of p50-activating and p58-inhibitory natural killer cell receptors. Proc Natl Acad Sci U S A (1998) 95:14326–31. 10.1073/pnas.95.24.14326

Venkataraman GM, Suciu D, Groh V, Boss JM, Spies T. Promoter region architecture and transcriptional regulation of the genes for the MHC class I-related chain A and B ligands of NKG2D. J Immunol. 2007 Jan 15;178(2):961-9. doi: 10.4049/jimmunol.178.2.961. PMID: 17202358.

Vivier E, Nunès JA, Vély F. Natural killer cell signaling pathways. Science. 2004 Nov 26;306(5701):1517-9. doi: 10.1126/science.1103478. PMID: 15567854.

Vivier E, Tomasello E, Baratin M, Walzer T, Ugolini S. Functions of natural killer cells. Nat Immunol. 2008 May;9(5):503-10. doi: 10.1038/ni1582. PMID: 18425107.

von Strandmann EP, Hansen HP, Reiners KS, Schnell R, Borchmann P, Merkert S, Simhadri VR, Draube A, Reiser M, Purr I, Hallek M, Engert A. A novel bispecific protein (ULBP2-BB4) targeting the NKG2D receptor on natural killer (NK) cells and CD138 activates NK cells and has potent antitumor activity against human multiple myeloma in vitro and in vivo. Blood. 2006 Mar 1;107(5):1955-62. doi: 10.1182/blood-2005-05-2177. Epub 2005 Oct 6. PMID: 16210338.

Voskoboinik I, Smyth MJ, Trapani JA. Perforin-mediated target-cell death and immune homeostasis. Nat Rev Immunol. 2006 Dec;6(12):940-52. doi: 10.1038/nri1983. PMID: 17124515.

Waldhauer I, Goehlsdorf D, Gieseke F, Weinschenk T, Wittenbrink M, Ludwig A, Stevanovic S, Rammensee HG, Steinle A. Tumor-associated MICA is shed by ADAM proteases. Cancer Res. 2008 Aug 1;68(15):6368-76. doi: 10.1158/0008-5472.CAN-07-6768. PMID: 18676862.

Walkiewicz K, Nowakowska-Zajdel E, Kozieł P, Muc-Wierzgoń M. The role of some ADAM-proteins and activation of the insulin growth factor-related pathway in colorectal cancer. Cent Eur J Immunol. 2018;43(1):109-113. doi: 10.5114/ceji.2018.74881. Epub 2018 Mar 30. PMID: 29731694; PMCID: PMC5927180.

Walzer T, Bléry M, Chaix J, Fuseri N, Chasson L, Robbins SH, Jaeger S, André P, Gauthier L, Daniel L, Chemin K, Morel Y, Dalod M, Imbert J, Pierres M, Moretta A, Romagné F, Vivier E. Identification, activation, and selective in vivo ablation of mouse NK cells via NKp46. Proc Natl Acad Sci U S A. 2007 Feb 27;104(9):3384-9. doi: 10.1073/pnas.0609692104. Epub 2007 Feb 20. PMID: 17360655; PMCID: PMC1805551.

Wang F, Hou H, Wu S, Tang Q, Liu W, Huang M, Yin B, Huang J, Mao L, Lu Y, Sun Z. TIGIT expression levels on human NK cells correlate with functional heterogeneity among healthy individuals. Eur J Immunol. 2015 Oct;45(10):2886-97. doi: 10.1002/eji.201545480. Epub 2015 Sep 7. PMID: 26171588.

Wang X, Lundgren AD, Singh P, Goodlett DR, Plymate SR, Wu JD. An six-amino acid motif in the alpha3 domain of MICA is the cancer therapeutic target to inhibit shedding. Biochem Biophys Res Commun. 2009 Sep 25;387(3):476-81. doi: 10.1016/j.bbrc.2009.07.062. Epub 2009 Jul 16. PMID: 19615970; PMCID: PMC2737406.

Warren HS, Kinnear BF. Quantitative analysis of the effect of CD16 ligation on human NK cell proliferation. J Immunol. 1999 Jan 15;162(2):735-42. PMID: 9916693.

Weinkove R, George P, Dasyam Net al.. Selecting costimulatory domains for chimeric antigen receptors: functional and clinical considerations. Clin Transl Immunology 2019;8(5):e1049. 10.1002/cti2.1049

Welte S, Kuttruff S, Waldhauer I, Steinle A. Mutual activation of natural killer cells and monocytes mediated by NKp80-AICL interaction. Nat Immunol. 2006 Dec;7(12):1334-42. doi: 10.1038/ni1402. Epub 2006 Oct 22. PMID: 17057721.

Welte SA, Sinzger C, Lutz SZ, Singh-Jasuja H, Sampaio KL, Eknigk U, Rammensee HG, Steinle A. Selective intracellular retention of virally induced NKG2D ligands by the human cytomegalovirus UL16 glycoprotein. Eur J Immunol. 2003 Jan;33(1):194-203. doi: 10.1002/immu.200390022. PMID: 12594848.

Whalen K, Naveen M, Meetze K, Gibson N, Michaelson J, BaeuerleP. 1395 CLN 619 a clinical stage MICA B specific IgG1 antibody which restores the MICA B-NKG2D axis requires Fc function for potent anti-tumor activity. Journal for ImmunoTherapy of Cancer. 2022;10**:** doi: 10.1136/jitc-2022-SITC2022.1395

Wiemann K, Mittrücker HW, Feger U, Welte SA, Yokoyama WM, Spies T, Rammensee HG, Steinle A. Systemic NKG2D down-regulation impairs NK and CD8 T cell responses in vivo. J Immunol. 2005 Jul 15;175(2):720-9. doi: 10.4049/jimmunol.175.2.720. PMID: 16002667.

Wolan DW, Teyton L, Rudolph MG, Villmow B, Bauer S, Busch DH, Wilson IA. Crystal structure of the murine NK cell-activating receptor NKG2D at 1.95 A. Nat Immunol. 2001 Mar;2(3):248-54. doi: 10.1038/85311. PMID: 11224525.

Wu J, Song Y, Bakker AB, Bauer S, Spies T, Lanier LL, Phillips JH. An activating immunoreceptor complex formed by NKG2D and DAP10. Science. 1999 Jul 30;285(5428):730-2. doi: 10.1126/science.285.5428.730. PMID: 10426994.

Yamanegi K, Yamane J, Kobayashi K, Kato-Kogoe N, Ohyama H, Nakasho K, Yamada N, Hata M, Nishioka T, Fukunaga S, Futani H, Okamura H, Terada N. Sodium valproate, a histone deacetylase inhibitor, augments the expression of cell-surface NKG2D ligands, MICA/B, without increasing their soluble forms to enhance susceptibility of human osteosarcoma cells to NK cell-mediated cytotoxicity. Oncol Rep. 2010 Dec;24(6):1621-7. doi: 10.3892/or_00001026. PMID: 21042760.

Yang X, Kuang S, Wang L, Wei Y. MHC class I chain-related A: Polymorphism, regulation and therapeutic value in cancer. Biomed Pharmacother. 2018 Jul;103:111-117. doi: 10.1016/j.biopha.2018.03.177. Epub 2018 Apr 7. PMID: 29635123.

Yang Y, Li C, Liu T, Dai X, Bazhin AV. Myeloid-Derived Suppressor Cells in Tumors: From Mechanisms to Antigen Specificity and Microenvironmental Regulation. Front Immunol. 2020 Jul 22;11:1371. doi: 10.3389/fimmu.2020.01371. PMID: 32793192; PMCID: PMC7387650.

Yasunaga M. Antibody therapeutics and immunoregulation in cancer and autoimmune disease. Semin Cancer Biol. 2020 Aug;64:1-12. doi: 10.1016/j.semcancer.2019.06.001. Epub 2019 Jun 7. PMID: 31181267.

Yin X, Liu T, Wang Z, Ma M, Lei J, Zhang Z, Fu S, Fu Y, Hu Q, Ding H, Han X, Xu J, Shang H, Jiang Y. Expression of the Inhibitory Receptor TIGIT Is Up-Regulated Specifically on NK Cells With CD226 Activating Receptor From HIV-Infected Individuals. Front Immunol. 2018 Oct 10;9:2341. doi: 10.3389/fimmu.2018.02341. PMID: 30364127; PMCID: PMC6192288.

Zamai L, Ahmad M, Bennett IM, Azzoni L, Alnemri ES, Perussia B. Natural killer (NK) cell-mediated cytotoxicity: differential use of TRAIL and Fas ligand by immature and mature primary human NK cells. J Exp Med. 1998 Dec 21;188(12):2375-80. doi: 10.1084/jem.188.12.2375. PMID: 9858524; PMCID: PMC2212426.

Zhang C, Liu J, Zhong JF, Zhang X. Engineering CAR-T cells. Biomark Res. 2017 Jun 24;5:22. doi: 10.1186/s40364-017-0102-y. PMID: 28652918; PMCID: PMC5482931.

Zhang C, Röder J, Scherer A, et al. Bispecific antibody-mediated redirection of NKG2D-CAR natural killer cells facilitates dual targeting and enhances antitumor activity. Journal for ImmunoTherapy of Cancer 2021;9:e002980. doi:10.1136/jitc-2021-002980

Zhang C, Zhang J, Niu J, Zhou Z, Zhang J, Tian Z. Interleukin-12 improves cytotoxicity of natural killer cells via upregulated expression of NKG2D. Hum Immunol. 2008 Aug;69(8):490-500. doi: 10.1016/j.humimm.2008.06.004. Epub 2008 Jul 9. PMID: 18619507.

Zhang N, Zhang Z-M, Wang X-F. The roles of basophils in mediating the immune responses. European Journal of Inflammation. 2021;19. doi:10.1177/20587392211047644

Zhu S, Denman CJ, Cobanoglu ZS, Kiany S, Lau CC, Gottschalk SM, Hughes DP, Kleinerman ES, Lee DA. The narrow-spectrum HDAC inhibitor entinostat enhances NKG2D expression without NK cell toxicity, leading to enhanced recognition of cancer cells. Pharm Res. 2015 Mar;32(3):779-92. doi: 10.1007/s11095-013-1231-0. Epub 2013 Nov 8. PMID: 24203492; PMCID: PMC4014531.

Zingoni A, Cecere F, Vulpis E, Fionda C, Molfetta R, Soriani A, Petrucci MT, Ricciardi MR, Fuerst D, Amendola MG, Mytilineos J, Cerboni C, Paolini R, Cippitelli M, Santoni A. Genotoxic Stress Induces Senescence-Associated ADAM10-Dependent Release of NKG2D MIC Ligands in Multiple Myeloma Cells. J Immunol. 2015 Jul 15;195(2):736-48. doi: 10.4049/jimmunol.1402643. Epub 2015 Jun 12. PMID: 26071561.

Zingoni A, Fionda C, Borrelli C, Cippitelli M, Santoni A, Soriani A. Natural Killer Cell Response to Chemotherapy-Stressed Cancer Cells: Role in Tumor Immunosurveillance. Front Immunol. 2017 Sep 25;8:1194. doi: 10.3389/fimmu.2017.01194. PMID: 28993779; PMCID: PMC5622151.

Zocchi MR, Catellani S, Canevali P, Tavella S, Garuti A, Villaggio B, Zunino A, Gobbi M, Fraternali-Orcioni G, Kunkl A, Ravetti JL, Boero S, Musso A, Poggi A. High ERp5/ADAM10 expression in lymph node microenvironment and impaired NKG2D ligands recognition in Hodgkin lymphomas. Blood. 2012 Feb 9;119(6):1479-89. doi: 10.1182/blood-2011-07-370841. Epub 2011 Dec 13. PMID: 22167753..

Erklärungen

§8 Abs. 1 lit. c der Promotionsordnung der TU Darmstadt

Ich versichere hiermit, dass die elektronische Version meiner Dissertation mit der schriftlichen Version übereinstimmt und für die Durchführung des Promotionsverfahrens vorliegt.

§8 Abs. 1 lit. d der Promotionsordnung der TU Darmstadt

Ich versichere hiermit, dass zu einem vorherigen Zeitpunkt noch keine Promotion versucht wurde und zu keinem früheren Zeitpunkt an einer in- oder ausländischen Hochschule eingereicht wurde. In diesem Fall sind nähere Angaben über Zeitpunkt, Hochschule, Dissertationsthema und Ergebnis dieses Versuchs mitzuteilen.

§9 Abs. 1 der Promotionsordnung der TU Darmstadt

Ich versichere hiermit, dass die vorliegende Dissertation selbstständig und nur unter Verwendung der angegebenen Quellen verfasst wurde.

§9 Abs. 2 der Promotionsordnung der TU Darmstadt

Die Arbeit hat bisher noch nicht zu Prüfungszwecken gedient.

Darmstadt, den 17.05.2023

Veronika Liptáková

Acknowledgements

I would like to sincerely thank my supervisor Prof. Dr. Alexander Steinle from the Institute for Molecular Medicine, Goethe University Frankfurt. Thank you for giving me the opportunity to work on such exciting projects, for your excellent supervision and continuous support. That is something that I will forever value.

I would also like to thank Prof. Dr. Harald Kolmar from the TU Darmstadt for kindly accepting me for the doctoral supervision. I appreciate your support.

Thank you to all members (previous and current) of AG Steinle and AG Krueger. Your friendship made this journey a lot easier. My thanks go to Julian with whom we shared great and inspiring scientific and also not too scientific discussions for all those years. Thank you for all the help, support and encouragement when the times got too overwhelming. Thank you Mariya and Rachel for the friendship and emotional and scientific support. Thank you to Young who introduced me to the MICA world and taught me many things that I know today. I appreciate it.

Rada by som sa poďakovala aj všetkým kamošom, čo ma po celé tie roky podporovali. Diky Sodoma! A hlavne ďakujem môjmu Bajtíkovi. Za všetko. Že sa ti vždy podarí vyčariť mi úsmev na tvári keď sa to zdá v tej chvíli takmer nemožné. A ešte aj za horalky, tresku a gumené cukríky.

V neposlednom rade by som sa chcela poďakovať svojim rodičom. Za ich lásku a starostlivosť. Vážim si všetko, čo ste pre mňa urobili a stále robíte. Preto by som vám dvom chcela túto záverečnú prácu venovať. Práve vďaka vám dnes som kto som. Ďakujem. A samozrejme ďakujem aj svojej malej sestre Peťke (stále budeš pre mňa moja malá sestra). Za tie dlhé rozhovory a za priateľstvo, ktoré vznikne len medzi sestrami.